Radially and azimuthally anisotropic shear-wave velocity model of the Earth’s upper mantle

François Lavoué, Sergei Lebedev, Nicolas L. Celli, Andrew J. Schaeffer

Institiúid Ard-Léinn Bhaile Átha Cliath | Dublin Institute for Advanced Studies

IRISH CENTRE FOR RESEARCH IN APPLIED GEOSCIENCES

TRINITY COLLEGE DUBLIN

Ireland’s European Structural and Investment Funds Programmes 2014-2020
Co-funded by the Irish Government and the European Union

European Union
European Regional Development Fund

Science Foundation Ireland For what’s next

Introduction: origin and importance of seismic anisotropy

Seismic anisotropy results from the preferential alignment of anisotropic cristals (e.g. olivine) due to deformation (mantle flow).

Important geodynamical implications in terms of **past and present deformation and flow in the mantle.**

But: (1) anisotropic models are less robust and much more debated than their isotropic counterpart.
(2) the geodynamical interpretation of seismic anisotropy is not straightforward.

(http://faculty.epss.ucla.edu/~cbeghein)

Seismic anisotropy and olivine lattice preferred orientation (LPO) - 1 Conventional model (Karato et al., 2008)

The geodynamical interpretation of seismic anisotropy is not straightforward…

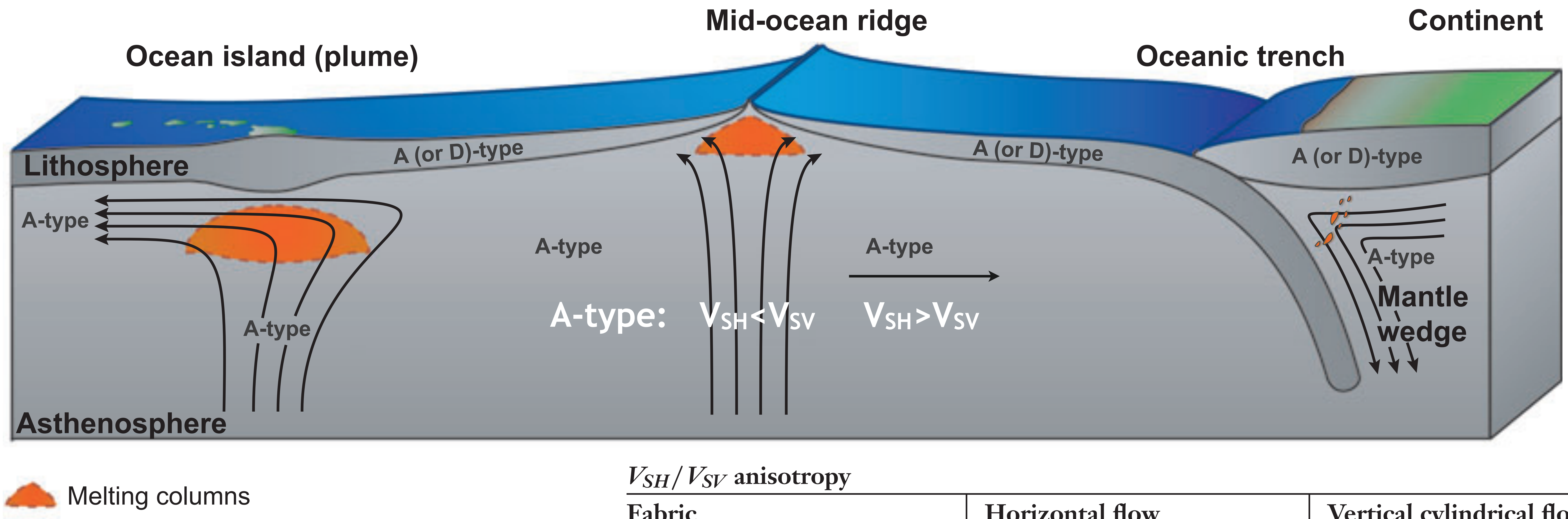

Conventional model of olivine LPO (Karato et al., 2008)

V_{SH}/V_{SV} **anisotropy**

Fabric	**Horizontal flow**	**Vertical cylindrical flow**
A-type	$V_{SH}/V_{SV} > 1$	$V_{SH}/V_{SV} < 1$
B-type	$V_{SH}/V_{SV} > 1$	$V_{SH}/V_{SV} > 1$ (weak)
C-type	$V_{SH}/V_{SV} < 1$	$V_{SH}/V_{SV} > 1$ (weak)
D-type	$V_{SH}/V_{SV} > 1$	$V_{SH}/V_{SV} < 1$
E-type	$V_{SH}/V_{SV} > 1$ (weak)	$V_{SH}/V_{SV} < 1$

Seismic anisotropy and olivine lattice preferred orientation (LPO) - 2 *New* model (Karato et al., 2008)

The geodynamical interpretation of seismic anisotropy is not straightforward...

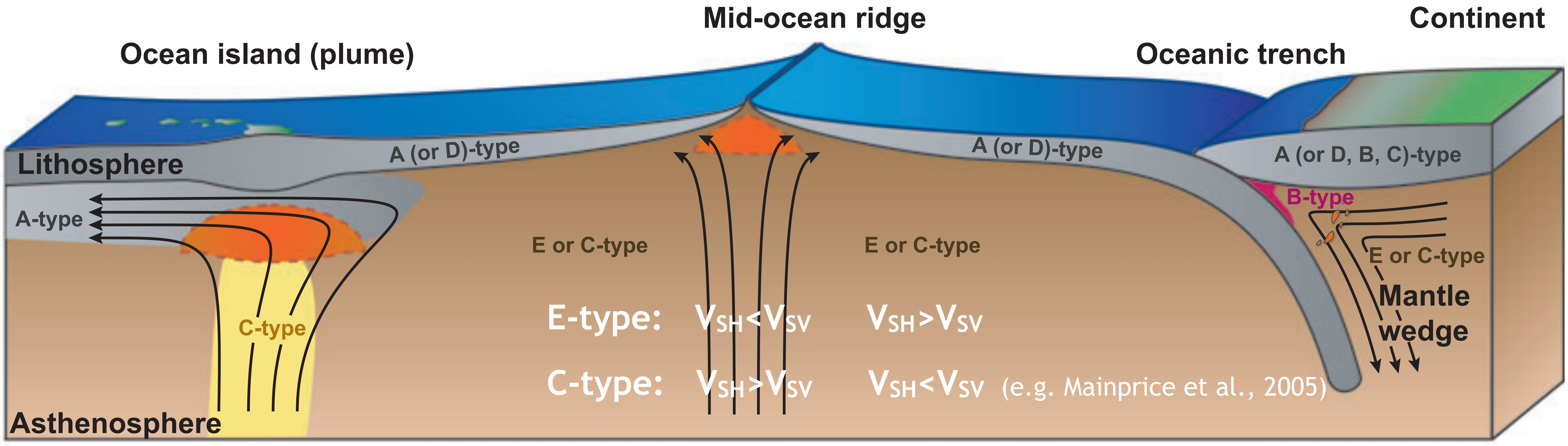

Melting columns

Karato's new model of olivine LPO (Karato et al., 2008)

V_{SH}/V_{SV} anisotropy

Fabric	Horizontal flow	Vertical cylindrical flow
A-type	$V_{SH}/V_{SV} > 1$	$V_{SH}/V_{SV} < 1$
B-type	$V_{SH}/V_{SV} > 1$	$V_{SH}/V_{SV} > 1$ (weak)
C-type	$V_{SH}/V_{SV} < 1$	$V_{SH}/V_{SV} > 1$ (weak)
D-type	$V_{SH}/V_{SV} > 1$	$V_{SH}/V_{SV} < 1$
E-type	$V_{SH}/V_{SV} > 1$ (weak)	$V_{SH}/V_{SV} < 1$

Our contribution: a new seismic model obtained by linearised waveform inversion of S and surface waves.

Large dataset of long-period, multicomponent waveform data.

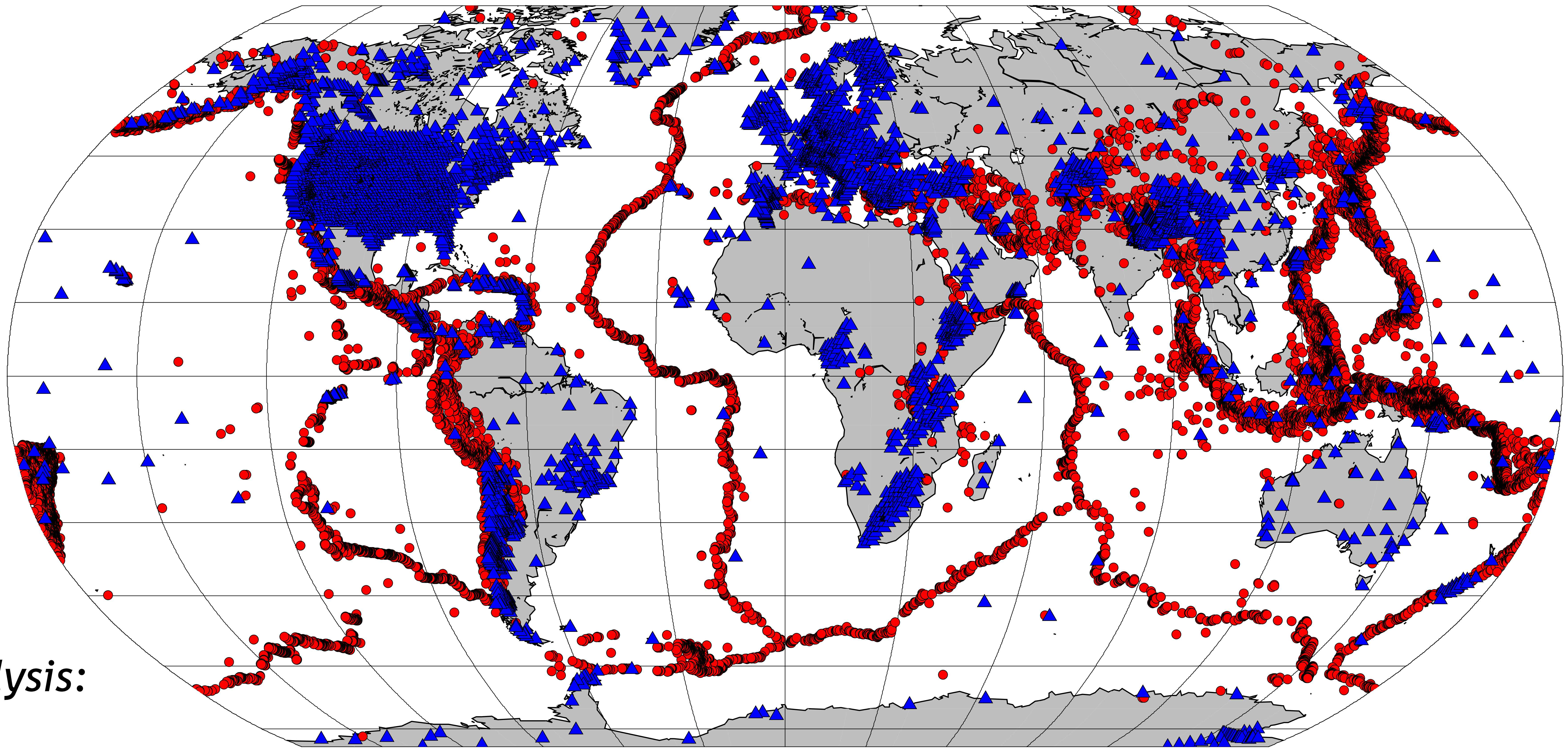

After outlier analysis:
- *24,802 events*
- *6,969 stations*
- *765,302 vertical-component seismograms (Rayleigh waves)*
- *243,736 transverse-component seismograms (Love waves)*
- *periods from 10 to 400 s*

Methodology: waveform fitting

Two-step partitioned inversion *(Nolet, 1990)*

1. Non-linear waveform fitting
within the JWKB approximation
via Automated Multimode Inversion
(AMI, Lebedev et al., 2005)

2. 3D linear tomography
(Lebedev and van der Hilst, 2008; Schaeffer and Lebedev, 2013)

Estimation of dV_{SH}, dV_{SV}, dV_P perturbations with respect to a reference model, and of V_{SH} and V_{SV} azimuthal anisotropy
(Smith & Dahlen, 1973; Montagner & Nataf, 1986)
on a 350-km grid and 18 predefined depths.

Regularisation (damping, horizontal and vertical smoothing) in terms of isotropic average perturbation and radial anisotropy:

$$dV_{S0} = (dV_{SH} + dV_{SV}) / 2$$

$$\delta = V_{SH} - V_{SV}$$

Reference model: modified AK135 + Crust2
(Kennett et al., 1995; Bassin et al., 2000)

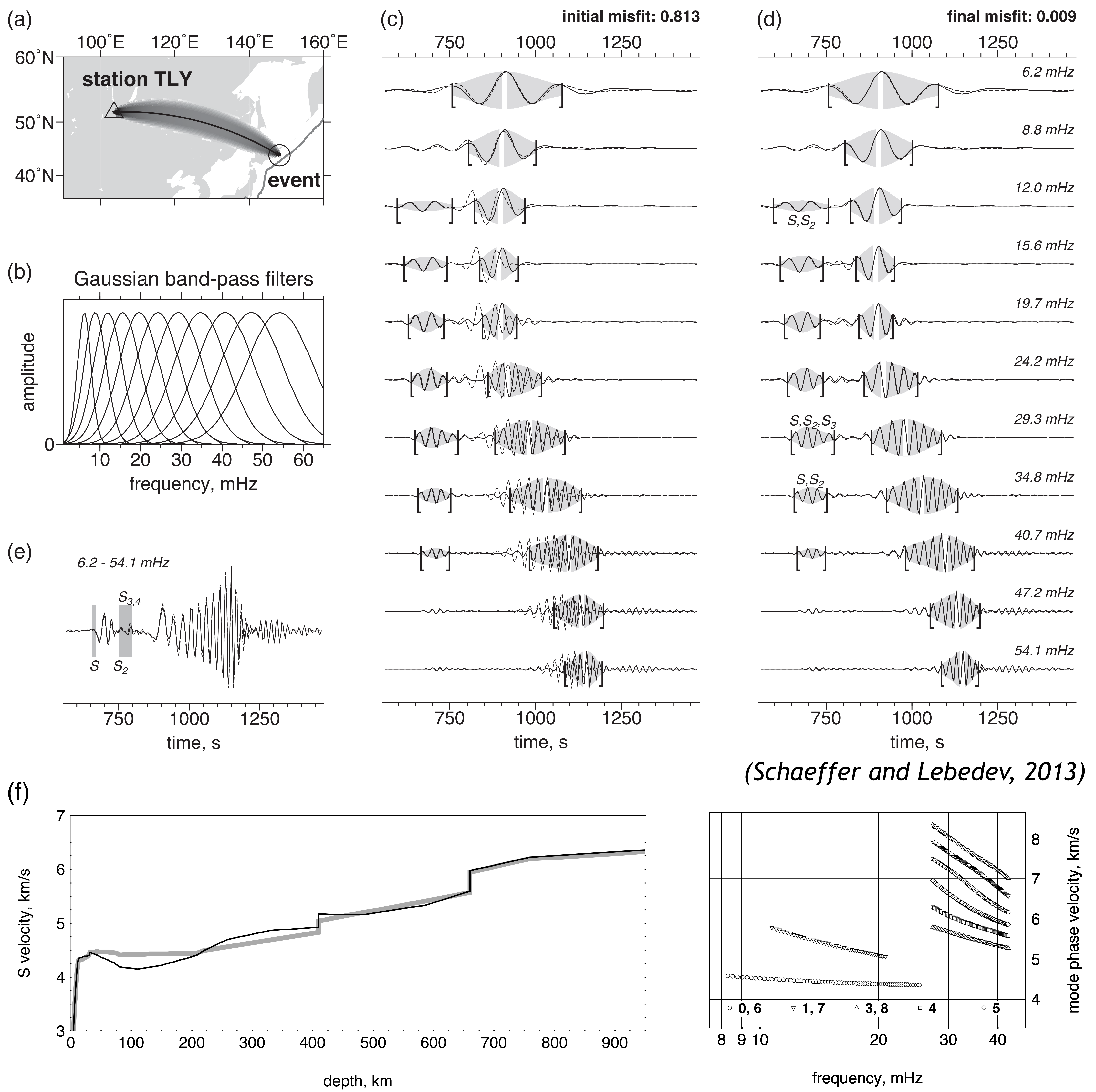

(Schaeffer and Lebedev, 2013)

Methodology: 3D tomography

Two-step partitioned inversion *(Nolet, 1990)*

1. **Non-linear waveform fitting**
   within the JWKB approximation
   via Automated Multimode Inversion
   (AMI, Lebedev et al., 2005)

2. **3D linear tomography**
   (Lebedev and van der Hilst, 2008;
   Schaeffer and Lebedev, 2013)

   Estimation of dV_{SH}, dV_{SV}, dV_P perturbations with respect to a reference model, and of V_{SH} and V_{SV} azimuthal anisotropy *(Smith & Dahlen, 1973; Montagner & Nataf, 1986)* on a 350-km grid and 18 predefined depths.

   Regularisation (damping, horizontal and vertical smoothing) in terms of isotropic average perturbation and radial anisotropy:

   $$dV_{S0} = (dV_{SH} + dV_{SV}) / 2$$

   $$\delta = V_{SH} - V_{SV}$$

Reference model: modified AK135 + Crust2
(Kennett et al., 1995; Bassin et al., 2000)

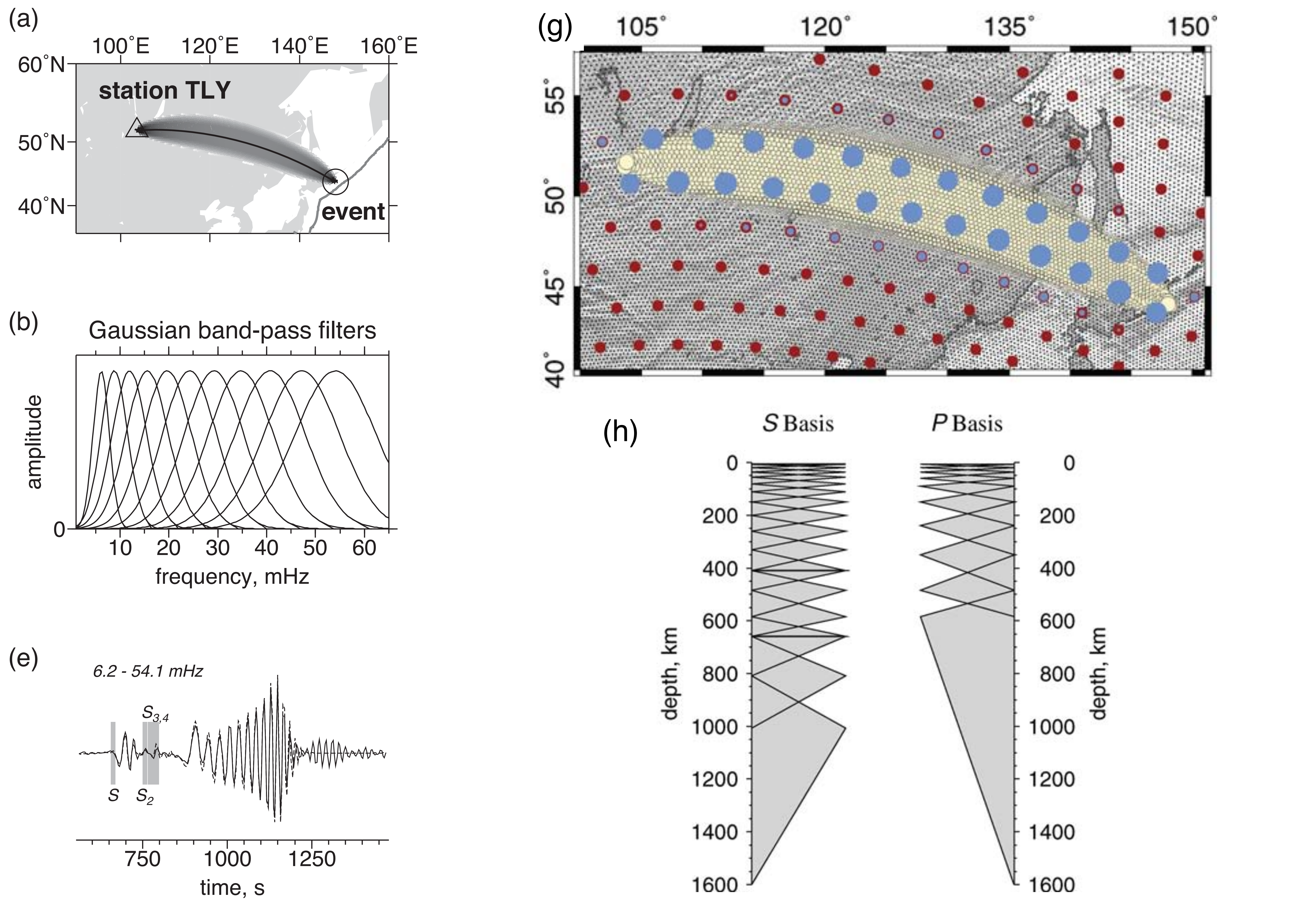

(Schaeffer and Lebedev, 2013)

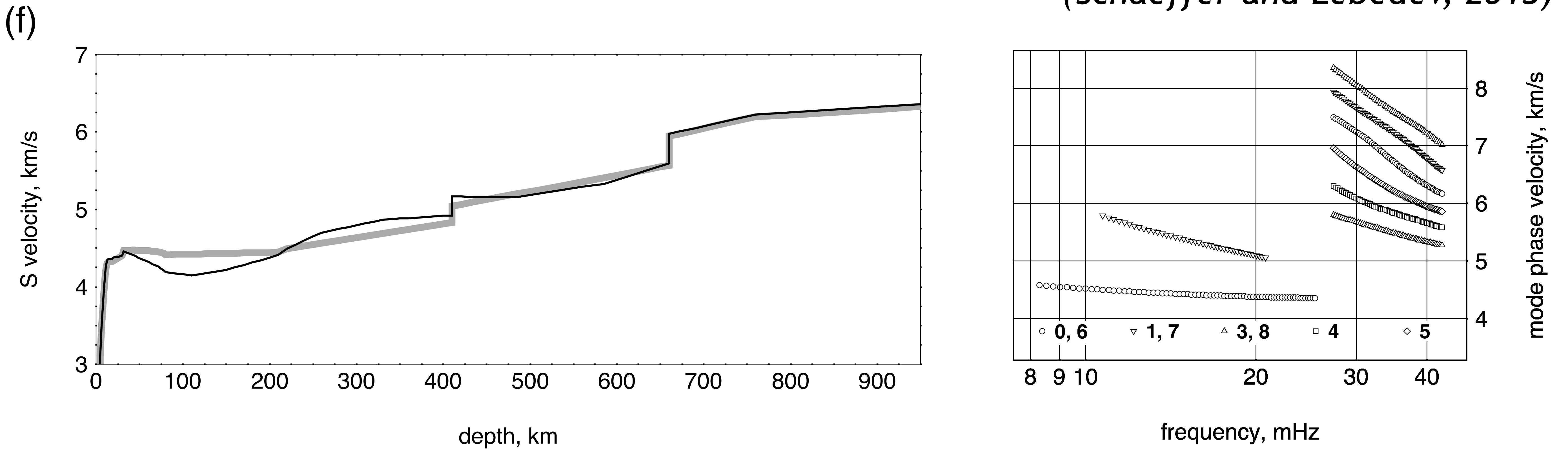

Methodology: outlier analysis

***Two-step partitioned inversion** (Nolet, 1990)*

1. Non-linear waveform fitting
within the JWKB approximation
via Automated Multimode Inversion
(AMI, Lebedev et al., 2005)

2. 3D linear tomography
(Lebedev and van der Hilst, 2008; Schaeffer and Lebedev, 2013)

Estimation of dV_{SH}, dV_{SV}, dV_P perturbations with respect to a reference model, and of V_{SH} and V_{SV} azimuthal anisotropy *(Smith & Dahlen, 1973; Montagner & Nataf, 1986)* on a 350-km grid and 18 predefined depths.

Regularisation (damping, horizontal and vertical smoothing) in terms of isotropic average perturbation and radial anisotropy:

$$dV_{S0} = (dV_{SH} + dV_{SV}) / 2$$

$$\delta = V_{SH} - V_{SV}$$

Reference model: modified AK135 + Crust2
(Kennett et al., 1995; Bassin et al., 2000)

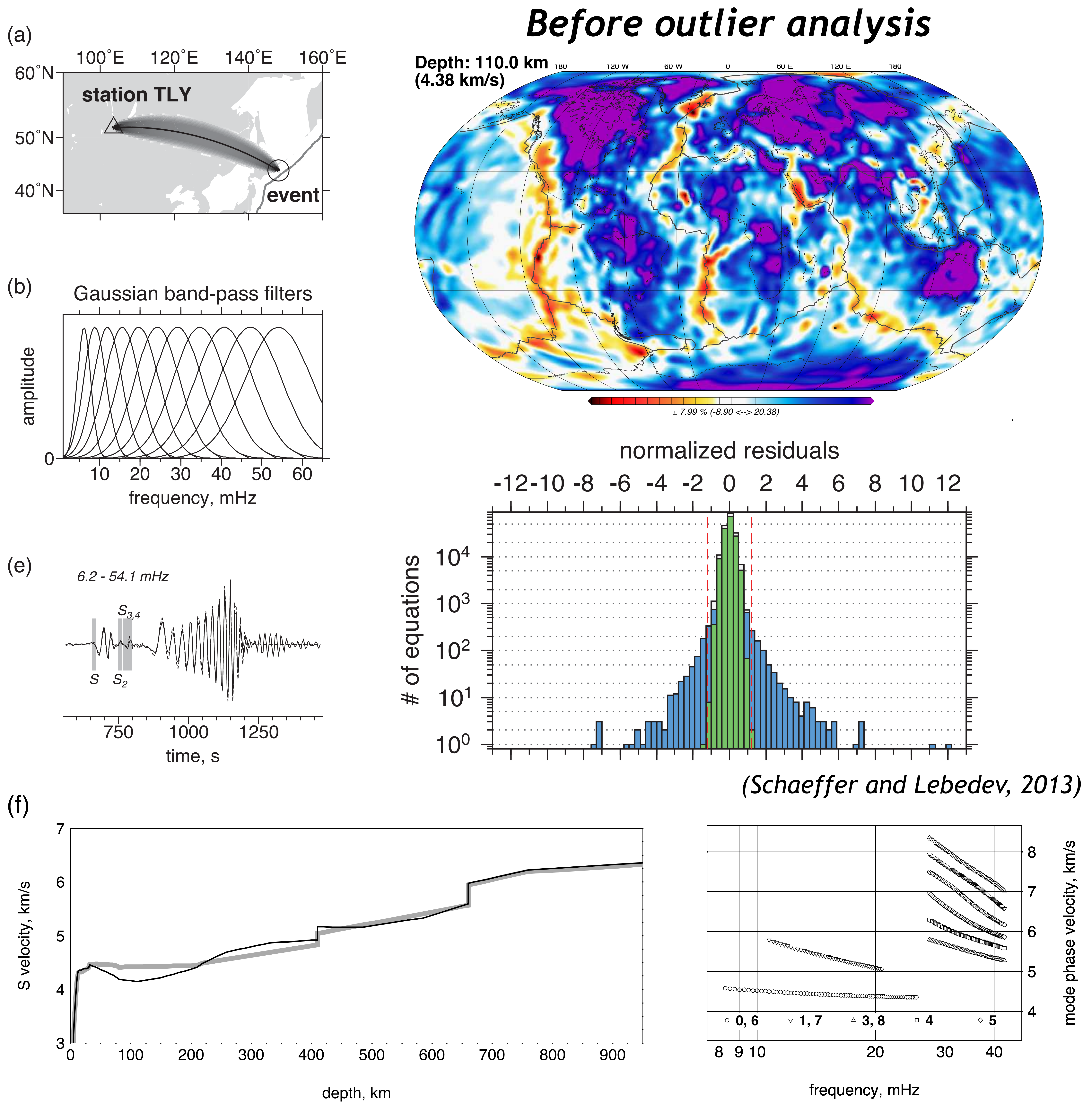

(Schaeffer and Lebedev, 2013)

Methodology: outlier analysis

Two-step partitioned inversion *(Nolet, 1990)*

1. **Non-linear waveform fitting**
   within the JWKB approximation
   via Automated Multimode Inversion
   (AMI, Lebedev et al., 2005)

2. **3D linear tomography**
   (Lebedev and van der Hilst, 2008; Schaeffer and Lebedev, 2013)

   Estimation of dV_{SH}, dV_{SV}, dV_P perturbations with respect to a reference model, and of V_{SH} and V_{SV} azimuthal anisotropy *(Smith & Dahlen, 1973; Montagner & Nataf, 1986)* on a 350-km grid and 18 predefined depths.

   Regularisation (damping, horizontal and vertical smoothing) in terms of isotropic average perturbation and radial anisotropy:

   $$dV_{S0} = (dV_{SH} + dV_{SV}) \;/\; 2$$

   $$\delta = V_{SH} - V_{SV}$$

Reference model: modified AK135 + Crust2
(Kennett et al., 1995; Bassin et al., 2000)

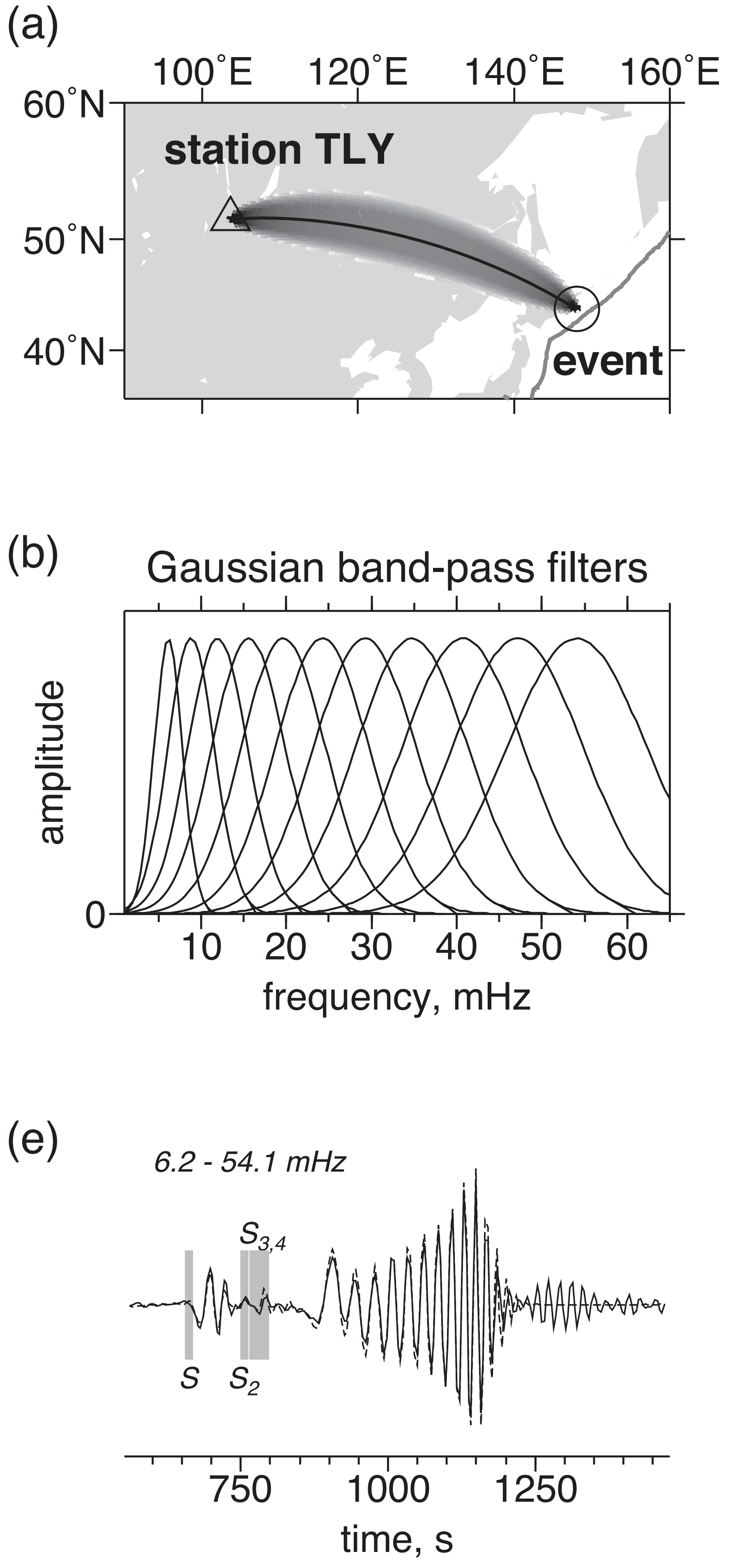

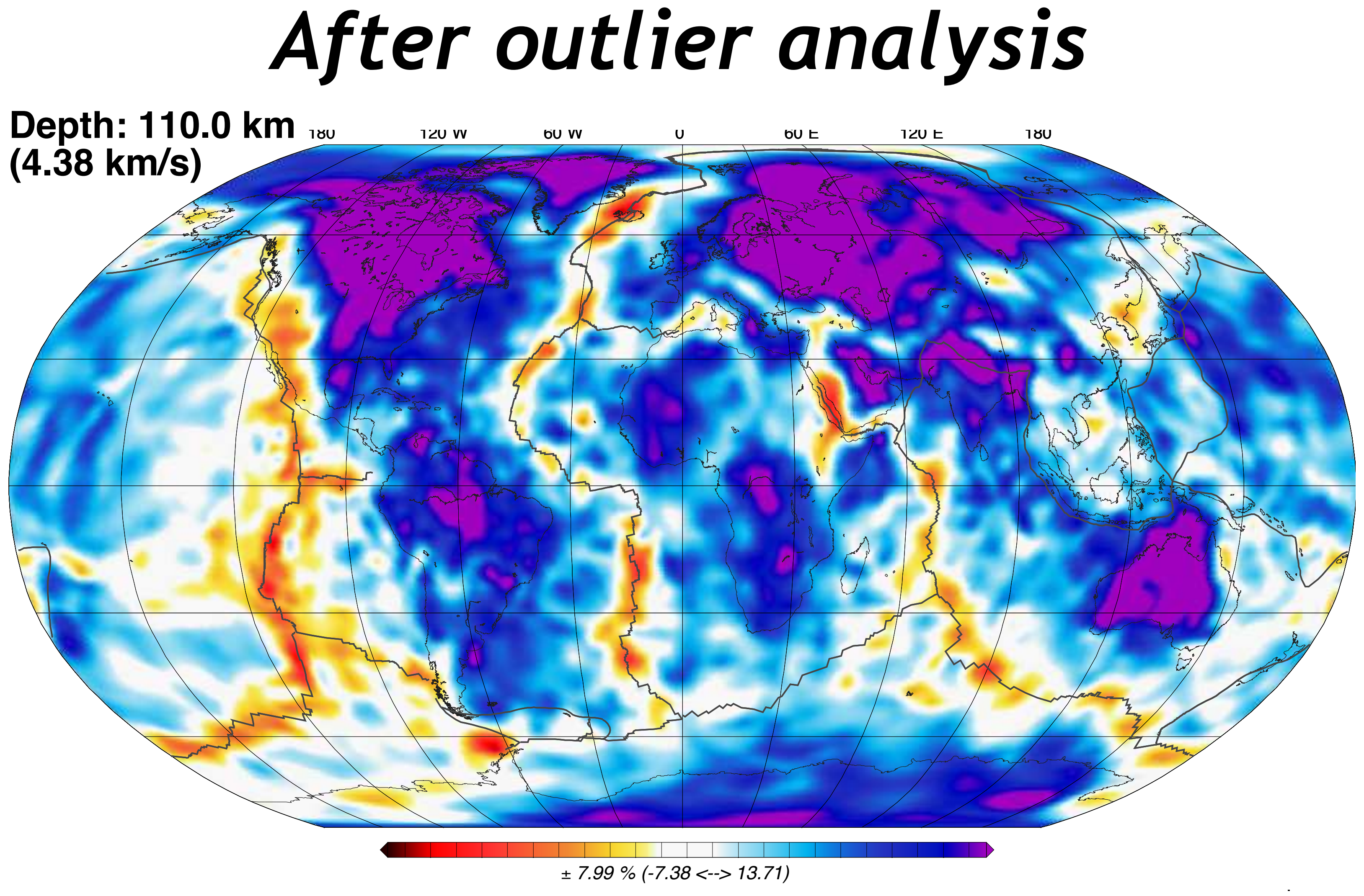

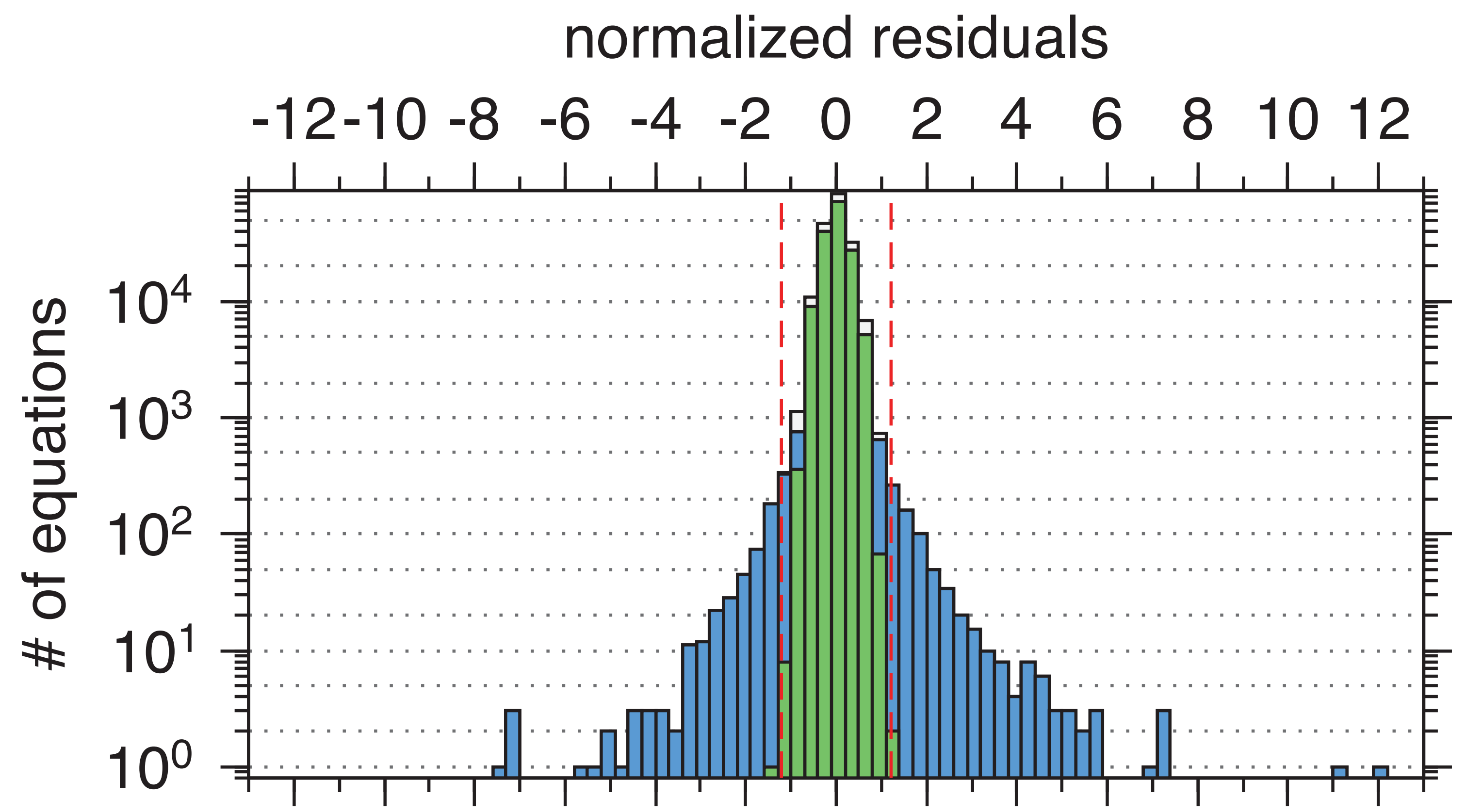

(Schaeffer and Lebedev, 2013)

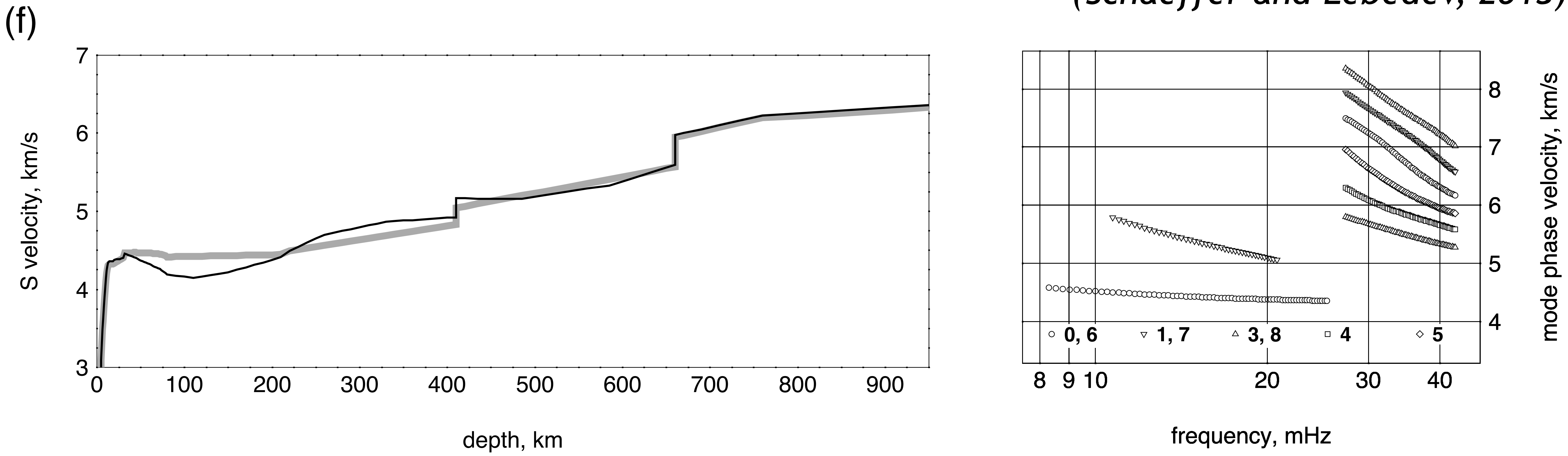

Results at 110 km

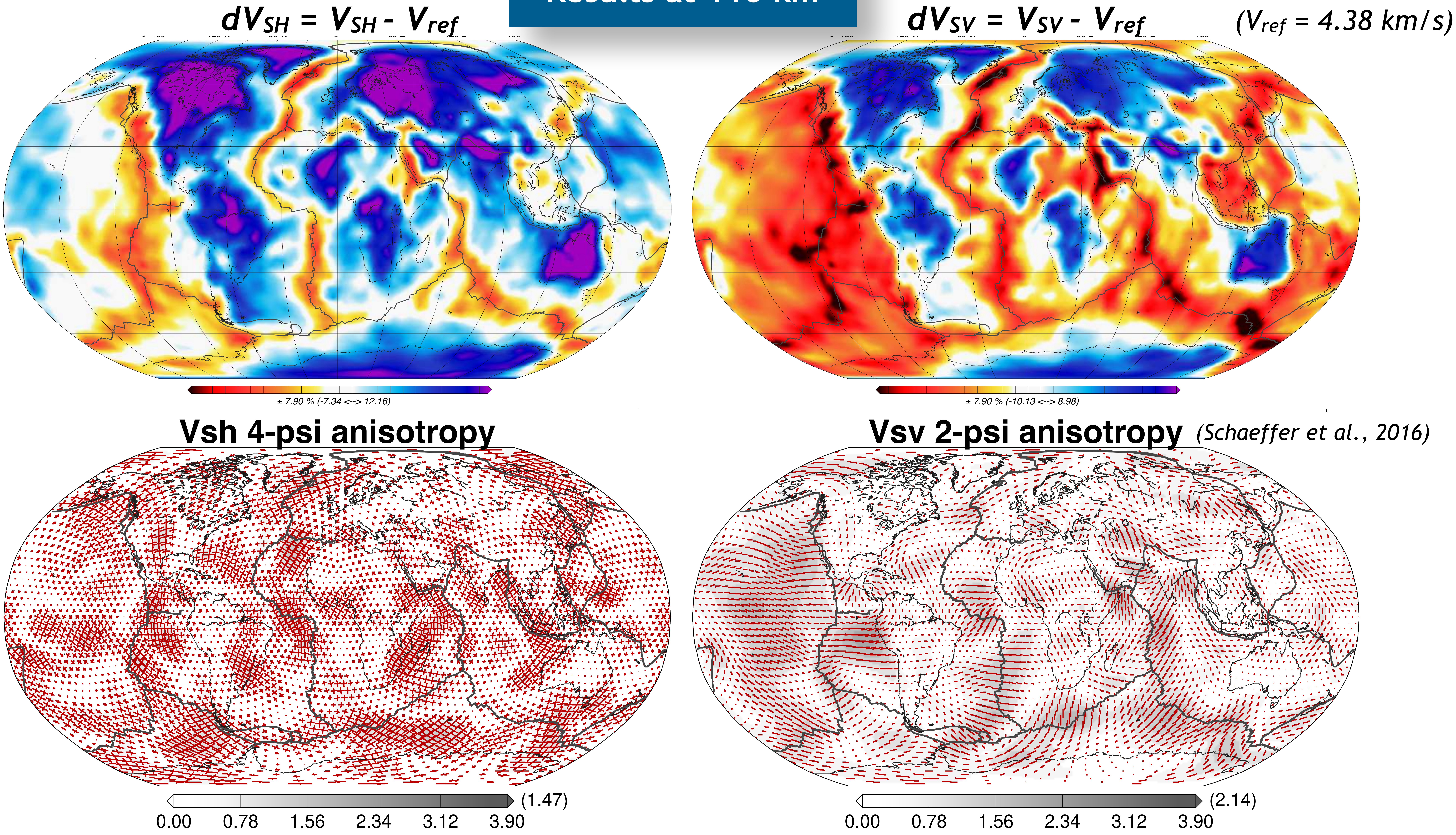

Radially-anisotropic model (V_{S0}, δ) at 36 km depth (template for next slides)

Isotropic average perturbation (dV_{S0})

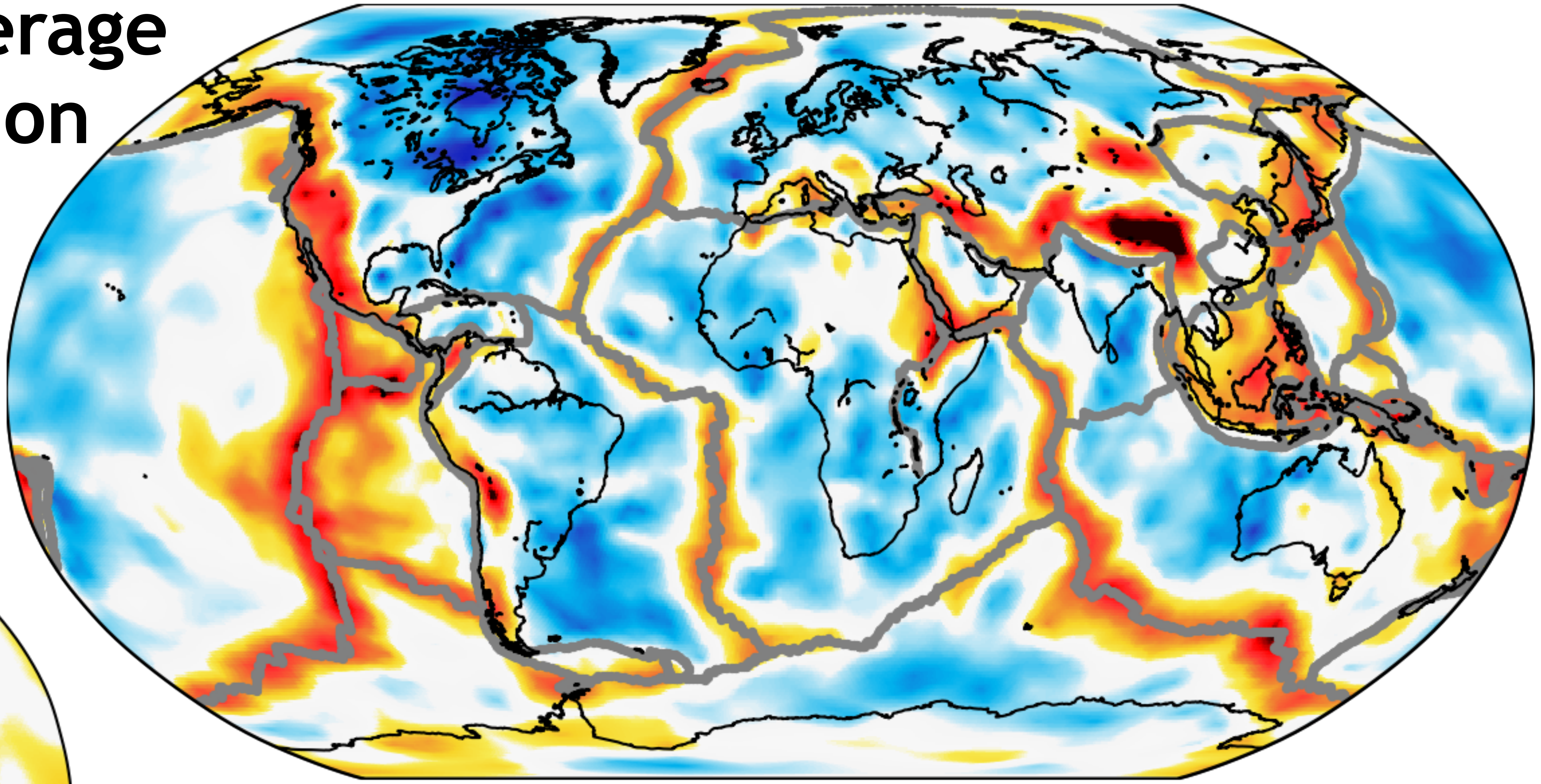

Full, relative, radial anisotropy (in %):

$\delta_r = (V_{SH} - V_{SV}) / V_{ref}$

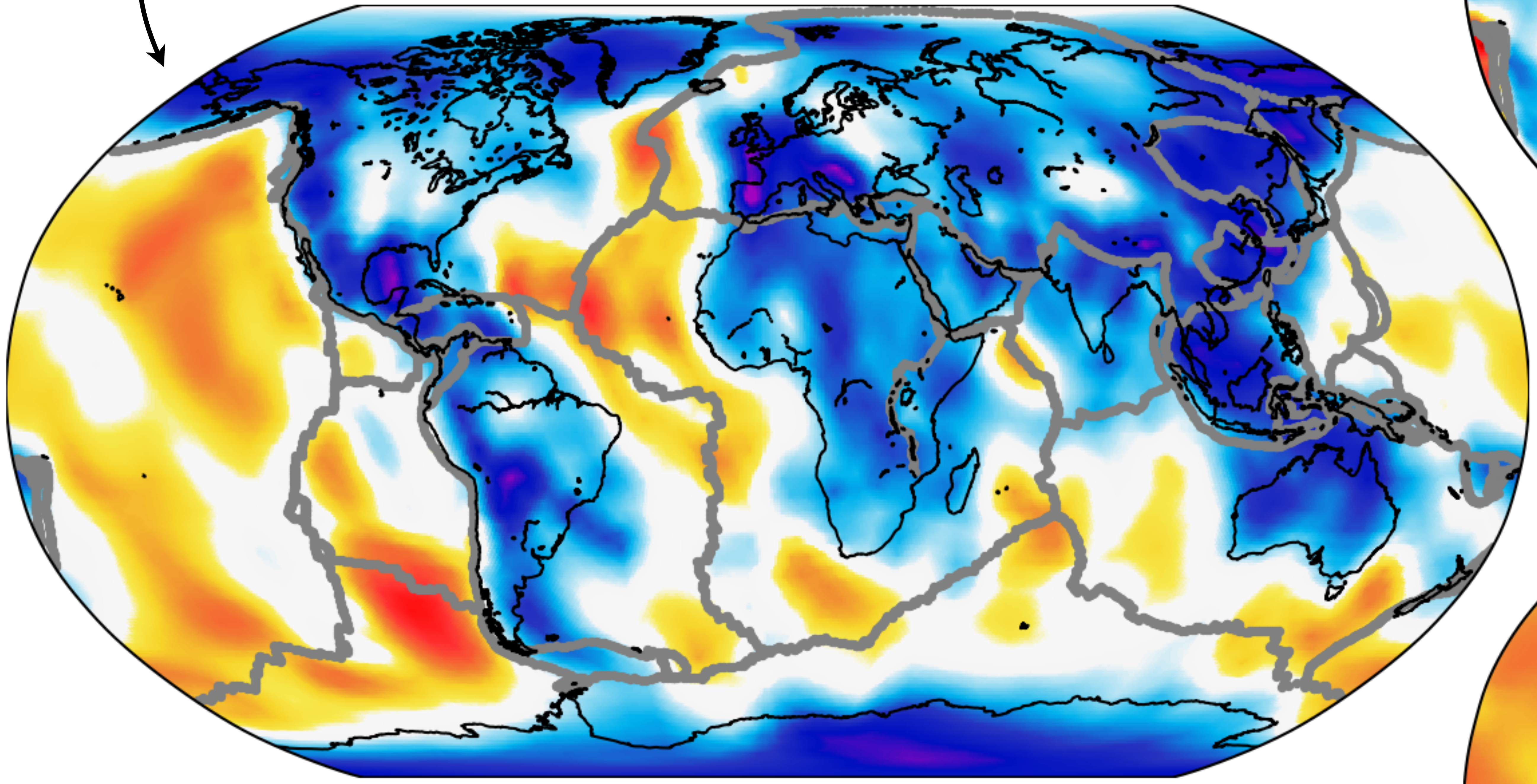

Anisotropy variations *wrt* depth average: $\delta_r - \delta_r^{avg.36km}$

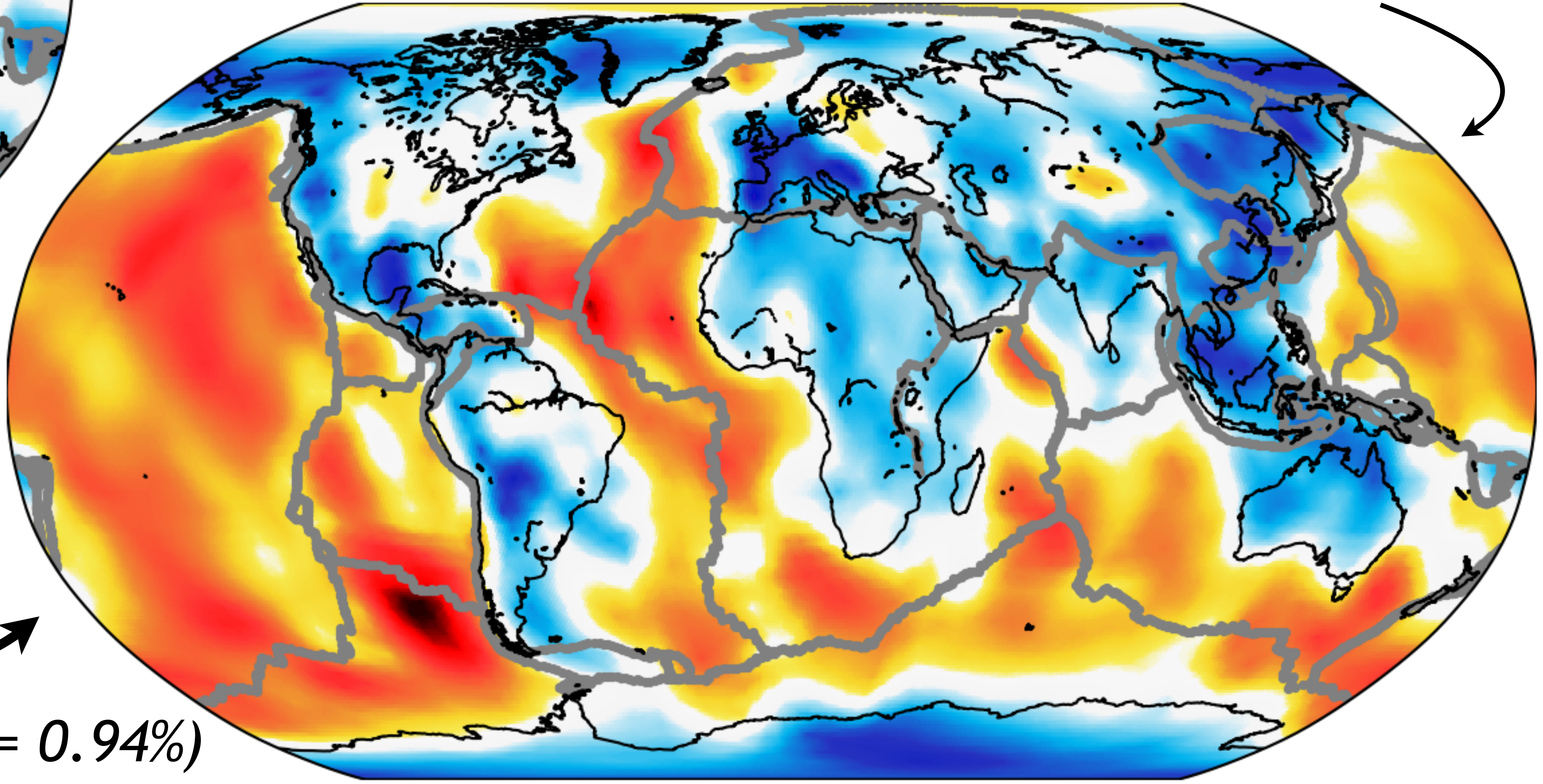

Anisotropy ($V_{SH} - V_{SV}$)

(-avg $\delta_r^{avg.36km} = 0.94\%$)

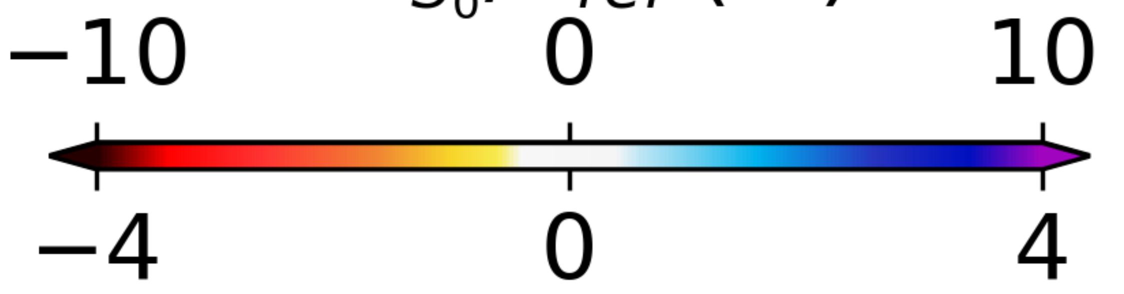

(V_{ref} = 4.32 km/s at 36 km depth)

V_{S0}, δ at 36 km

Note the difference in anisotropy between oceans and continents.

Isotropic average (dV_{S0})

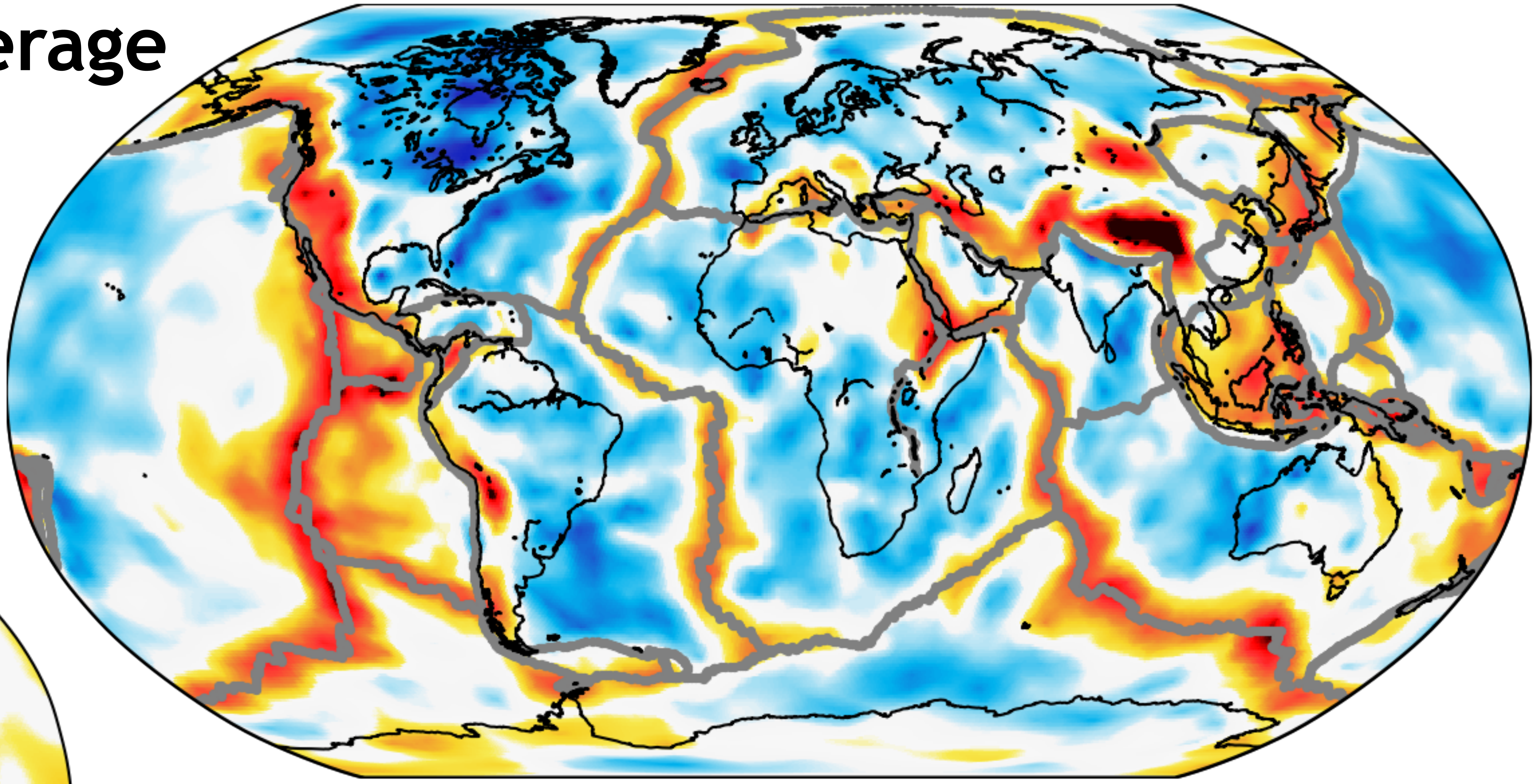

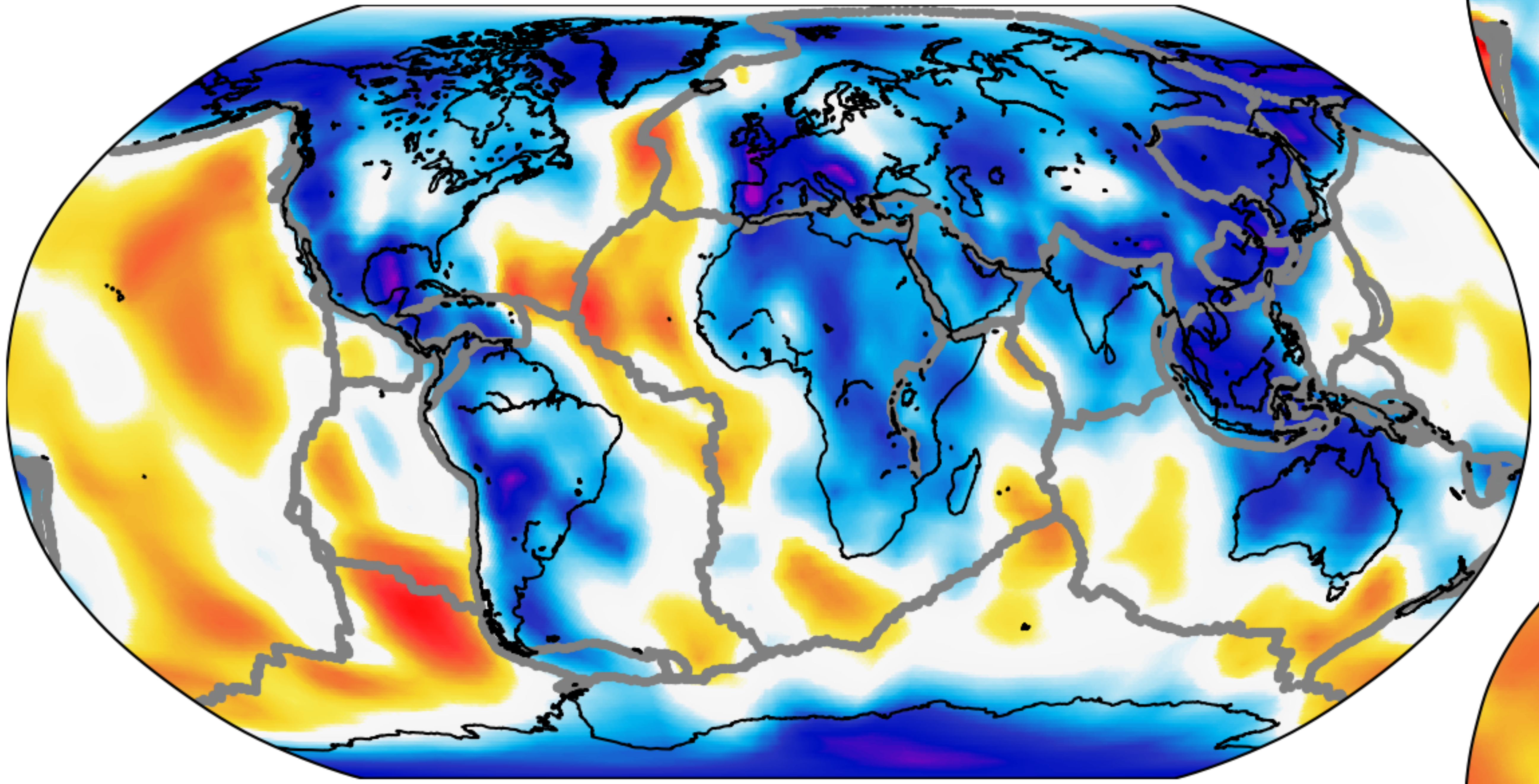

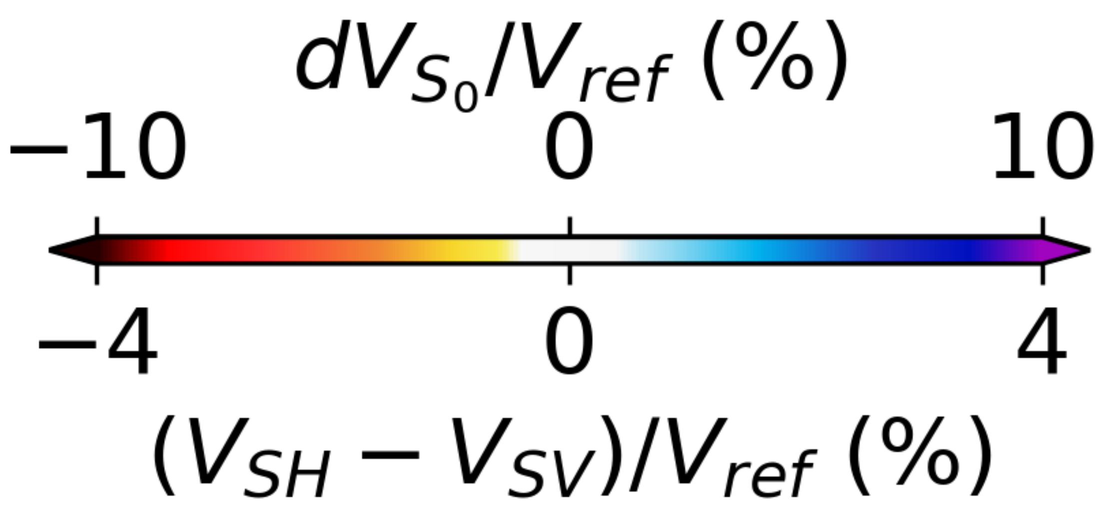

(V_{ref} = 4.32 km/s)

Anisotropy (V_{SH} - V_{SV})

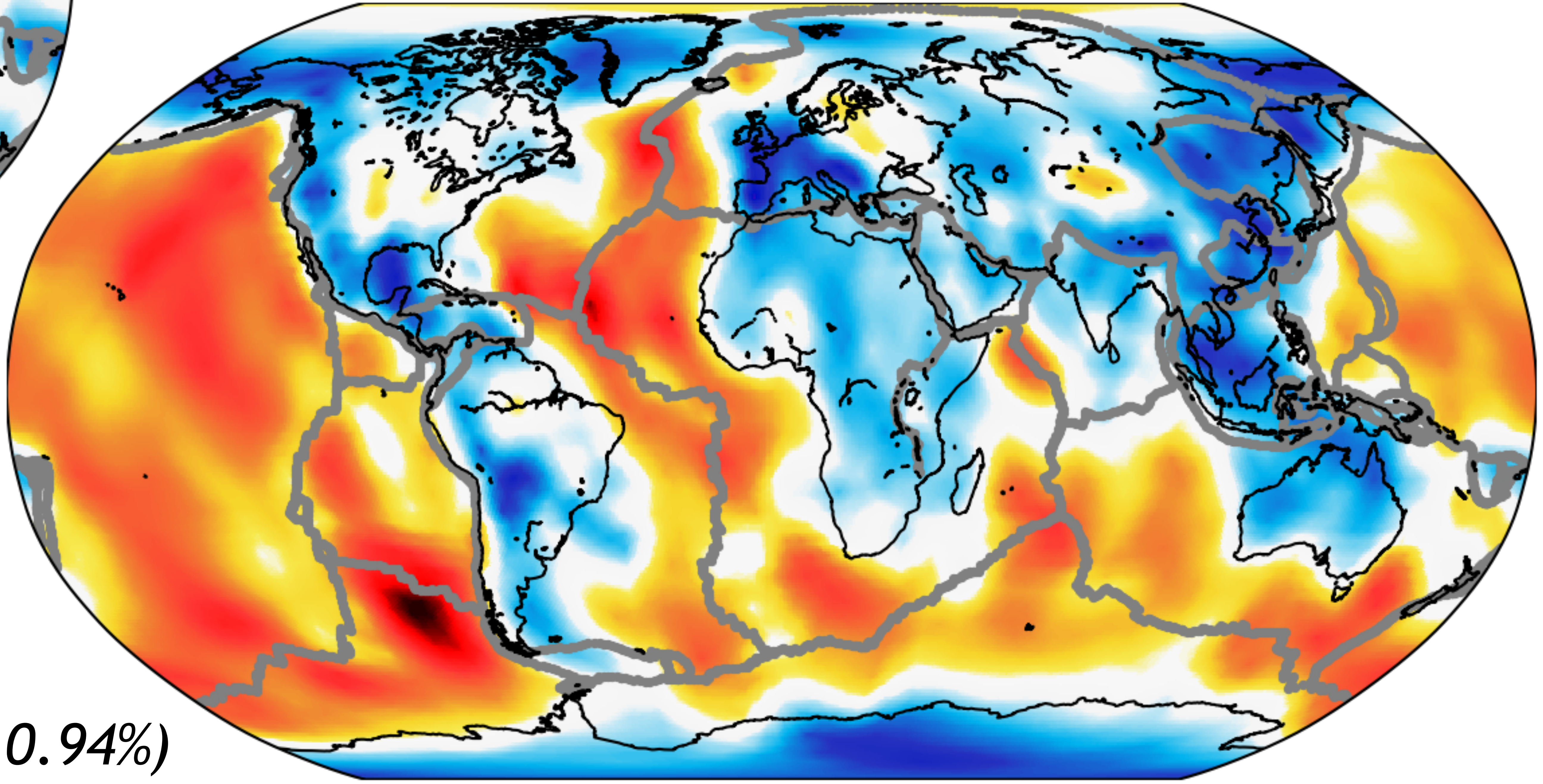

(-avg 0.94%)

V_{S0}, δ at 56 km

Isotropic average (dV_{S0})

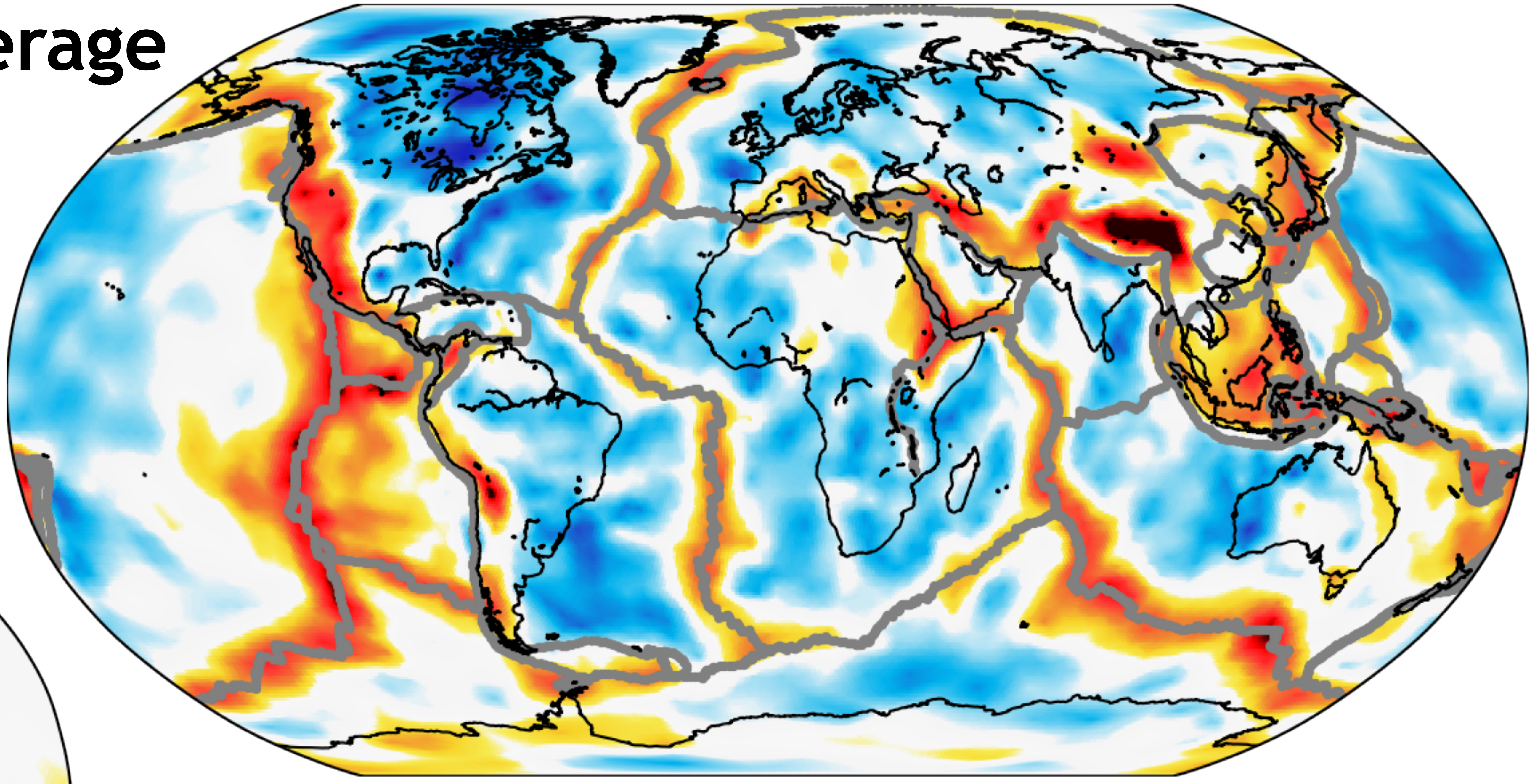

Note the difference in anisotropy between oceans and continents, and the strong positive anomalies under thick orogens.

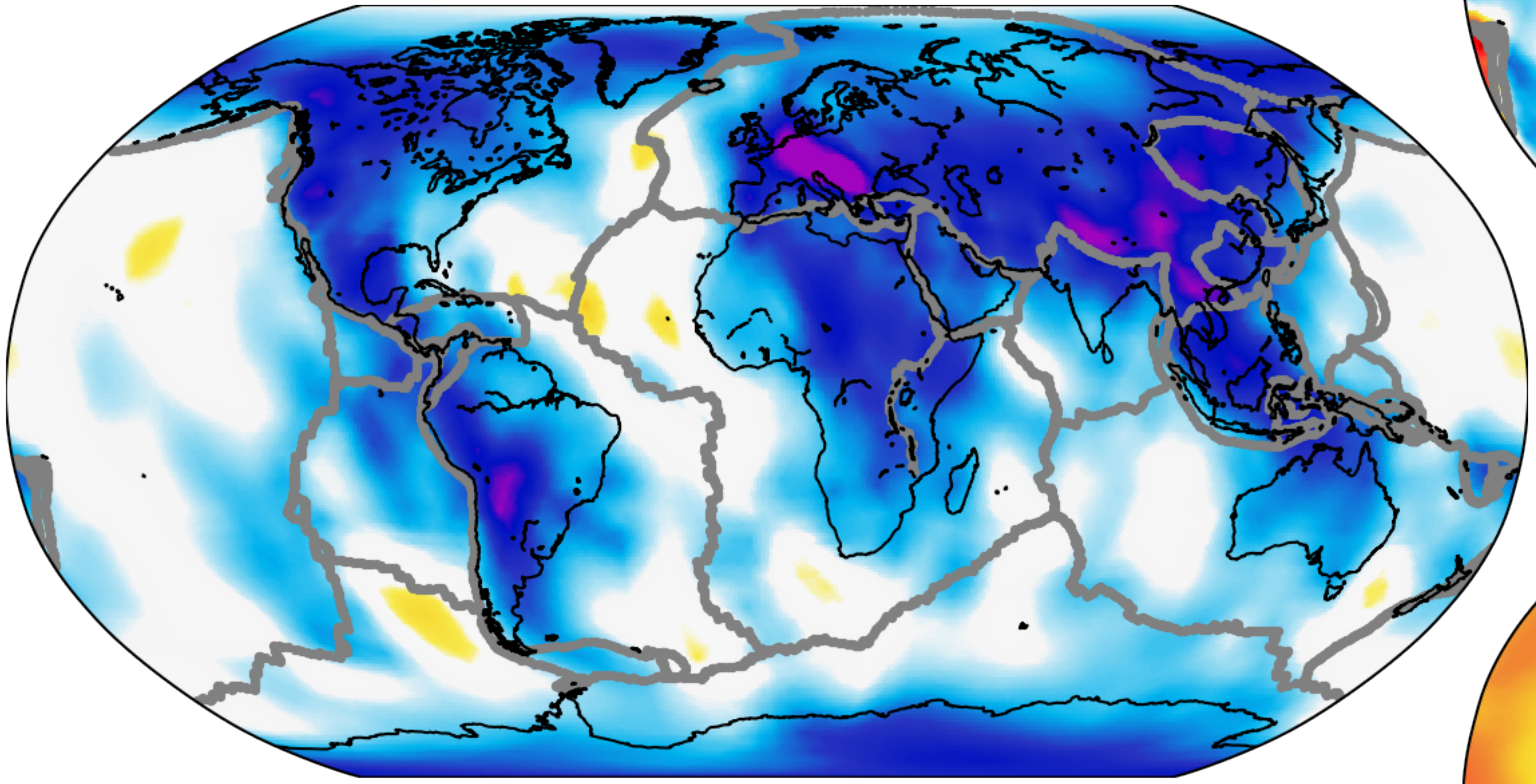

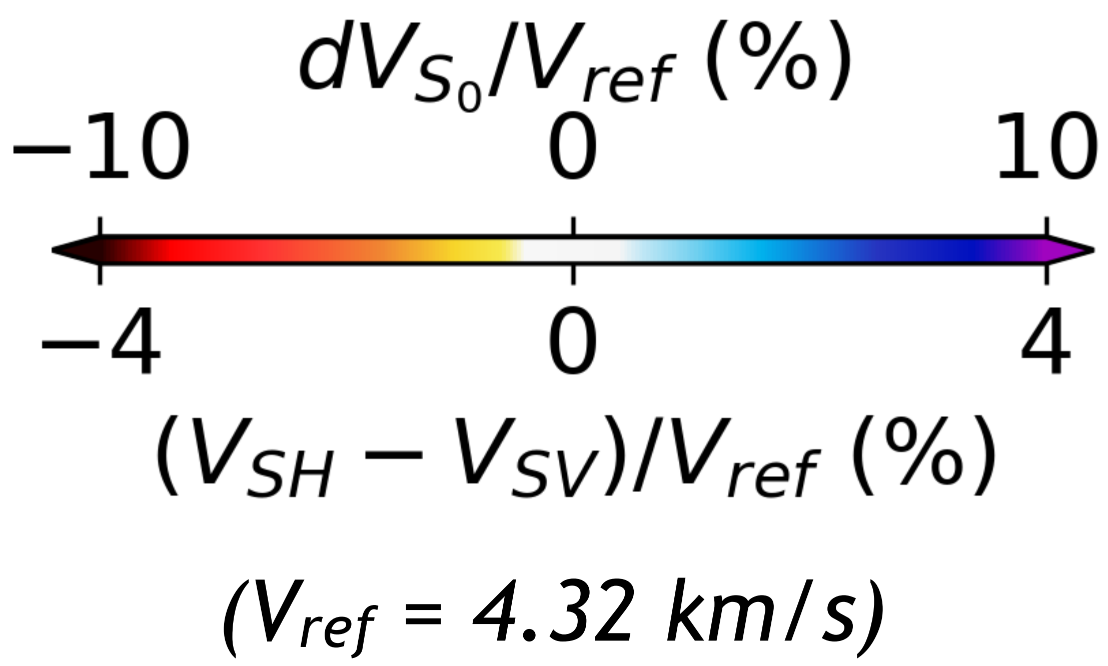

Anisotropy (V_{SH} - V_{SV})

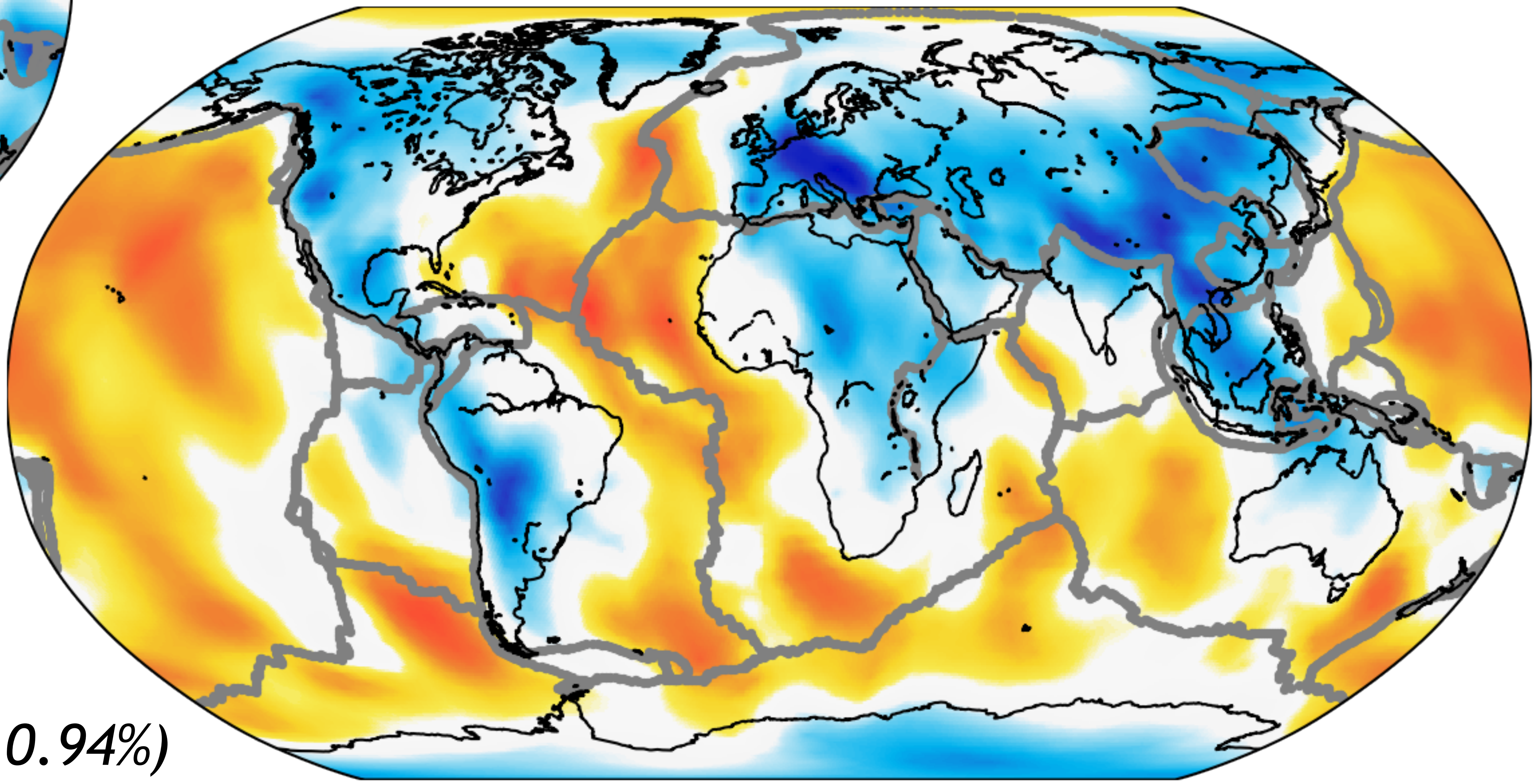

(-avg 0.94%)

V_{S0}, δ at 80 km

Isotropic average (dV_{S0})

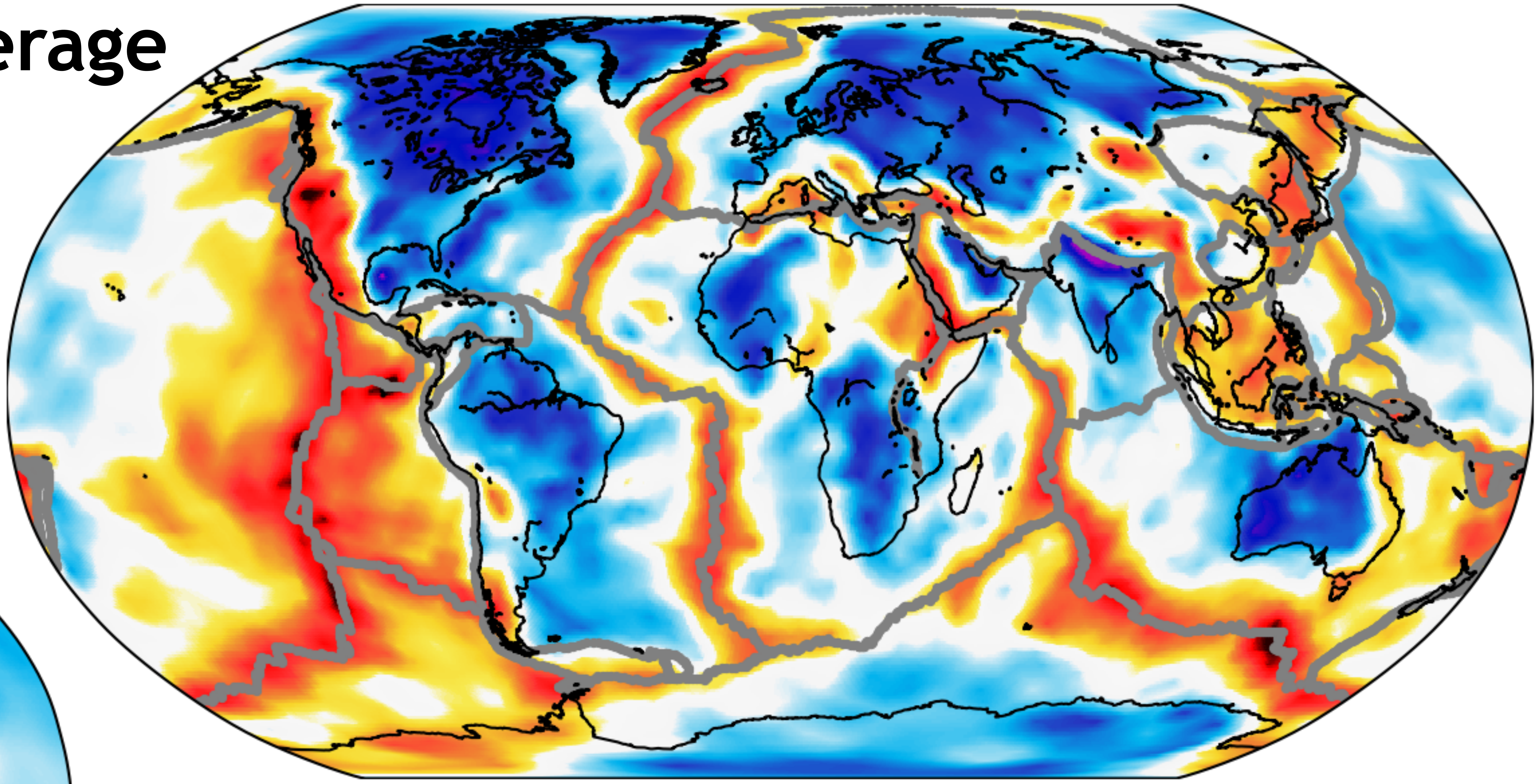

Global trend to positive anisotropy ($V_{SH} > V_{SV}$), consistent with horizontal shear under the lithosphere.

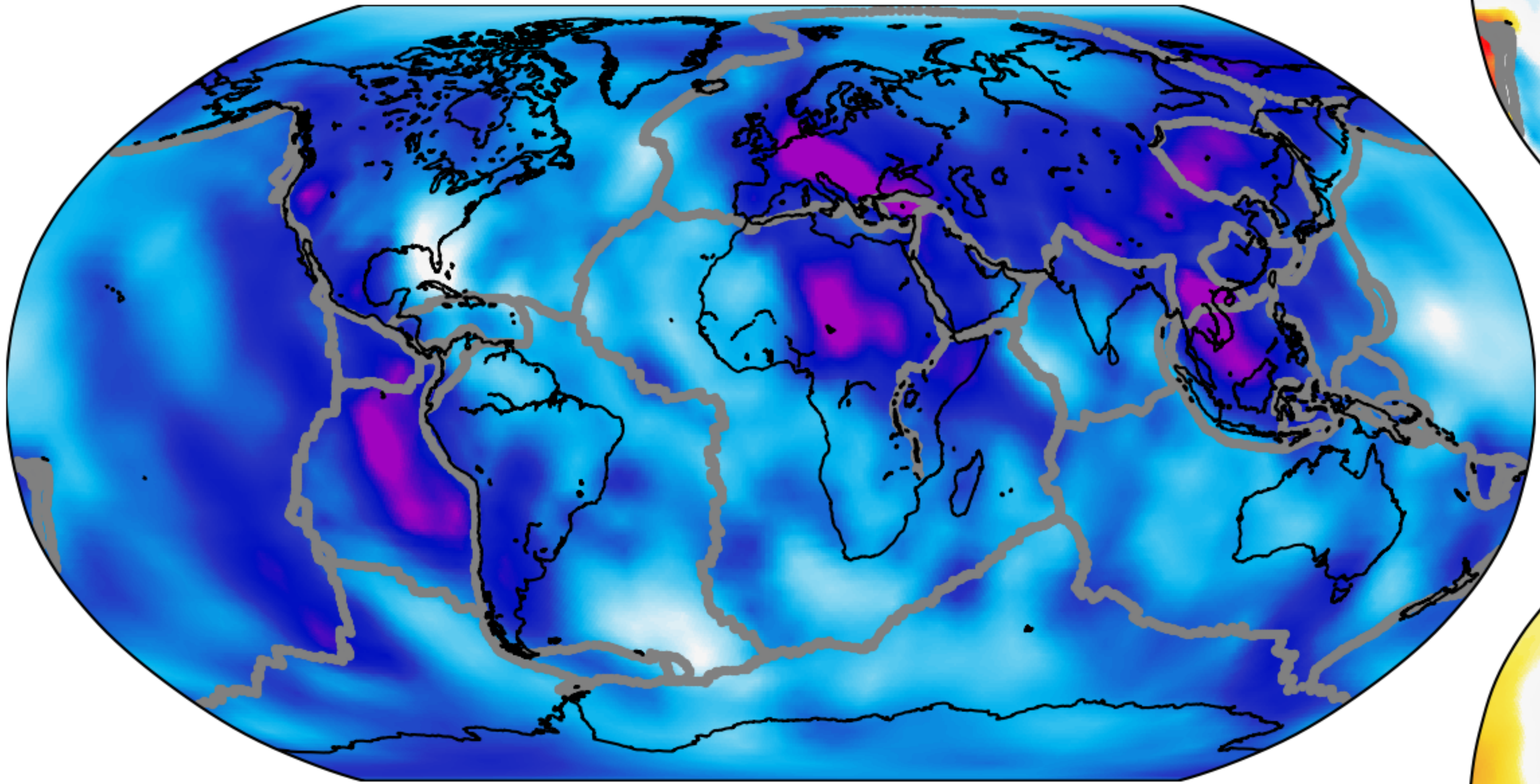

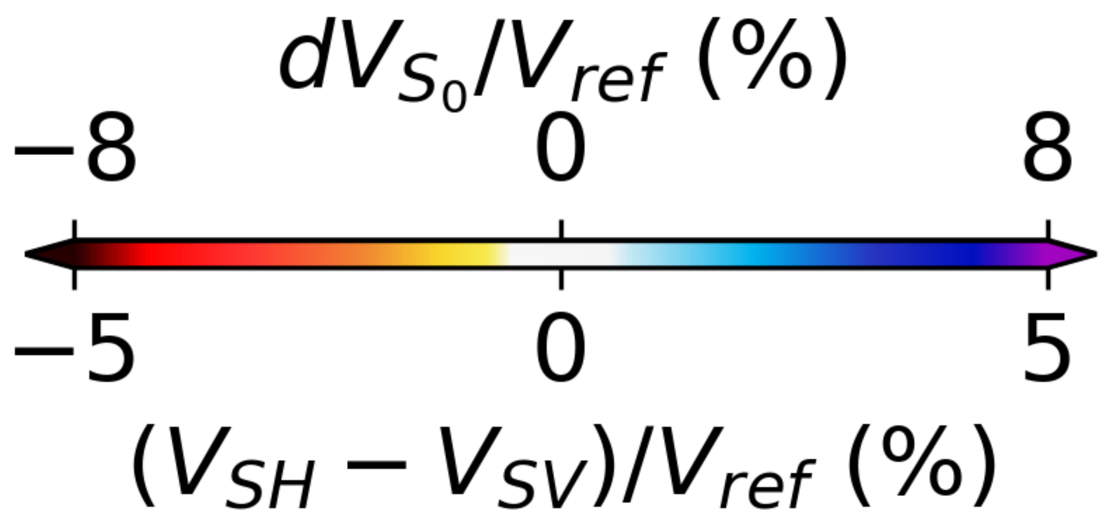

(V_{ref} = 4.43 km/s)

Anisotropy (V_{SH} - V_{SV})

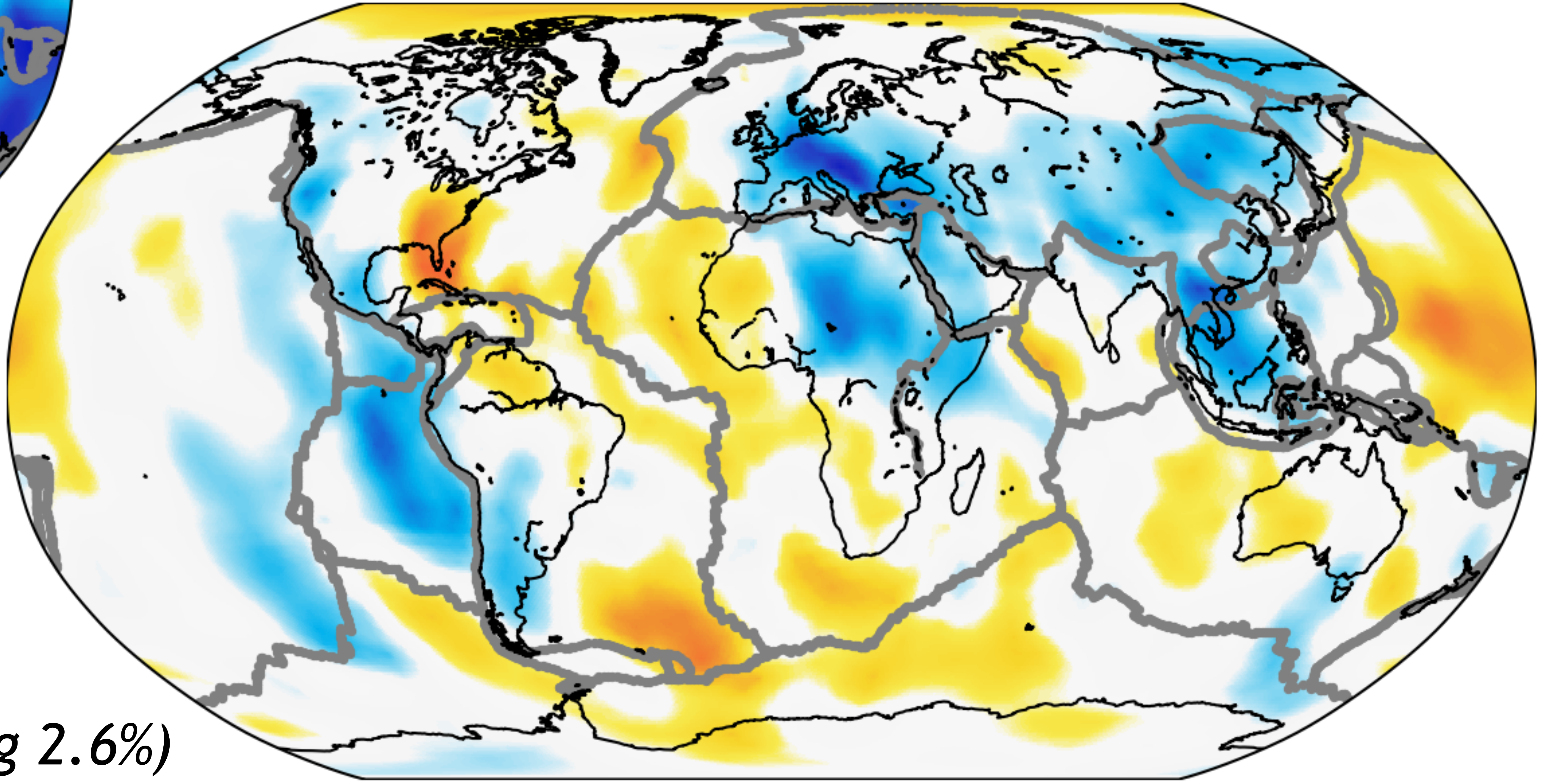

(-avg 2.6%)

V_{S0}, δ at 110 km

Global trend to positive anisotropy ($V_{SH} > V_{SV}$),
consistent with horizontal shear under the lithosphere,
especially under (some) subducting plates (Nazca, Philippines).

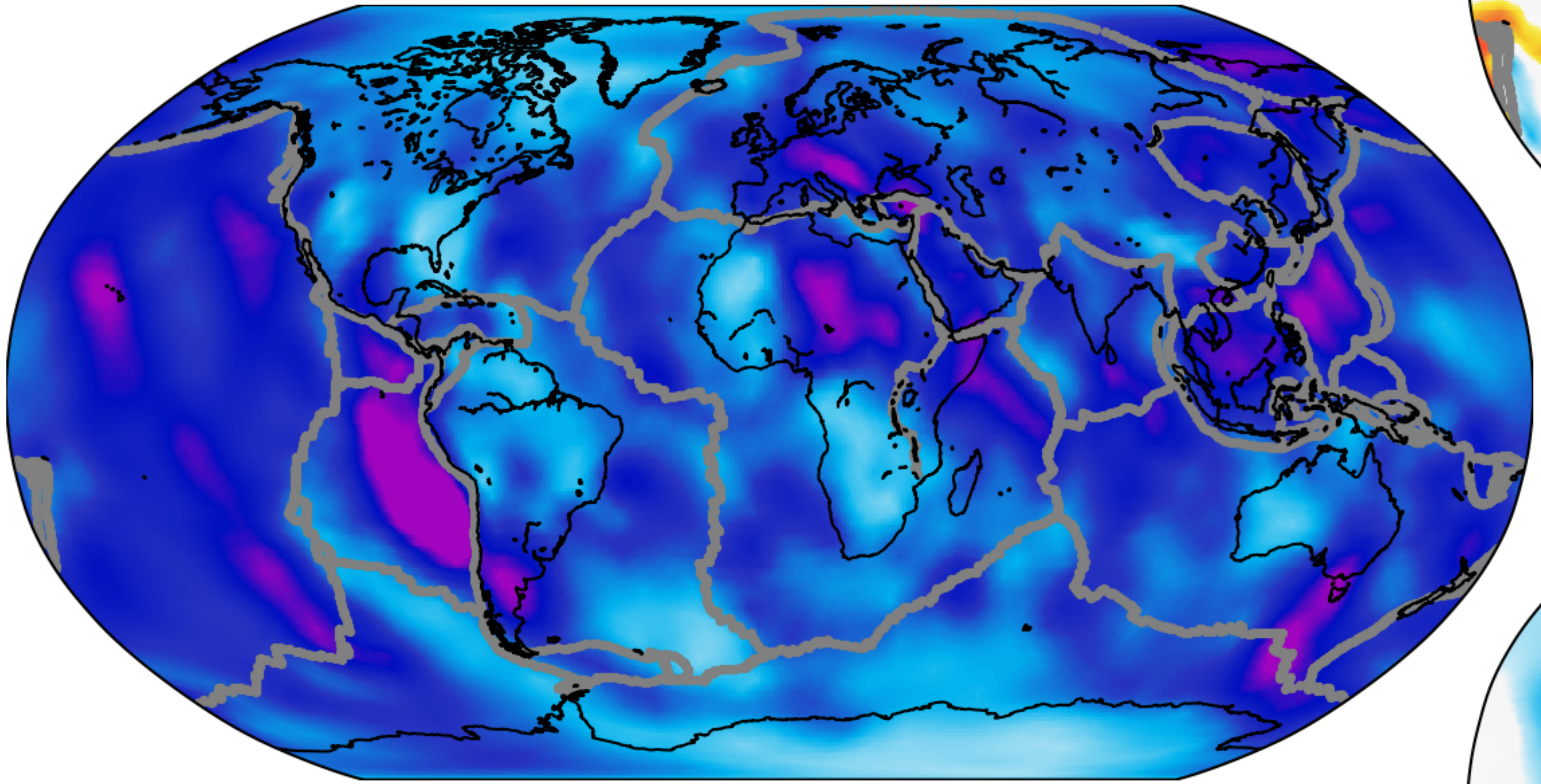

Isotropic average (dV_{S0})

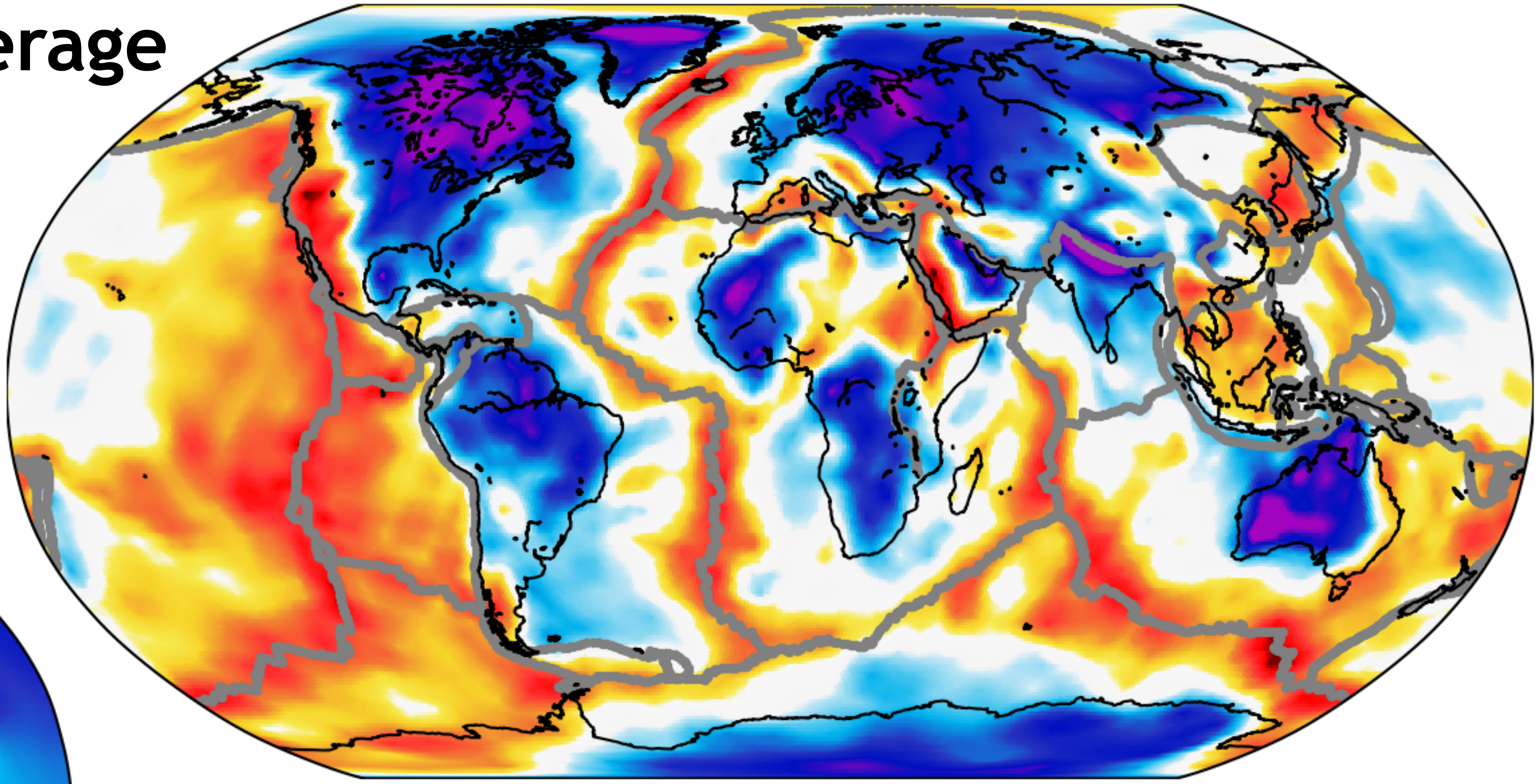

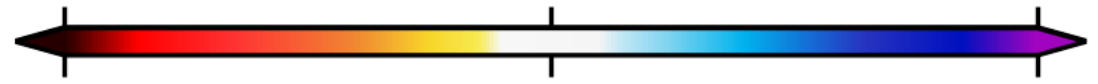

Anisotropy (V_{SH} - V_{SV})

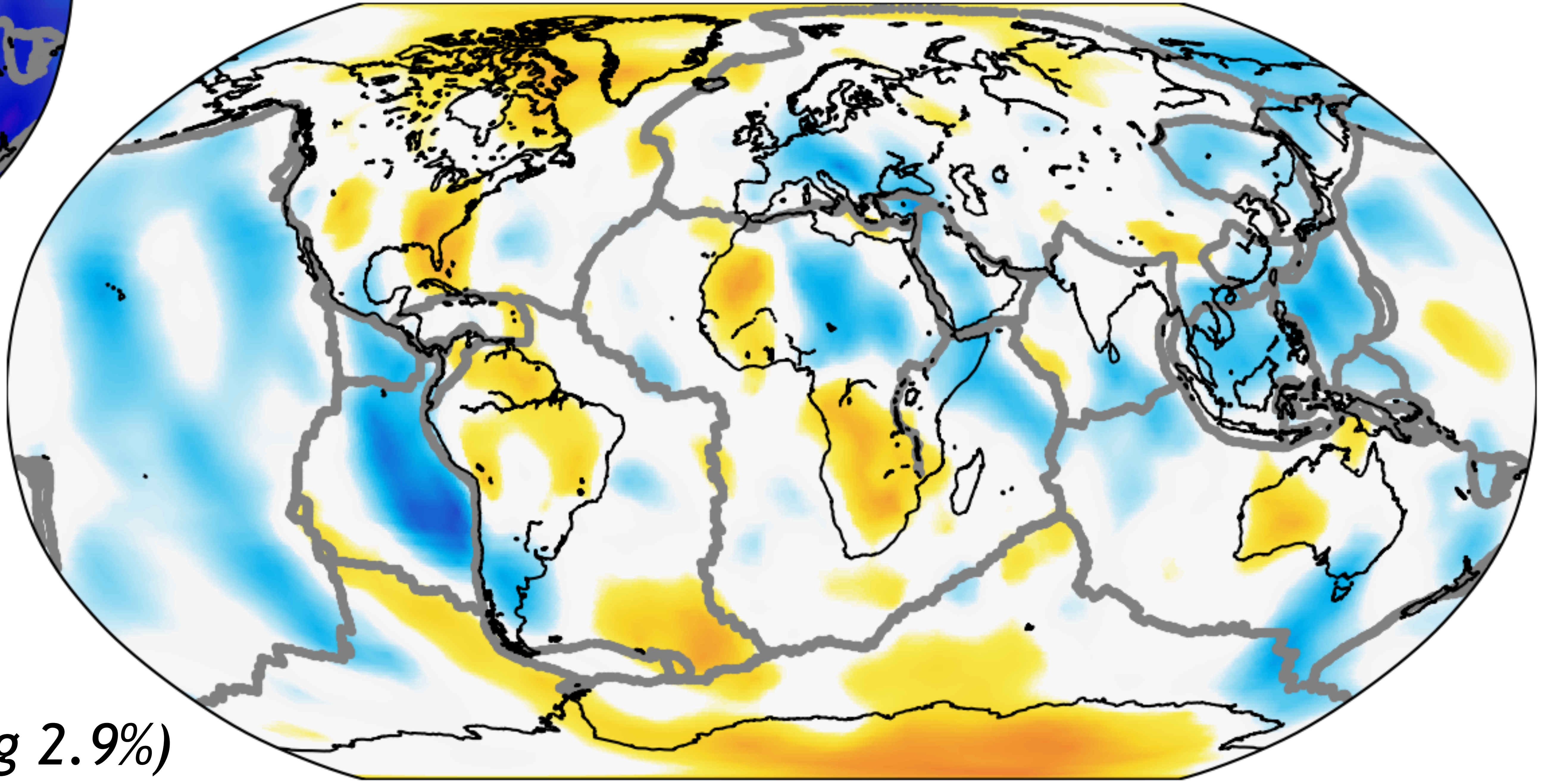

(-avg 2.9%)

V_{S0}, δ at 150 km

Global trend to positive anisotropy ($V_{SH} > V_{SV}$),
consistent with horizontal shear under the lithosphere,
especially under (some) subducting plates (Nazca, Philippines).

Isotropic average (dV_{S0})

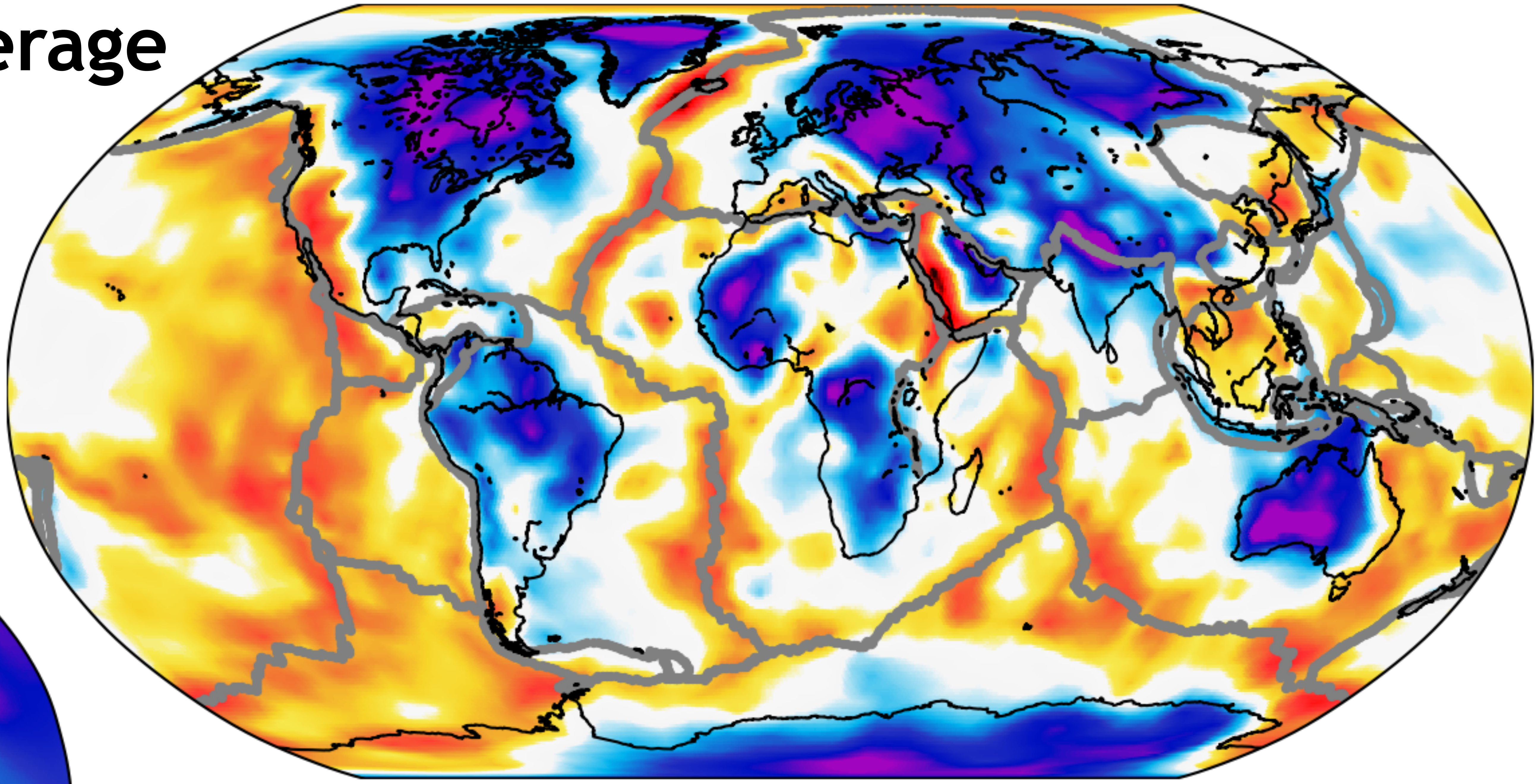

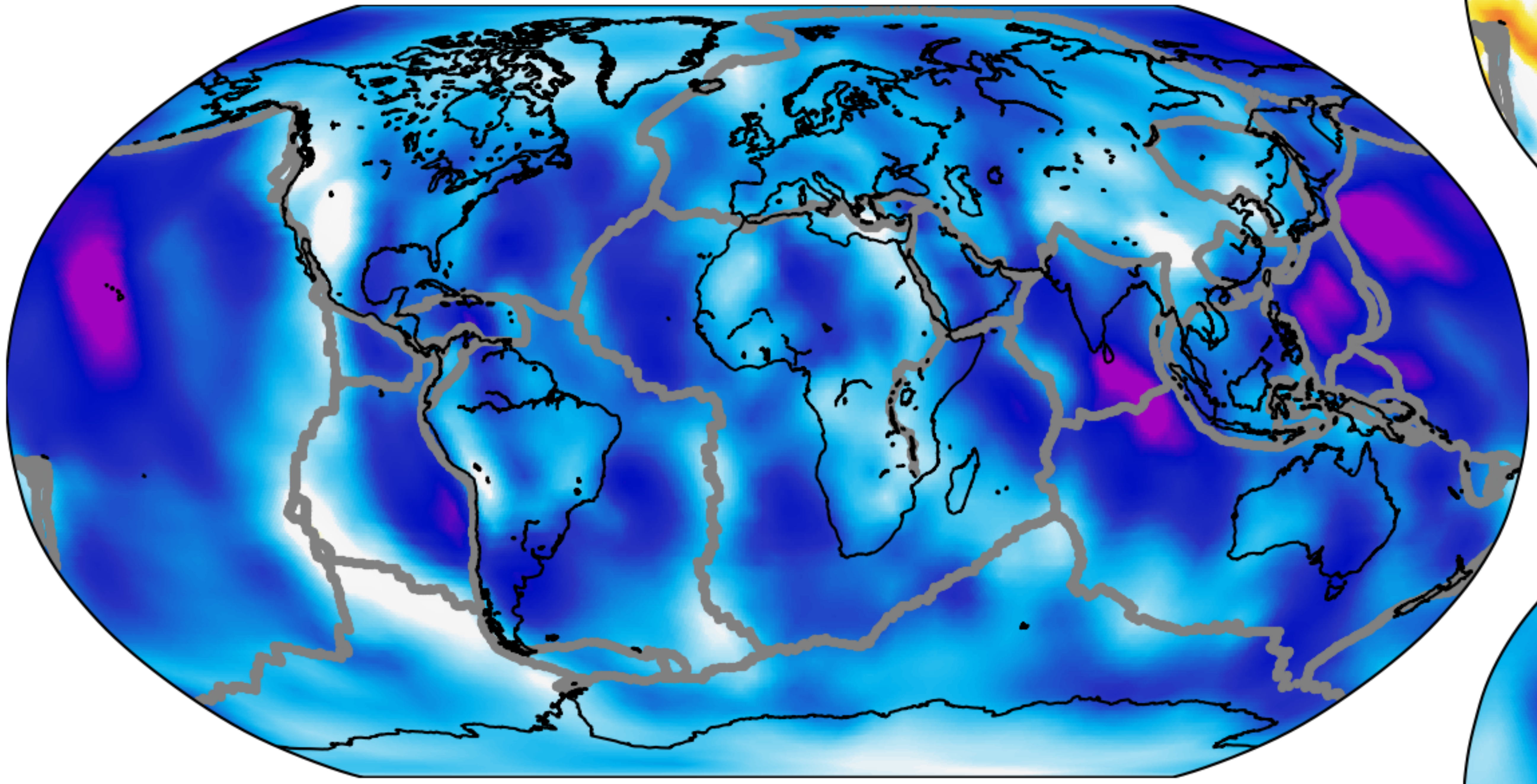

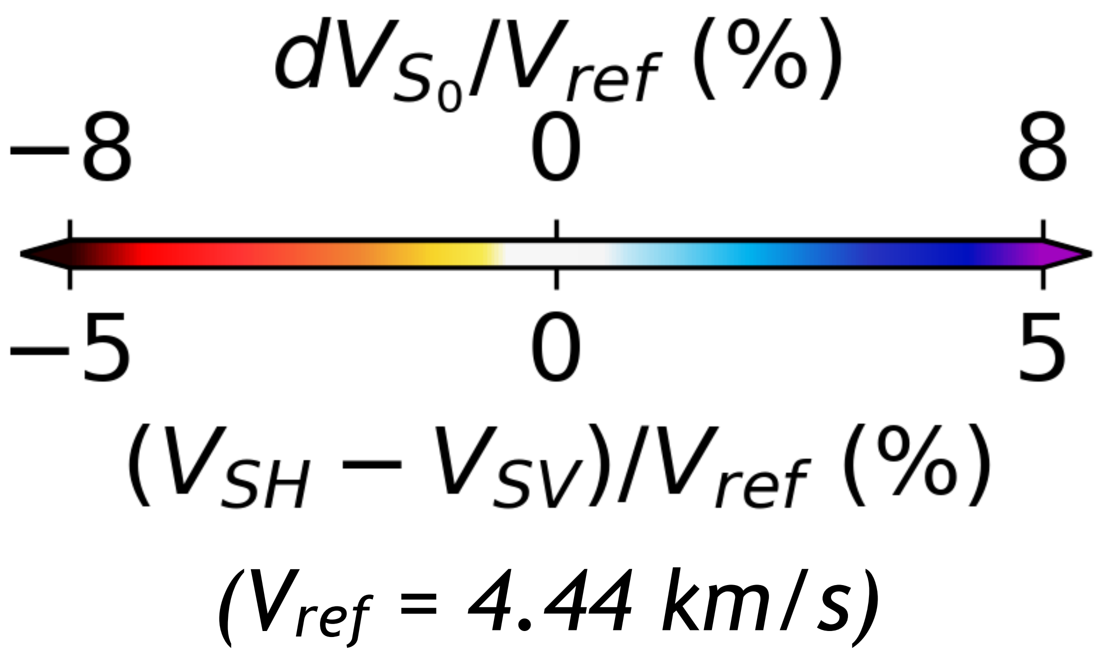

Anisotropy (V_{SH} - V_{SV})

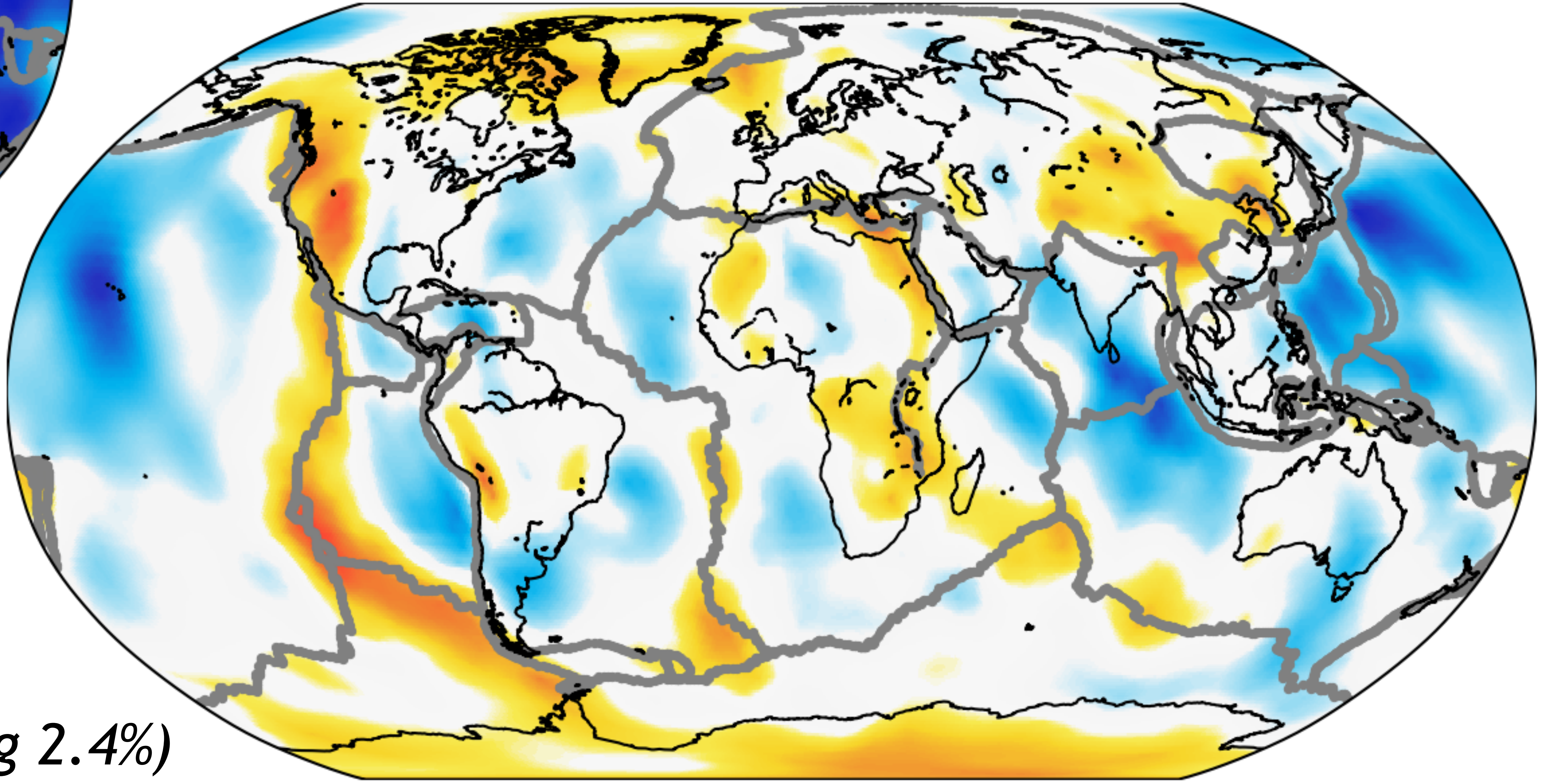

(-avg 2.4%)

V_{S0}, δ at 200 km

Negative anisotropy ($V_{SH} < V_{SV}$) under mid-ocean ridges.

Isotropic average (dV_{S0})

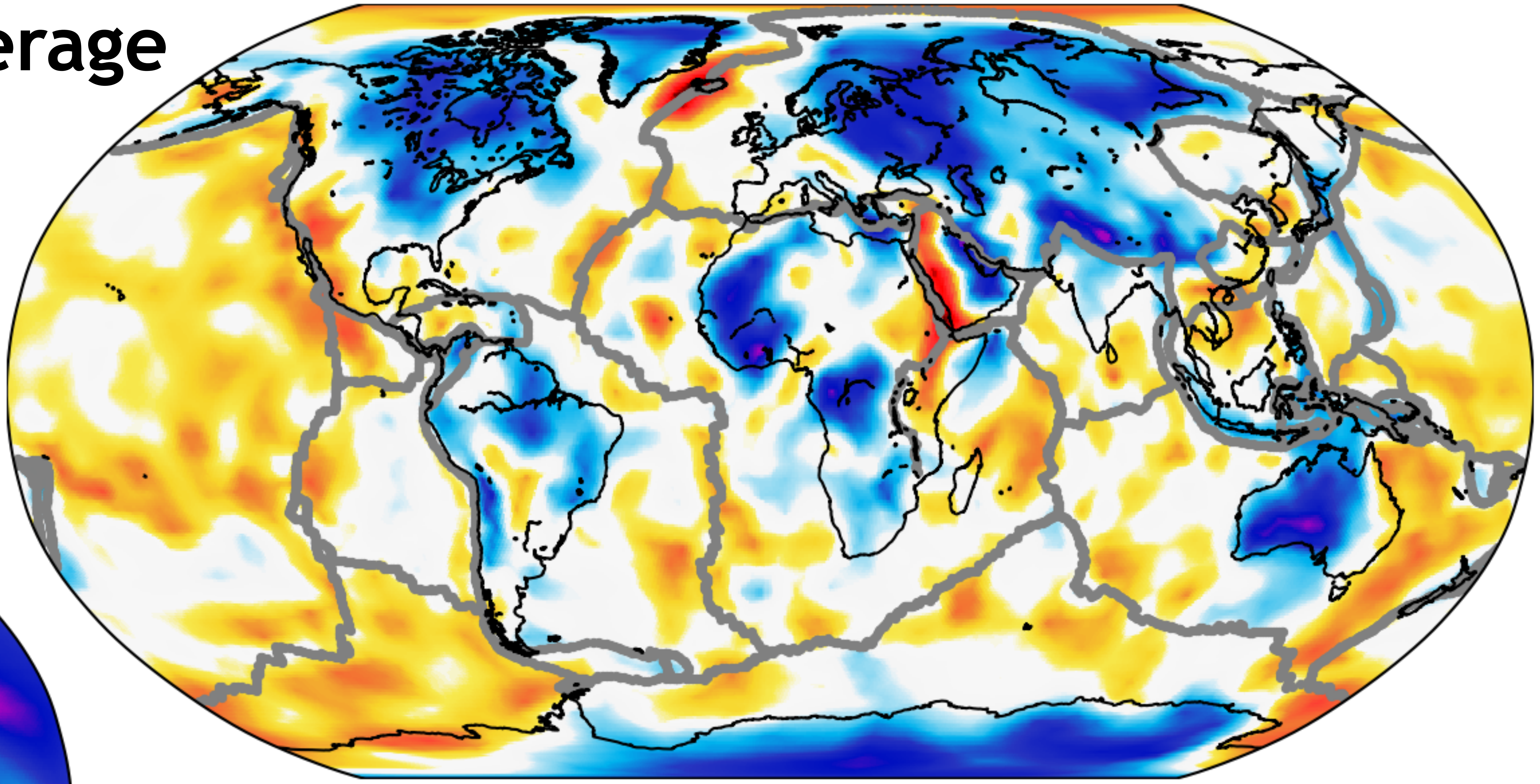

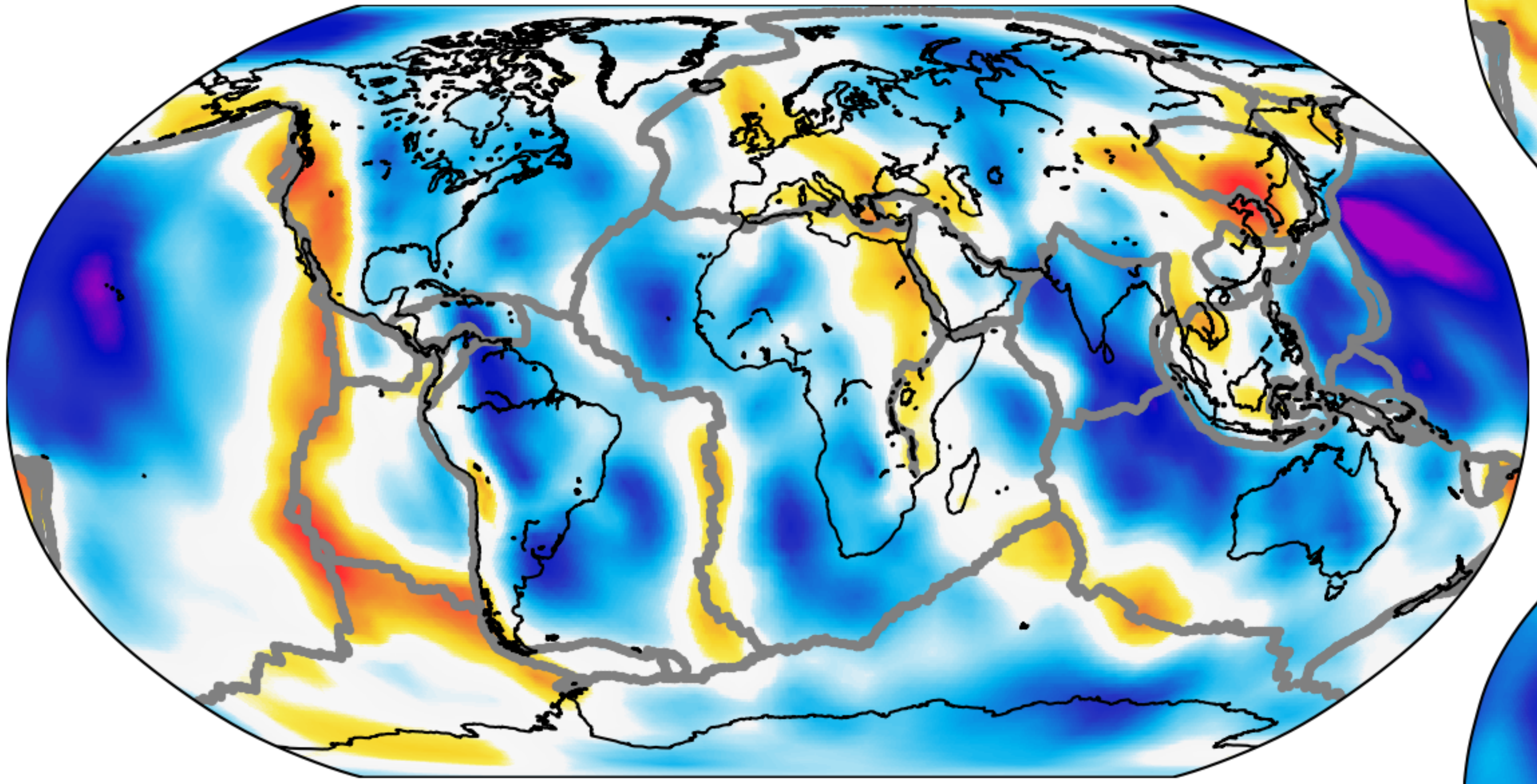

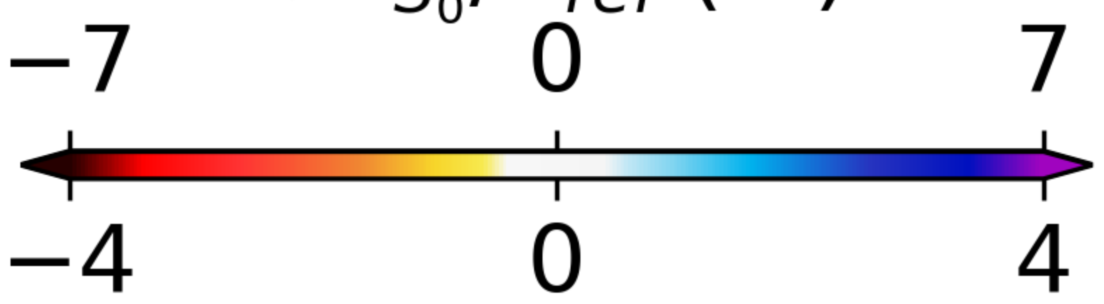

Anisotropy (V_{SH} - V_{SV})

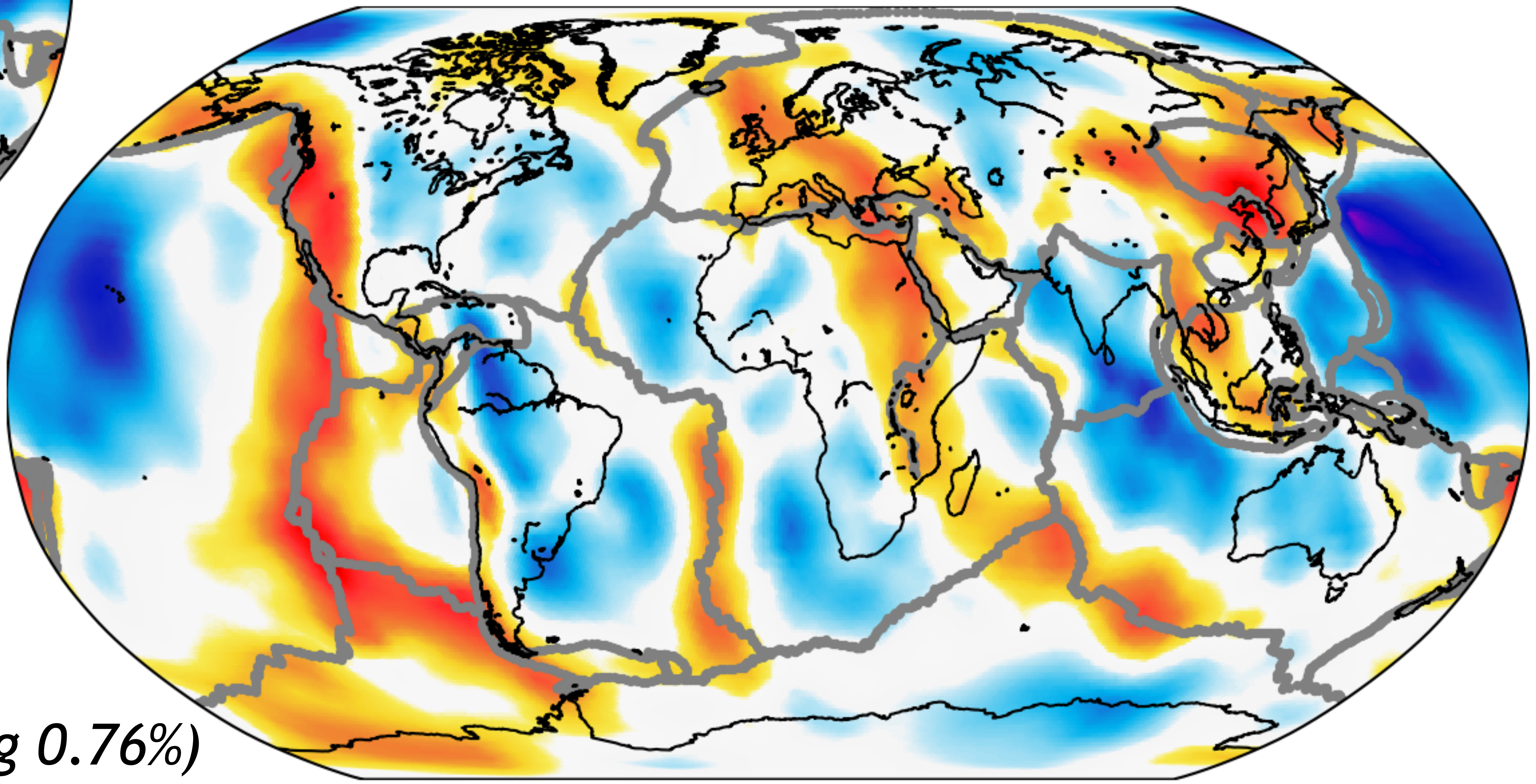

(-avg 0.76%)

V_{S0}, δ at 260 km

Isotropic average (dV_{S0})

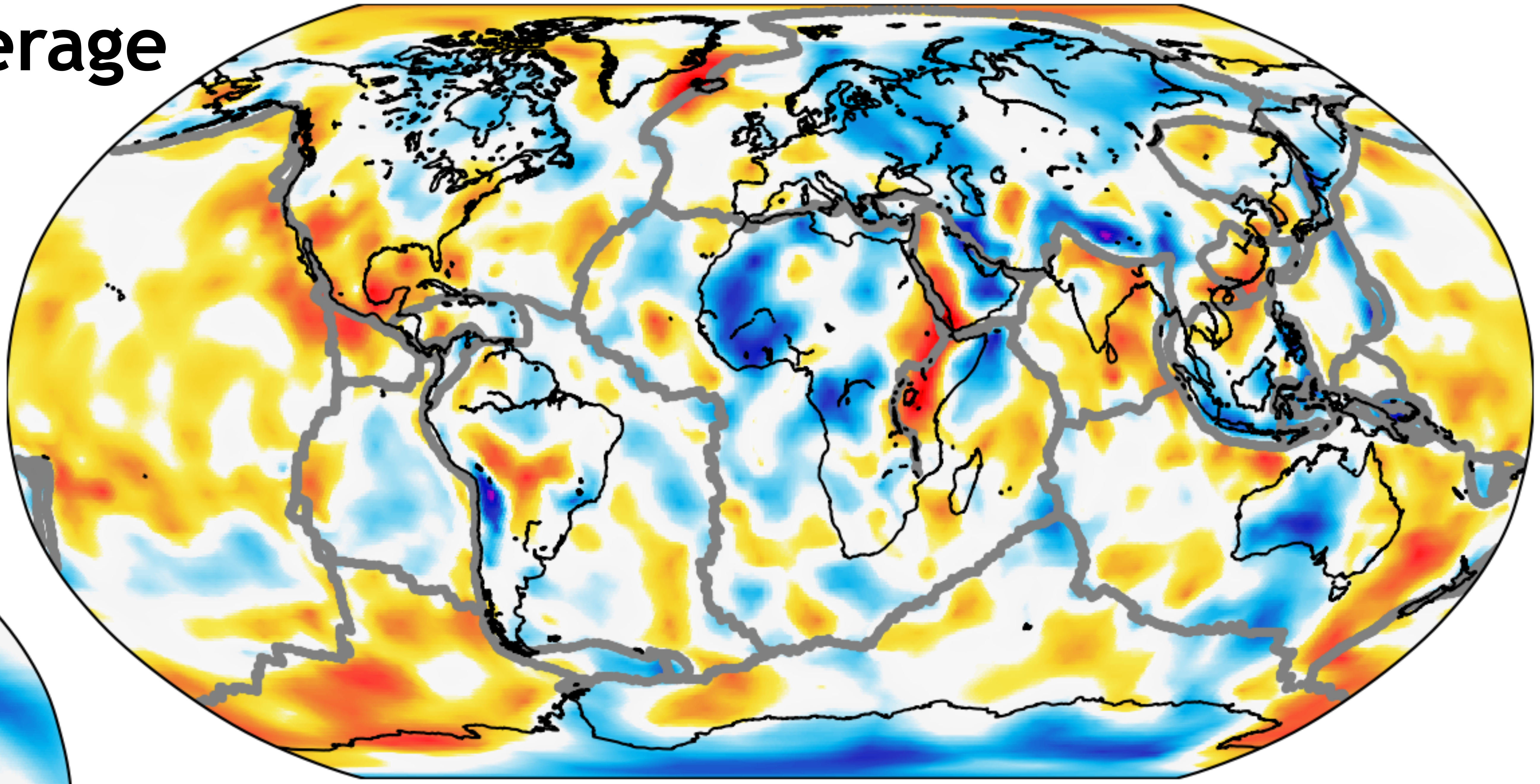

Negative anisotropy ($V_{SH} < V_{SV}$) under mid-ocean ridges, subductions, and backarcs.

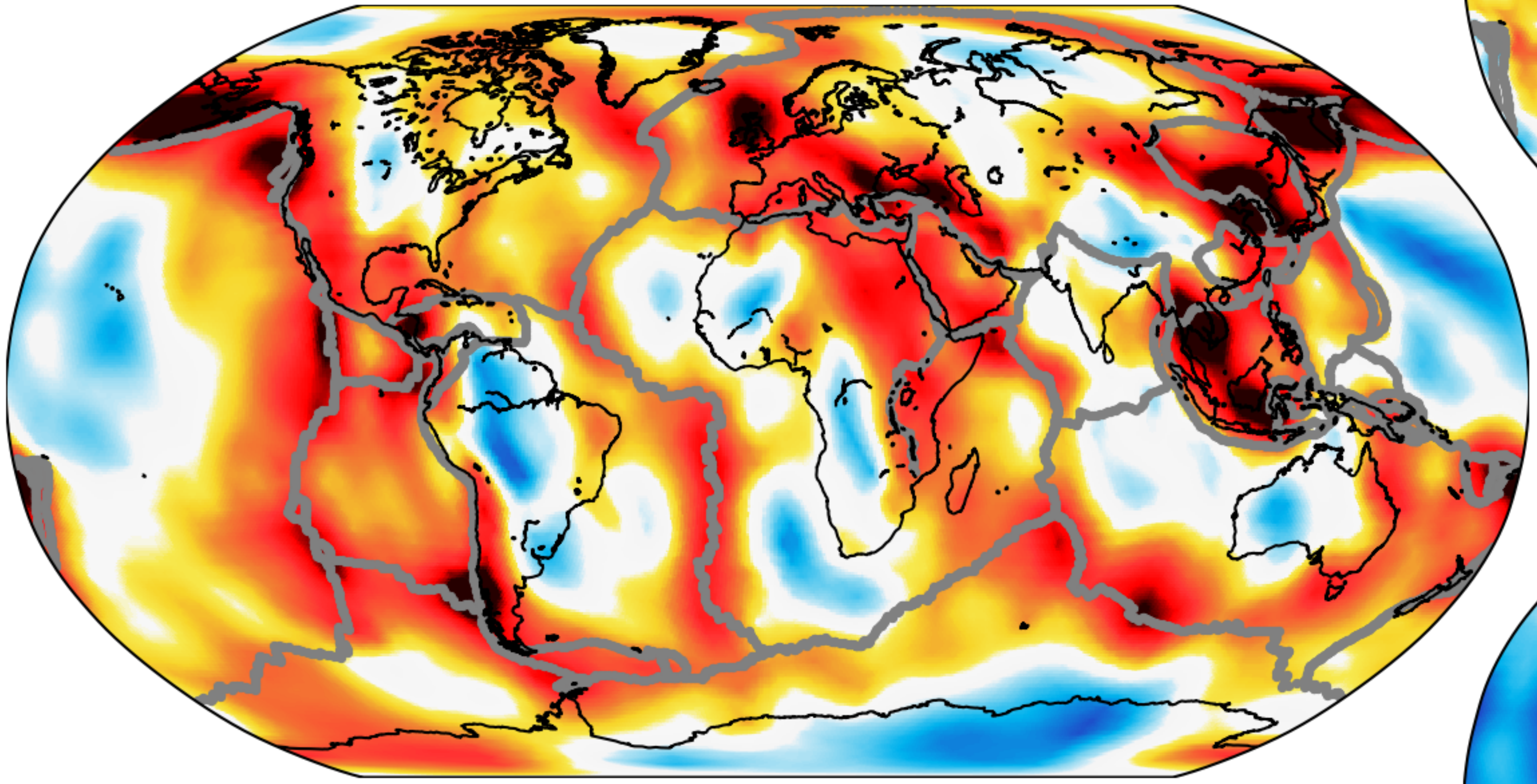

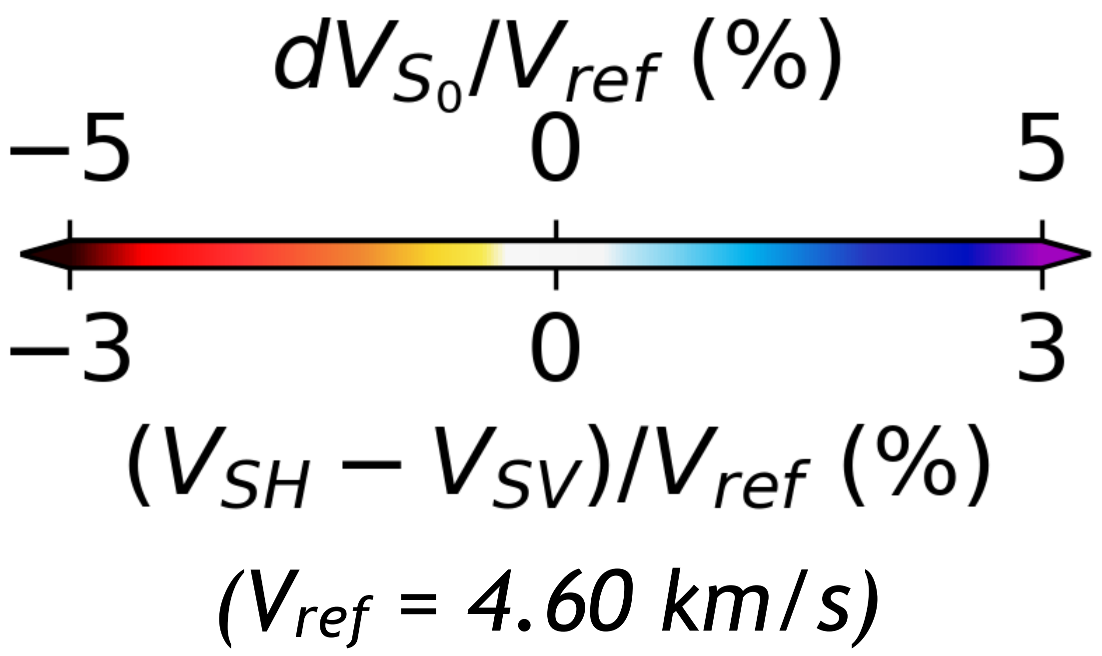

Anisotropy (V_{SH} - V_{SV})

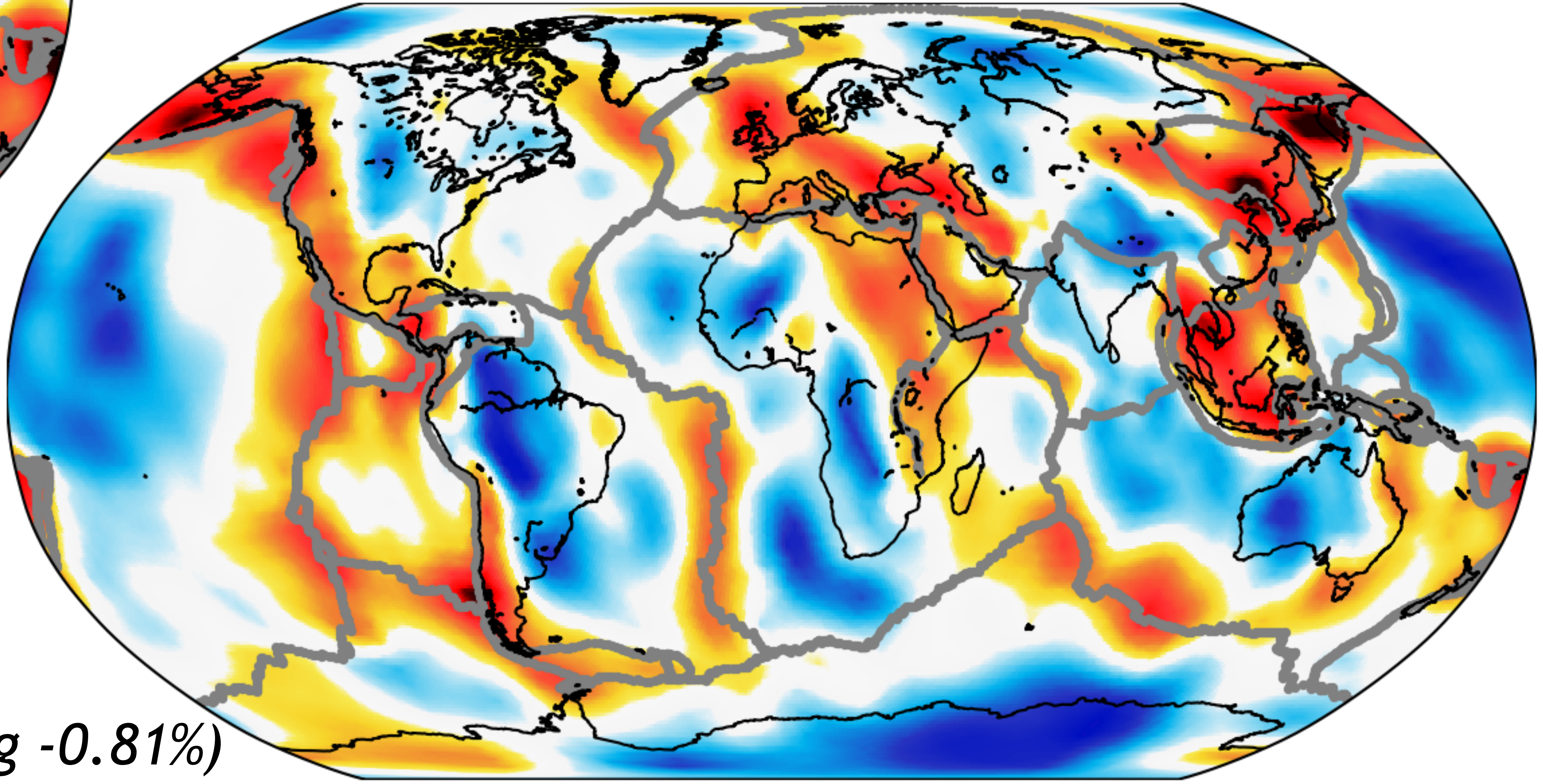

(-avg -0.81%)

V_{S0}, δ at 330 km

Global trend to negative anisotropy ($V_{SH} < V_{SV}$),
except under (some) cratons.

Isotropic average (dV_{S0})

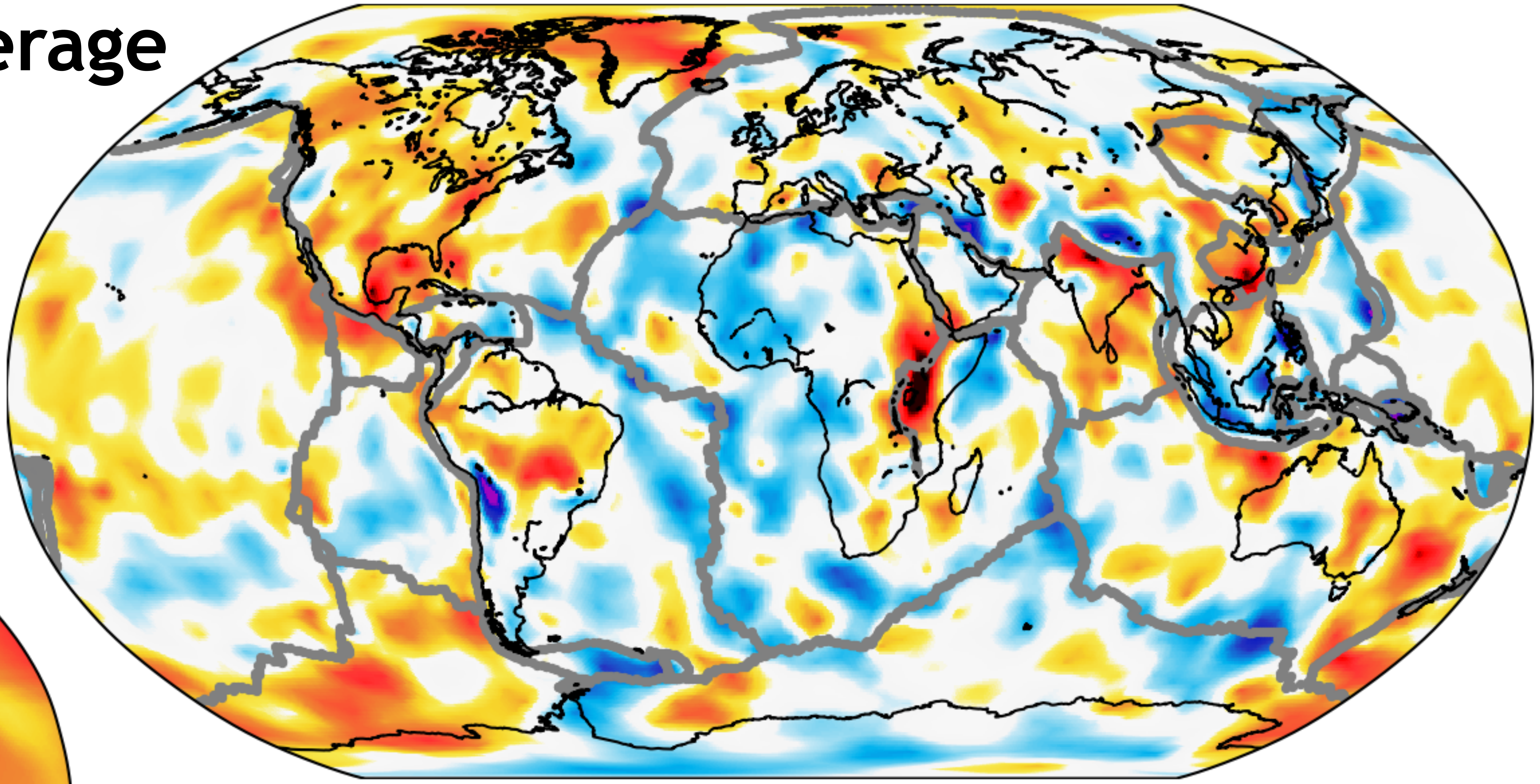

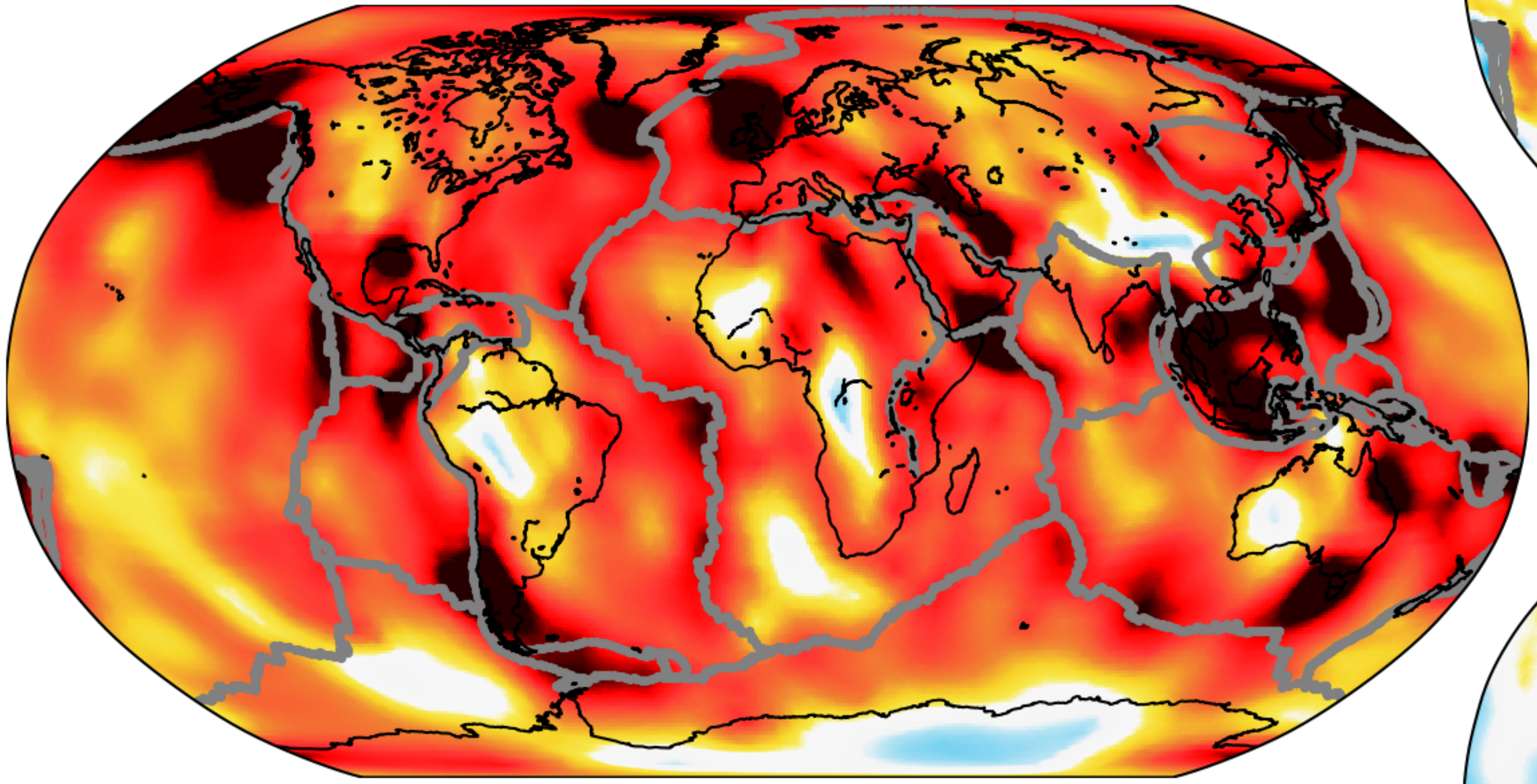

Anisotropy (V_{SH} - V_{SV})

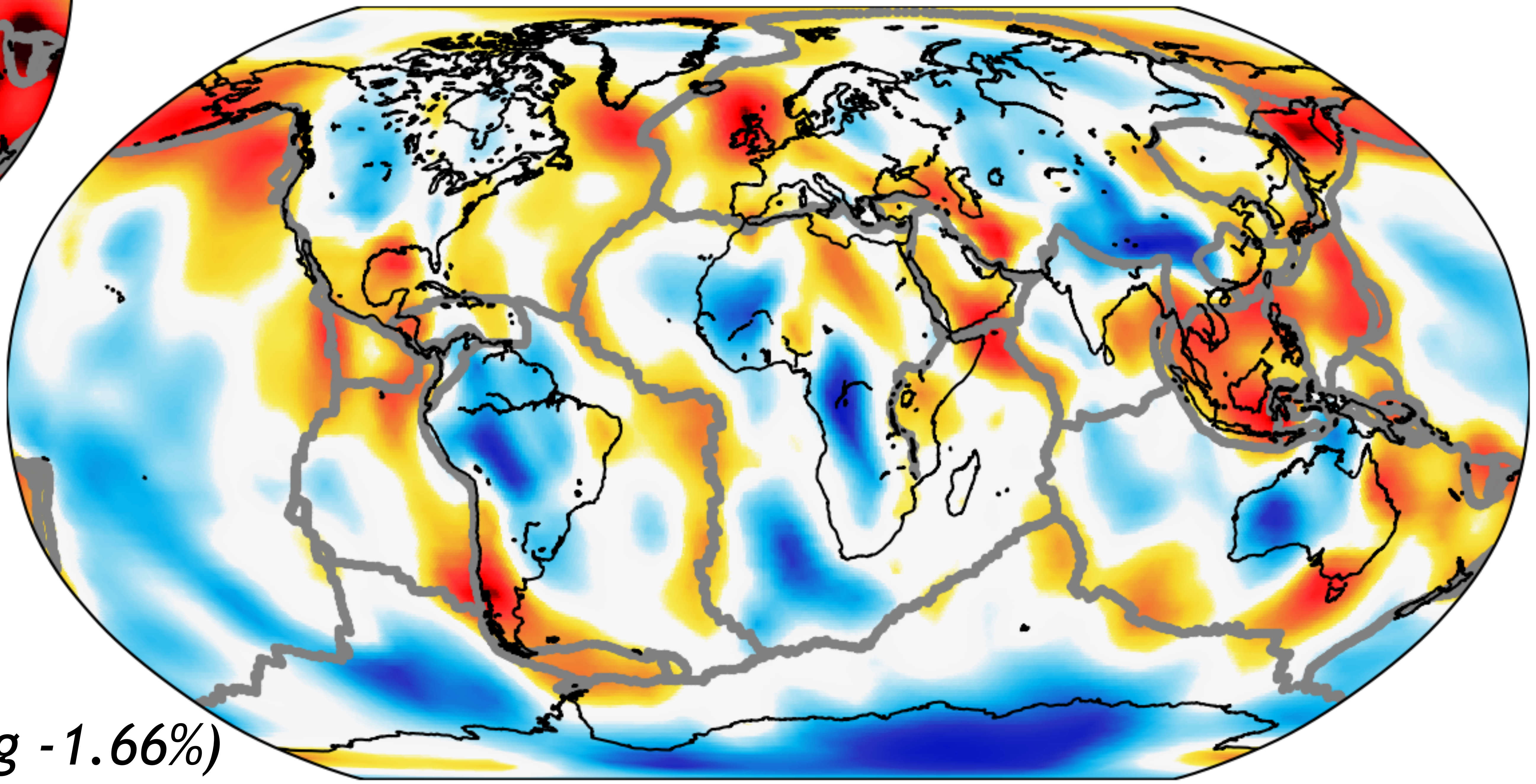

(-avg -1.66%)

What should we think about this model?
Let’s compare it with other models from the literature.

Model comparison at 110 km: isotropic average

There is a general agreement about large-scale isotropic structures, suggesting they are now robust and well-known. Most differences are small-scale discrepancies due to regularisation choices (smoothing), which we will not detail here.

Model comparison at 56 km: anisotropy

Much poorer agreement on anisotropic structures…
But several models seem to agree on the ocean-continent difference at shallow depths (BM12UM, SGLOBE-rani).

Model comparison at 80 km: anisotropy

All models agree on a global trend to positive anisotropy between 80 and 150 km depth, but the location of the strongest positive anomalies vary between models.

Model comparison at 110 km: anisotropy

All models agree on a global trend to positive anisotropy between 80 and 150 km depth, but the location of the strongest positive anomalies vary between models.

Model comparison at 150 km: anisotropy

Most models present less positive to slightly negative anisotropy under mid-ocean ridges, especially the EPR, as well as under subduction and backarc regions (Western US, Eastern Asia, Sunda plate).

Model comparison at 200 km: anisotropy

Most models present less positive to slightly negative anisotropy under mid-ocean ridges, especially the EPR, as well as under subduction and backarc regions (Western US, Eastern Asia, Sunda plate).

Model comparison at 260 km: anisotropy

Other models do not agree with our global trend to negative anisotropy between 260 and 410 km depth.

Model comparison at 330 km: anisotropy

Other models do not agree with our global trend to negative anisotropy between 260 and 410 km depth.

Model comparison at 330 km: anisotropy

Surprisingly, this negative trend is in better agreement with earlier models (e.g. Visser et al., 2008 [shown here], Montagner et al., 1998; Zhou et al., 2006; Nettles & Dziewonski, 2008; and, in a lesser extent, Panning and Romanowicz, 2006).

Global 1D averages

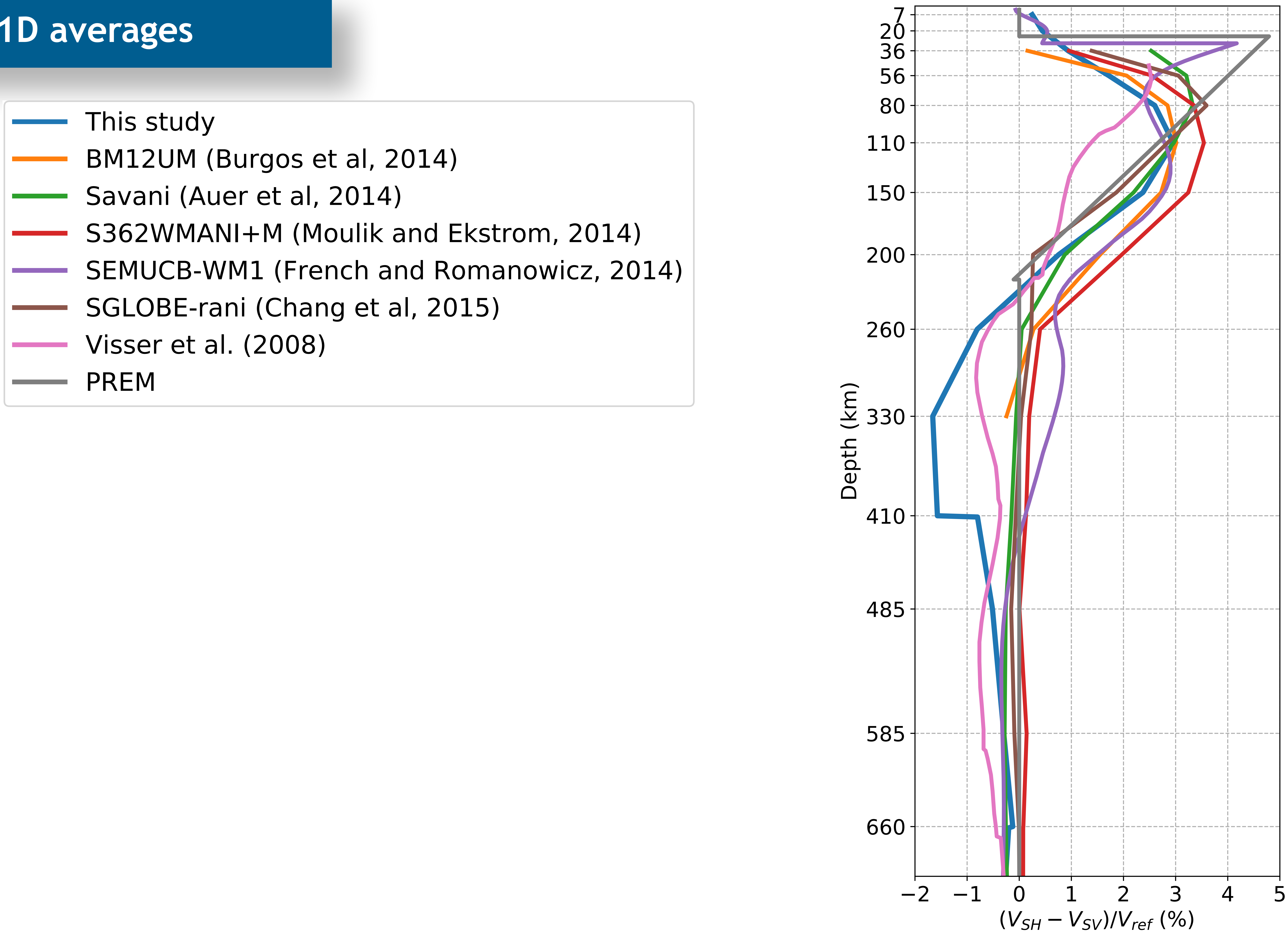

Global 1D averages

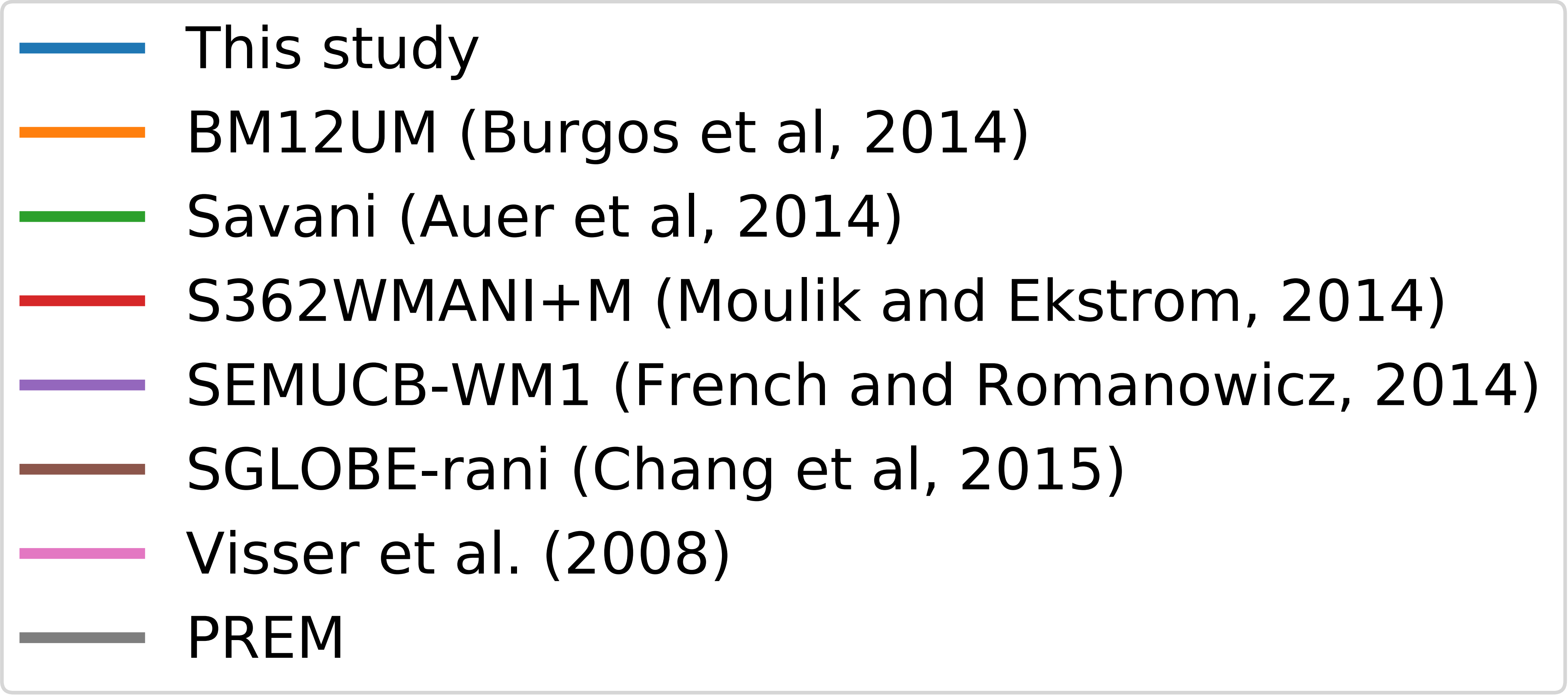

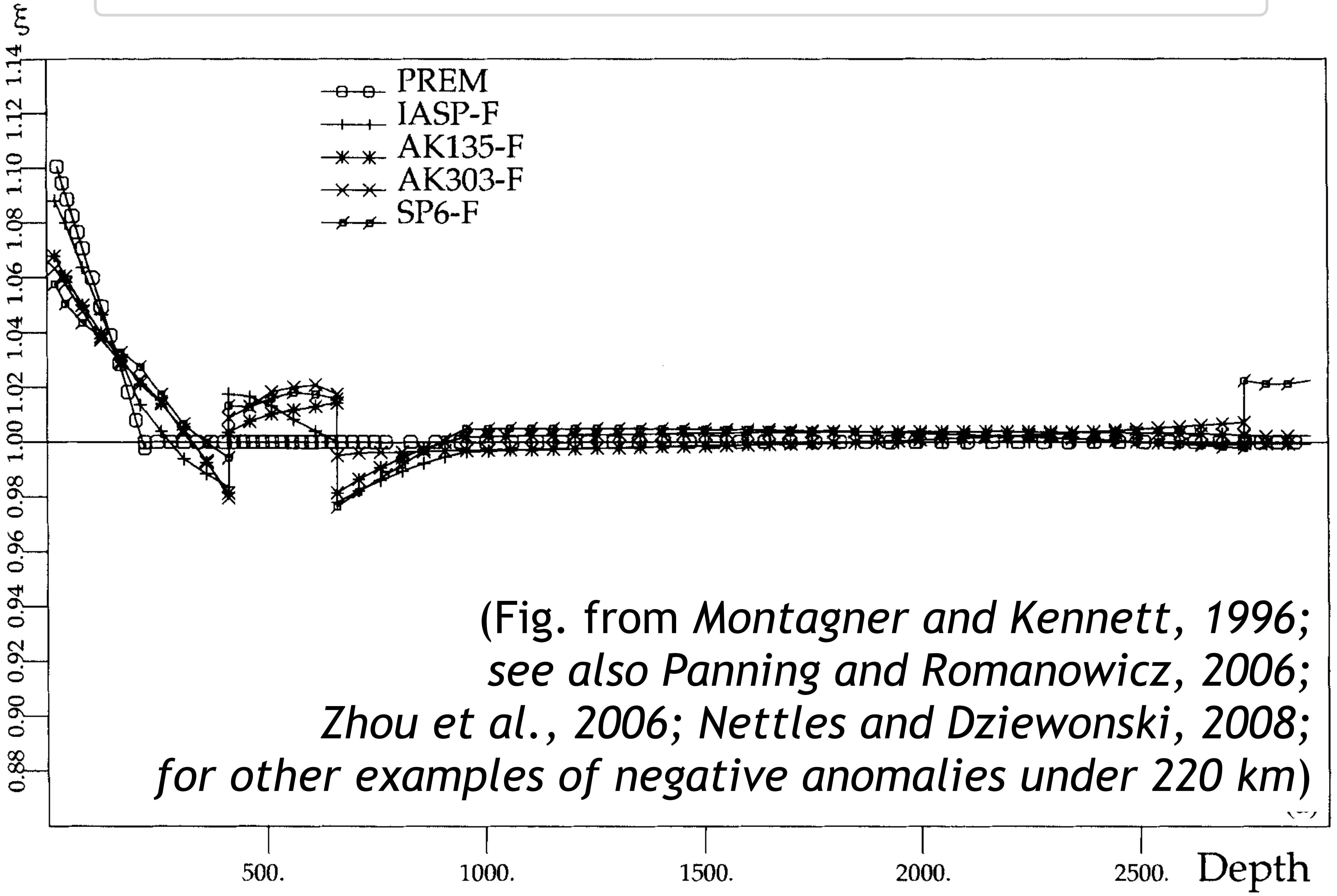

(Fig. from *Montagner and Kennett, 1996; see also Panning and Romanowicz, 2006; Zhou et al., 2006; Nettles and Dziewonski, 2008; for other examples of negative anomalies under 220 km*)

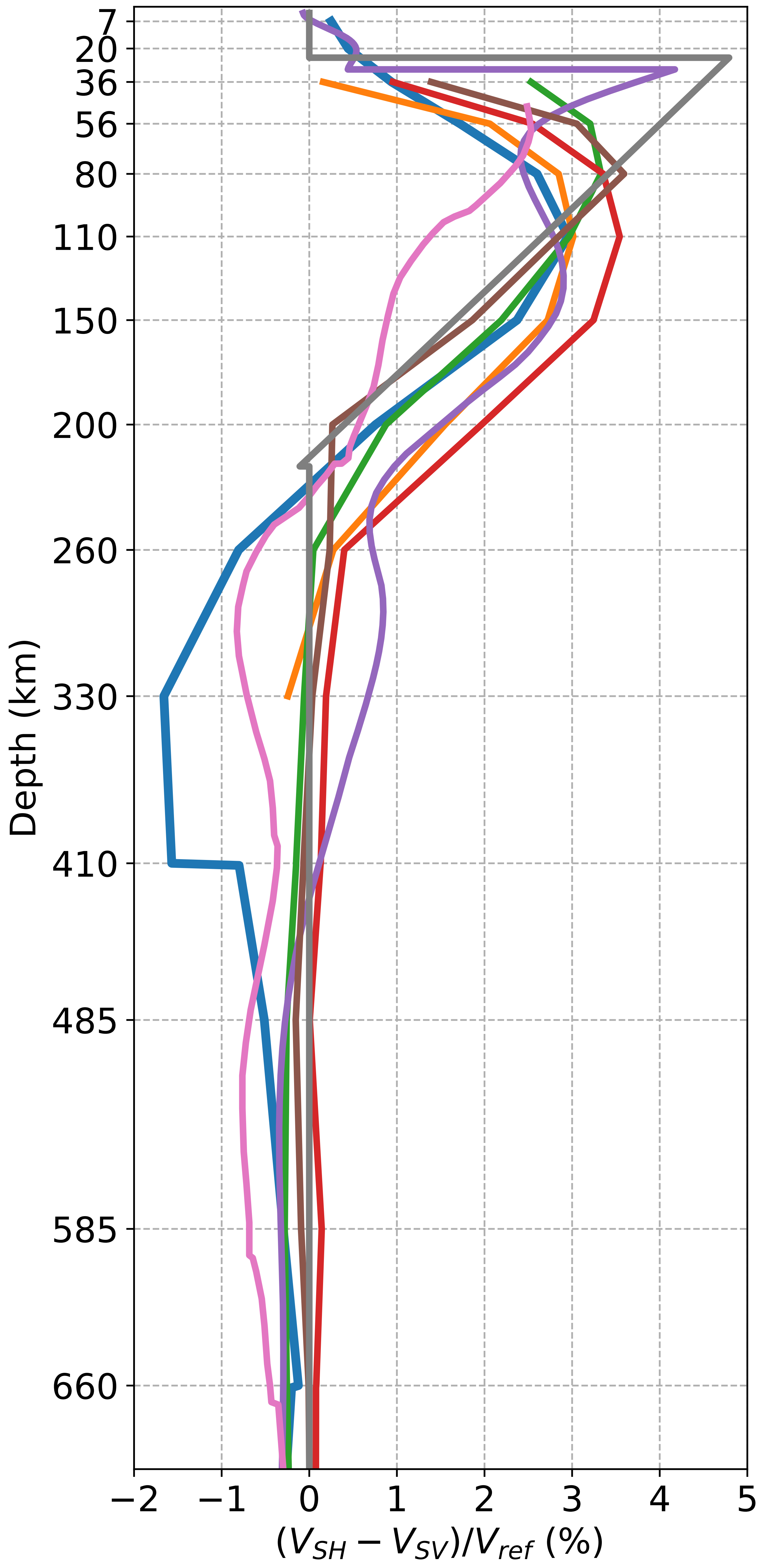

Synthetic tests demonstrate the robustness of our global anisotropy pattern

(except in the transition zone)

(a,b) Leakage and flip tests

- Preferred model
- Synthetic target model
- Retrieved model

(c) Regularization tests

- preferred model
- very smooth
- very rough
- anisotropic reference model
- other isotropic reference (LH2008)
- Love vs. Rayleigh weighting
- sensitivity-based reparameterization

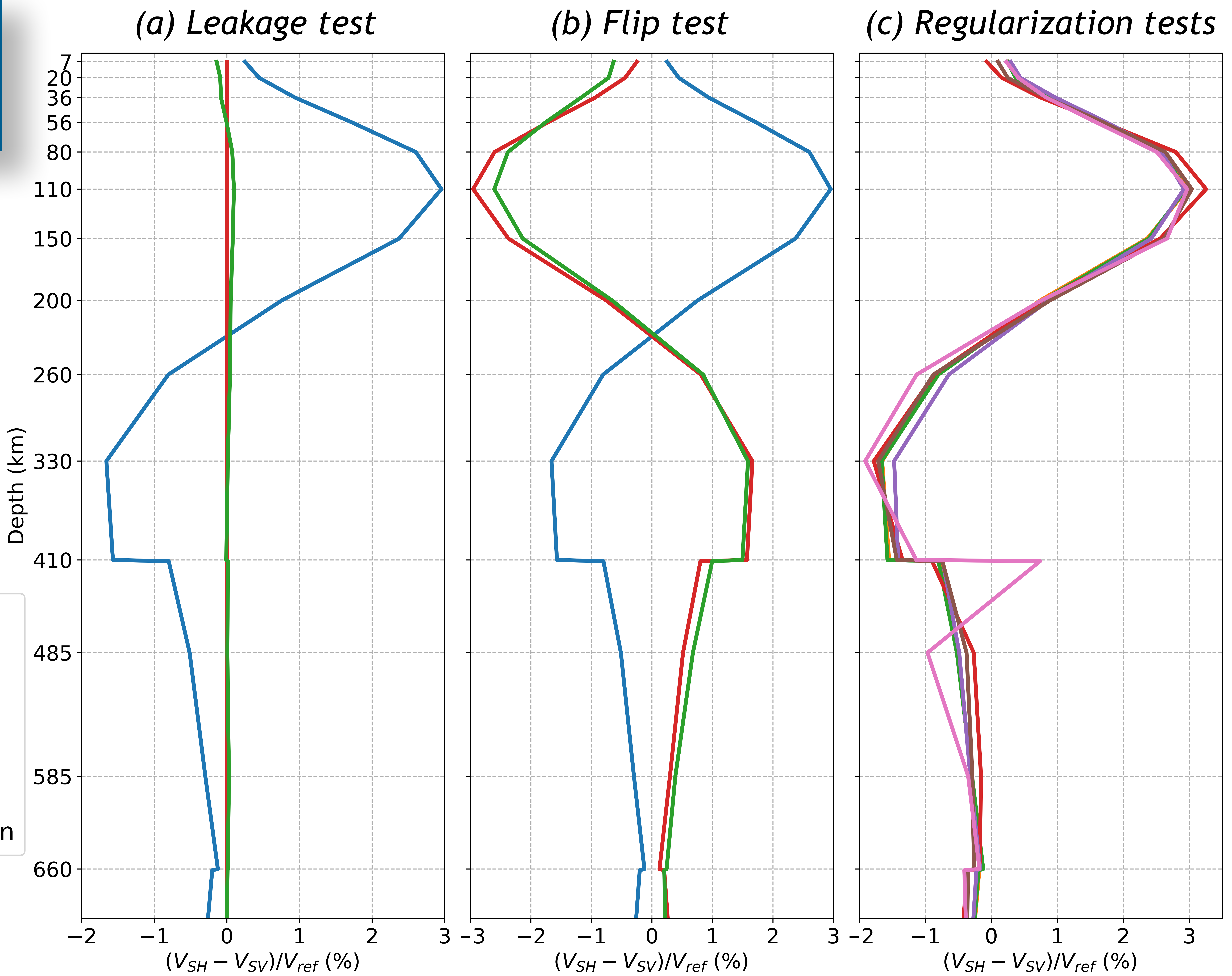

Regionalized 1D averages show interesting tectonic dependencies

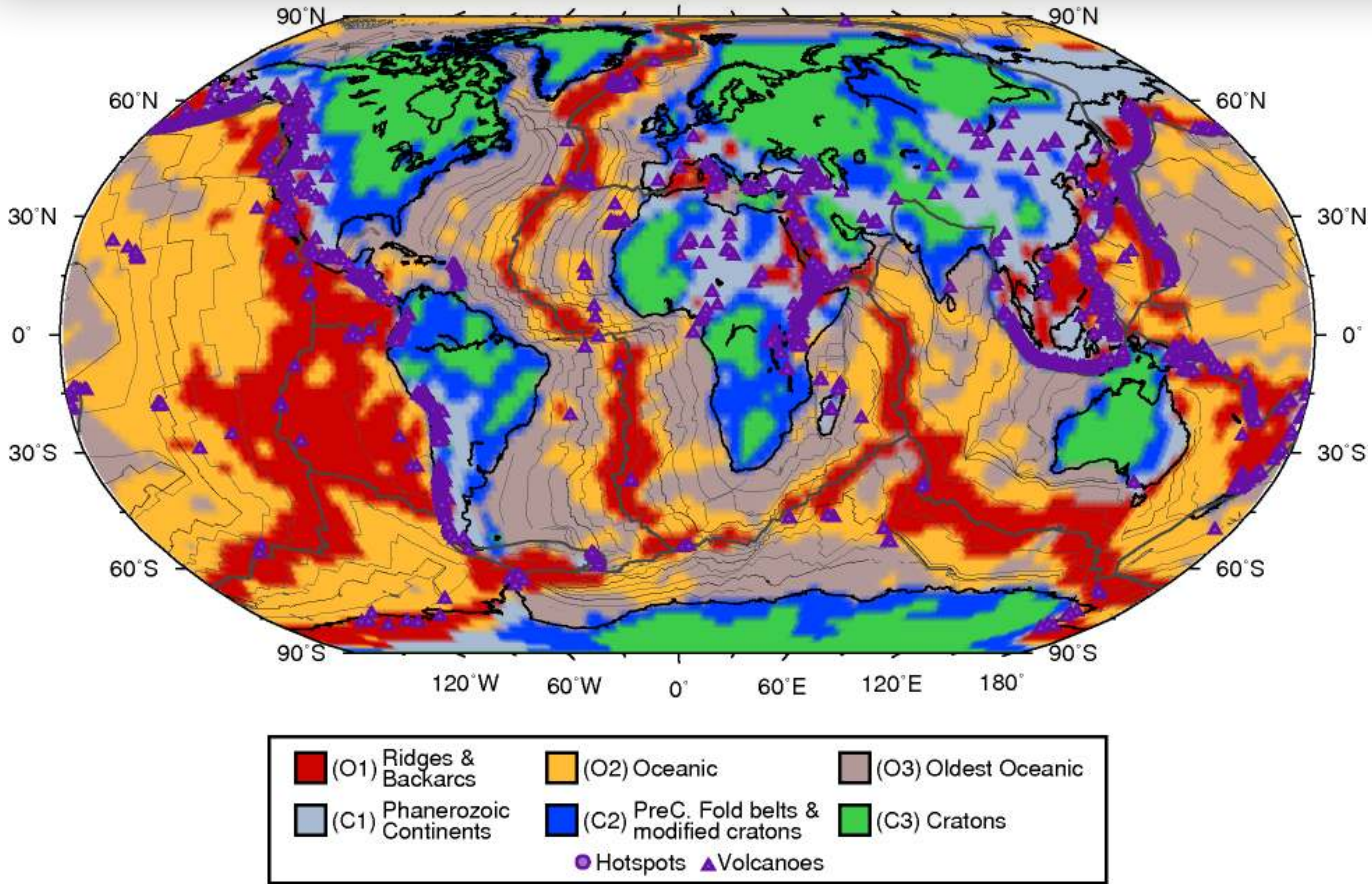

(Schaeffer and Lebedev, 2015)

global average
cratons
precambrian belts
phanerozoic continents
ridges and backarcs
intermediate oceans
oldest oceans

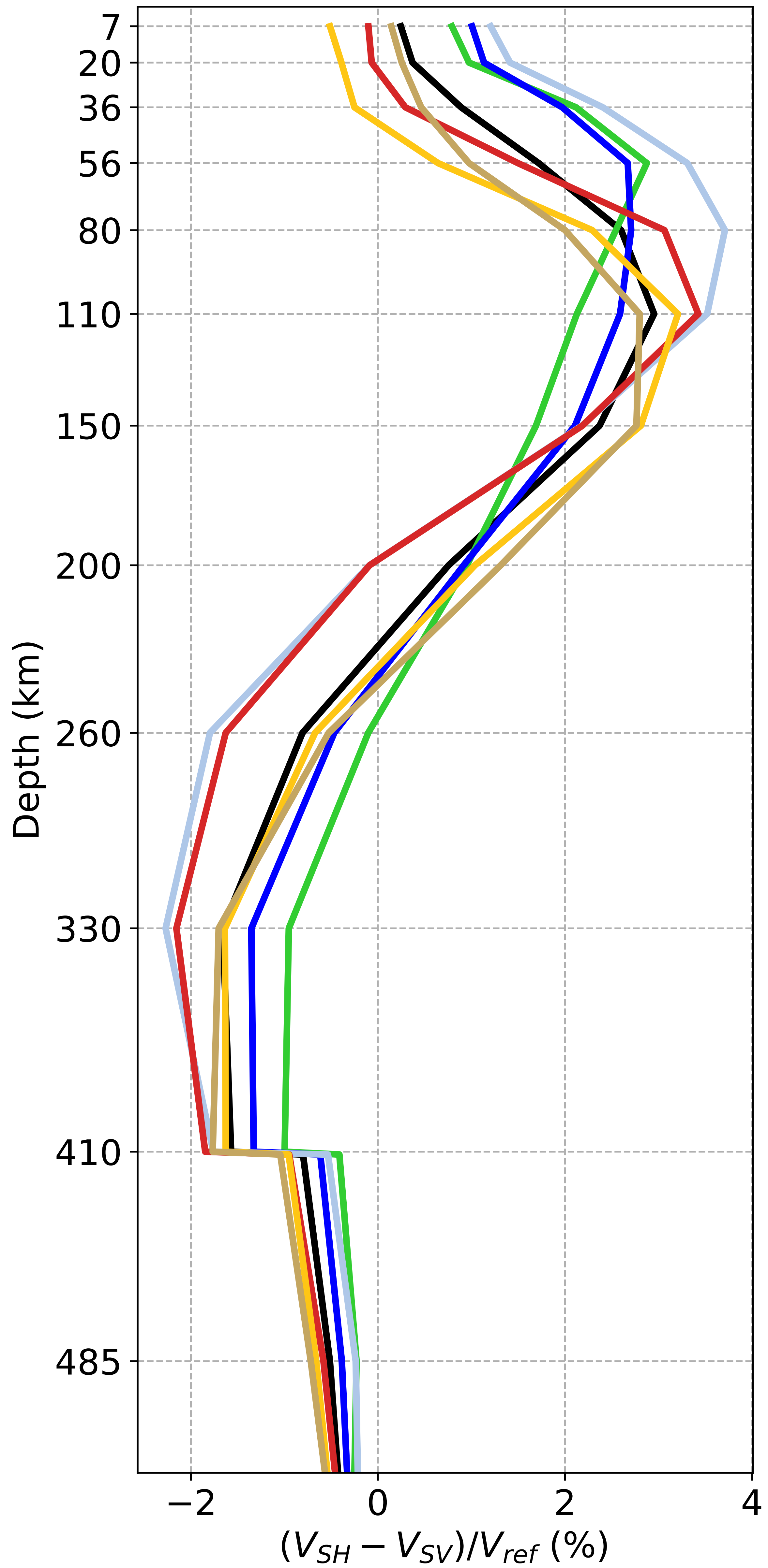

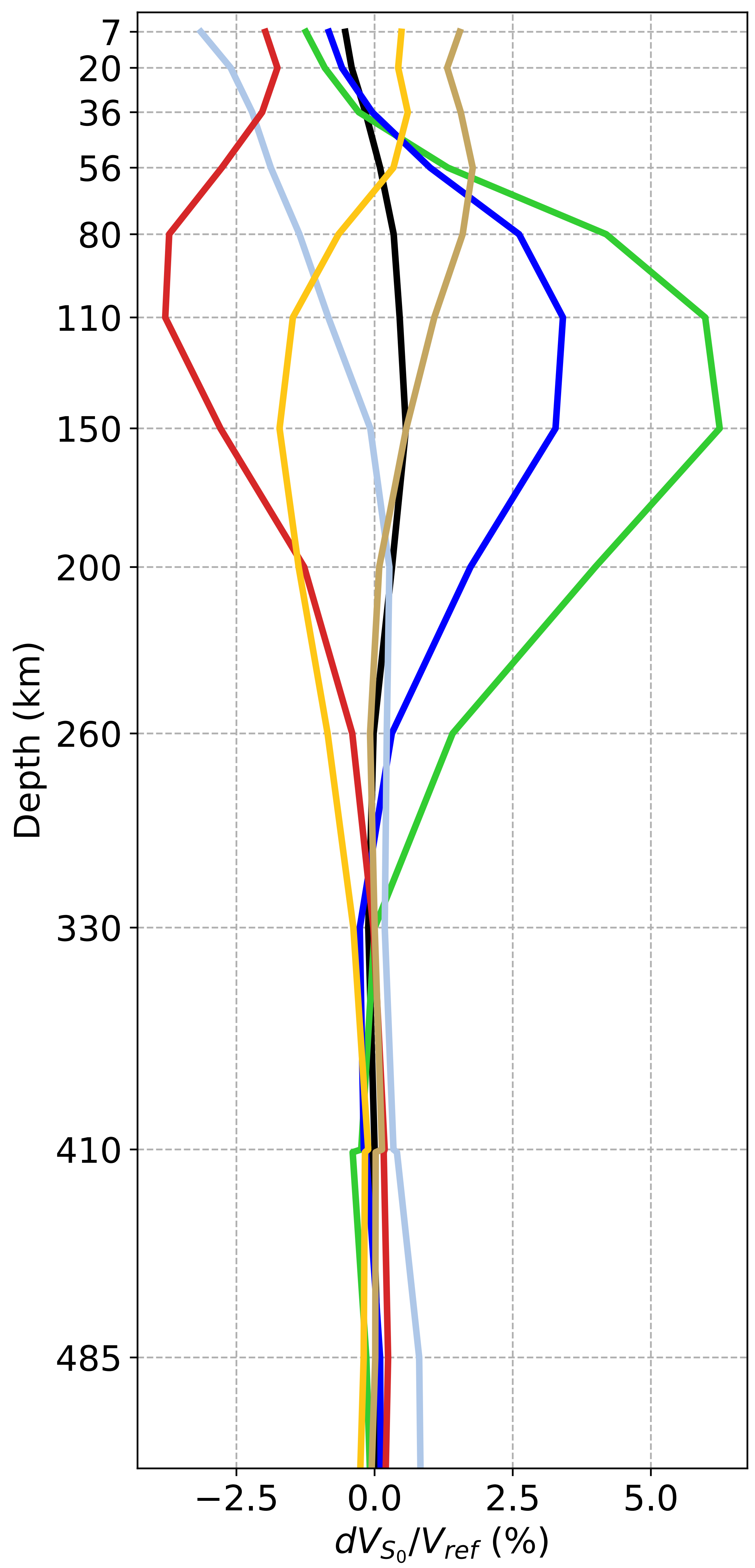

Vertical cross-sections

Vertical cross-sections

Vertical cross-sections

Seismic anisotropy and olivine lattice preferred orientation (LPO)

Remember that the geodynamical interpretation of seismic anisotropy is not straightforward…

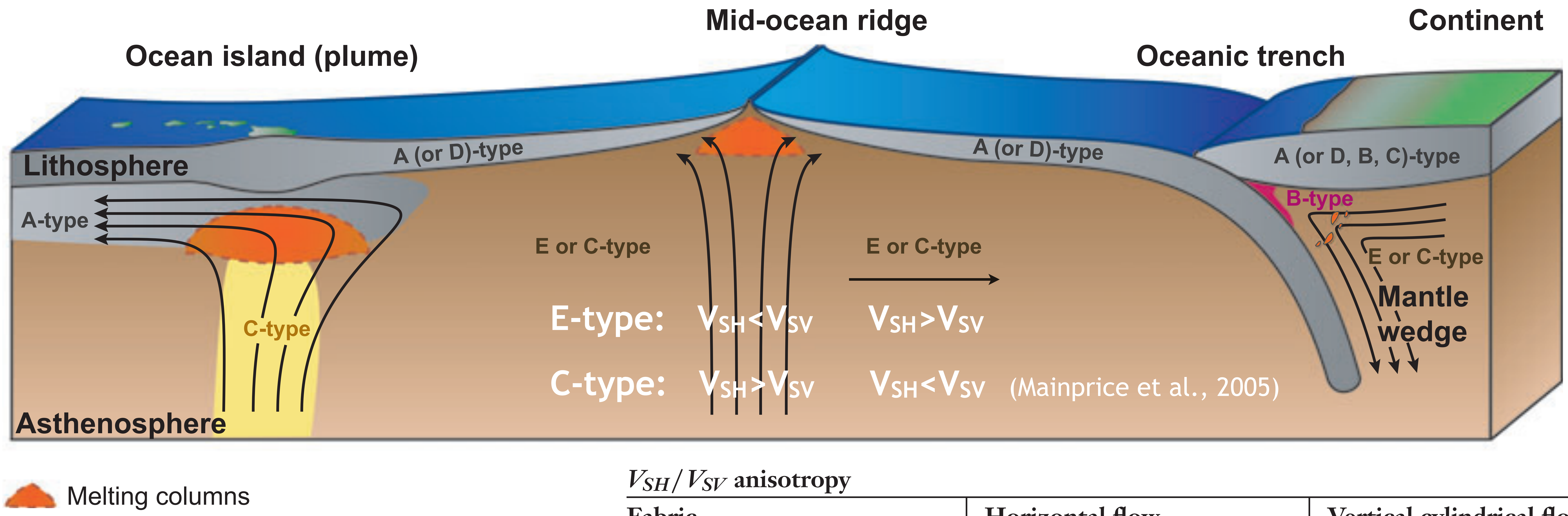

Karato's new model of olivine LPO (Karato et al., 2008)

V_{SH}/V_{SV} anisotropy

Fabric	Horizontal flow	Vertical cylindrical flow
A-type	$V_{SH}/V_{SV} > 1$	$V_{SH}/V_{SV} < 1$
B-type	$V_{SH}/V_{SV} > 1$	$V_{SH}/V_{SV} > 1$ (weak)
C-type	$V_{SH}/V_{SV} < 1$	$V_{SH}/V_{SV} > 1$ (weak)
D-type	$V_{SH}/V_{SV} > 1$	$V_{SH}/V_{SV} < 1$
E-type	$V_{SH}/V_{SV} > 1$ (weak)	$V_{SH}/V_{SV} < 1$

Regionalized 1D averages show interesting tectonic dependencies

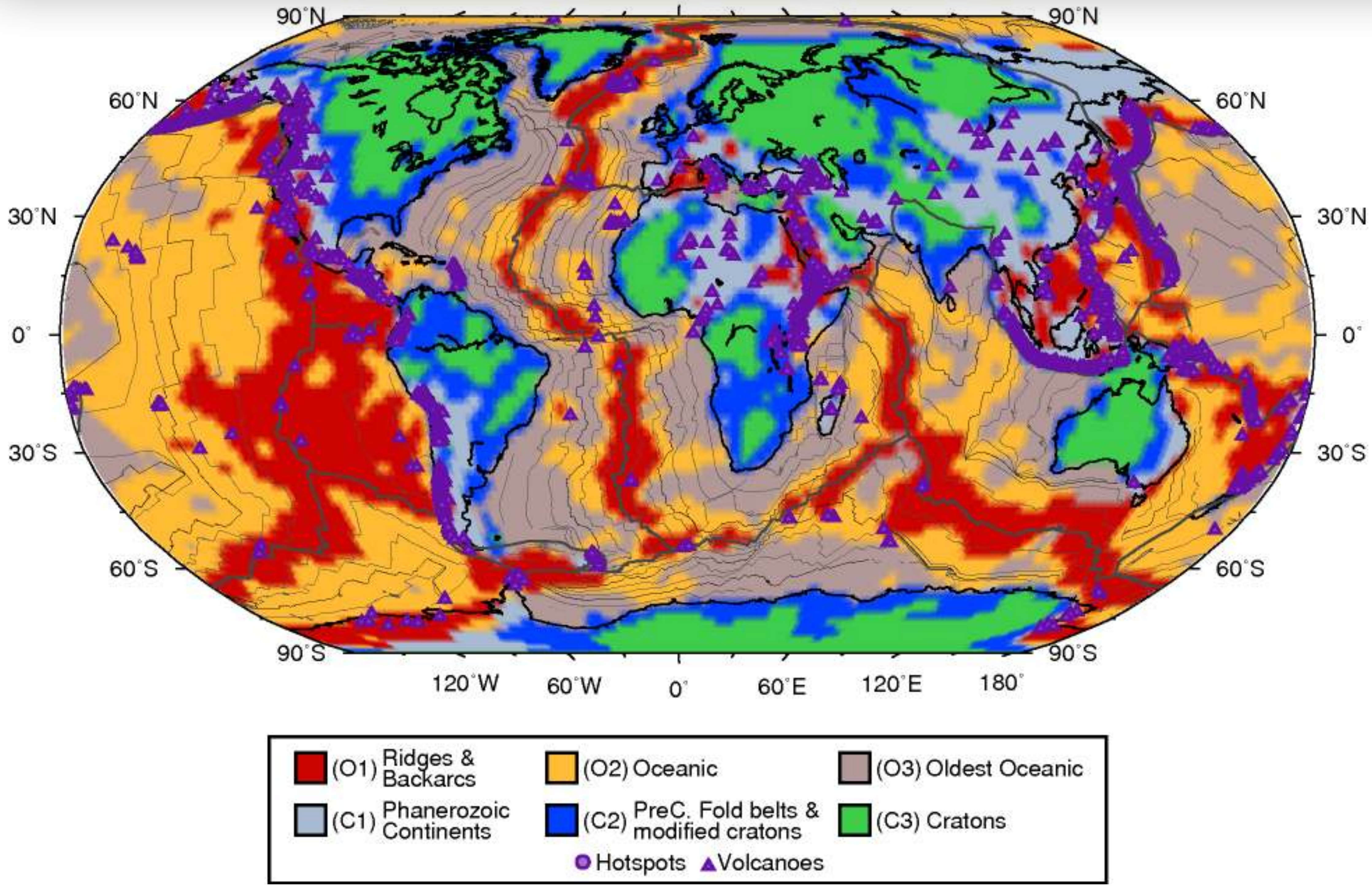

(Schaeffer and Lebedev, 2015)

- global average
- cratons
- precambrian belts
- phanerozoic continents
- ridges and backarcs
- intermediate oceans
- oldest oceans

Radial anisotropy

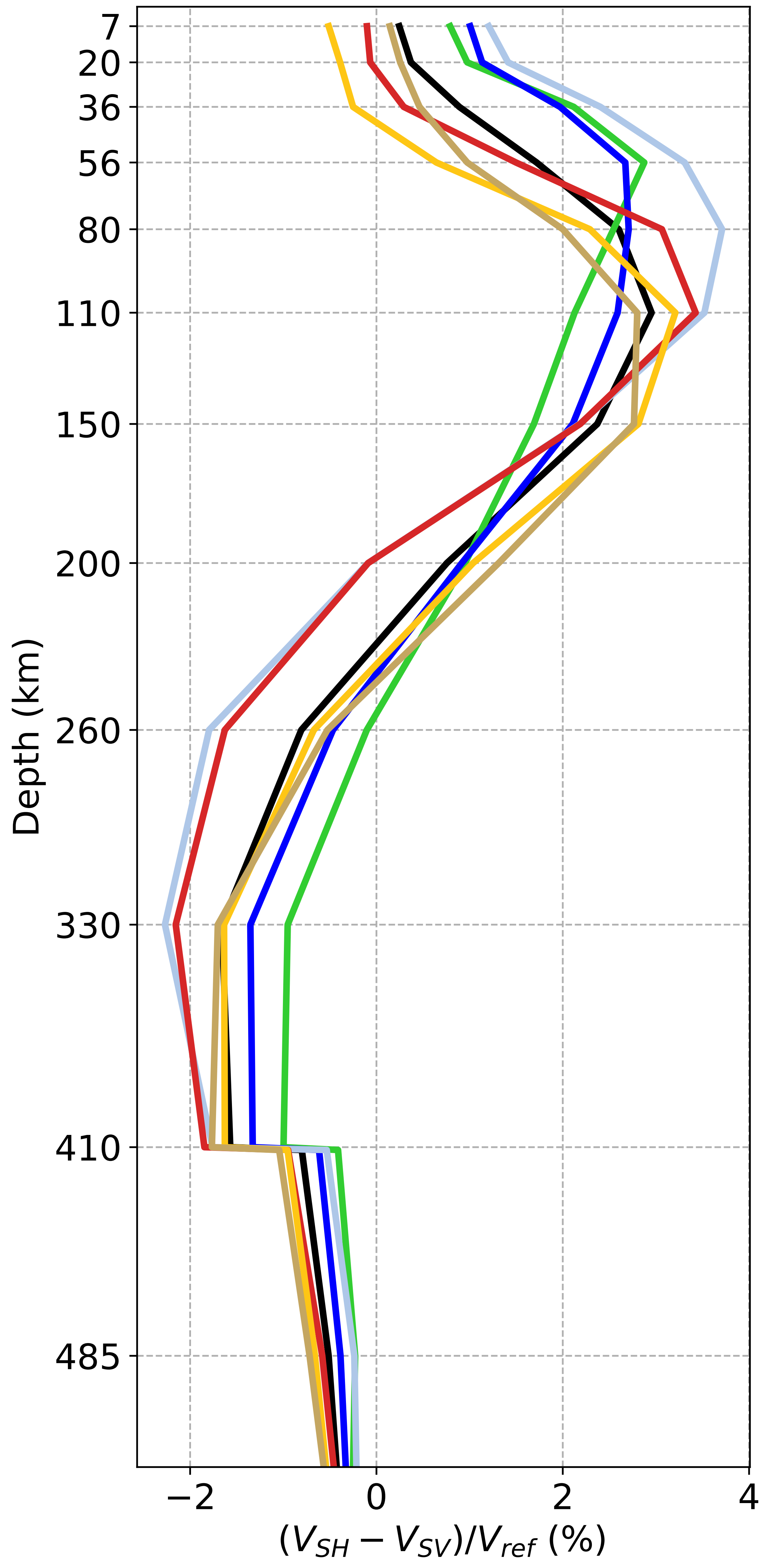

Isotropic velocity perturbation

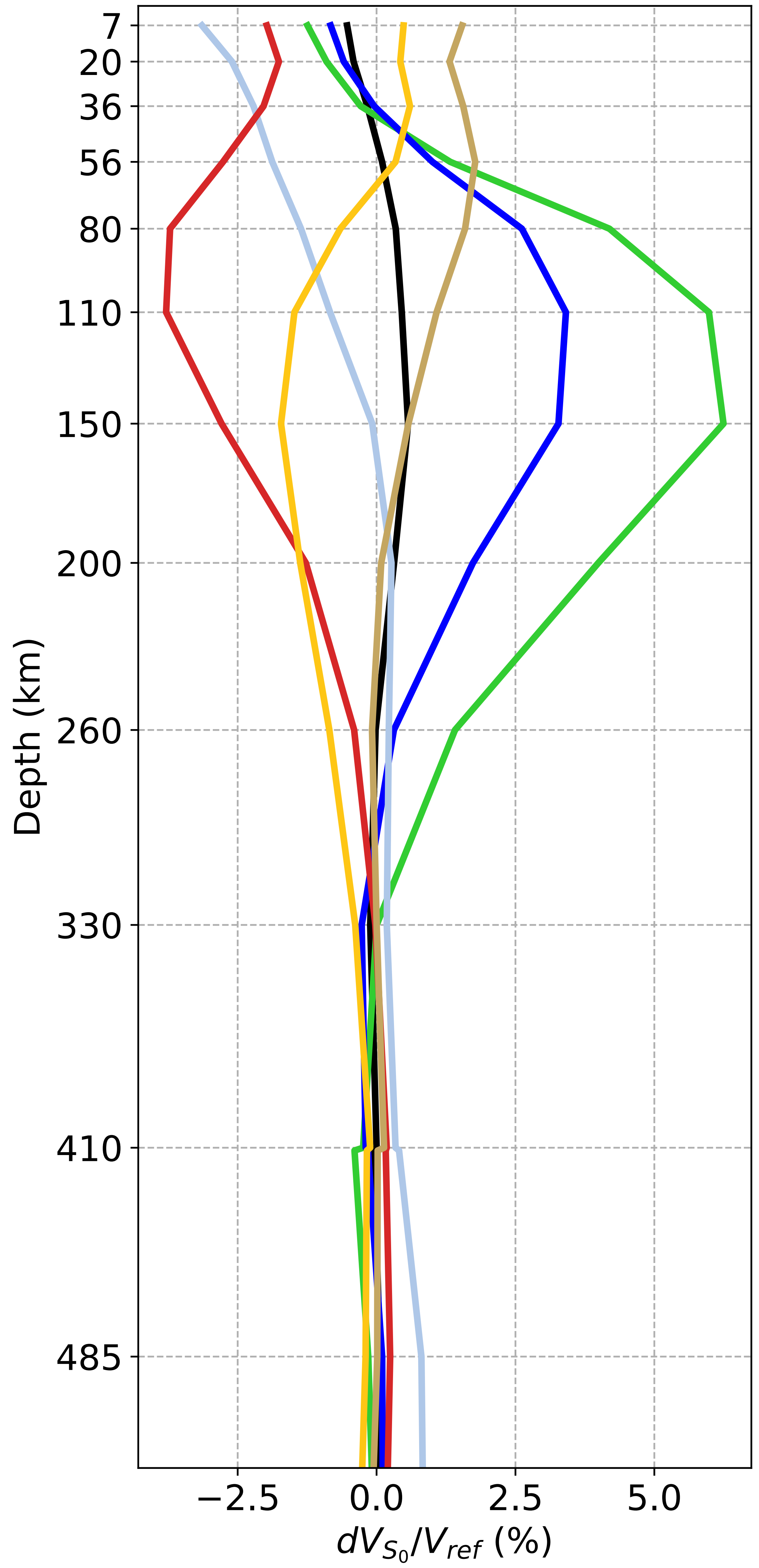

Can we characterize this anisotropy transition? (depth, temperature, Clapeyron slopes?)

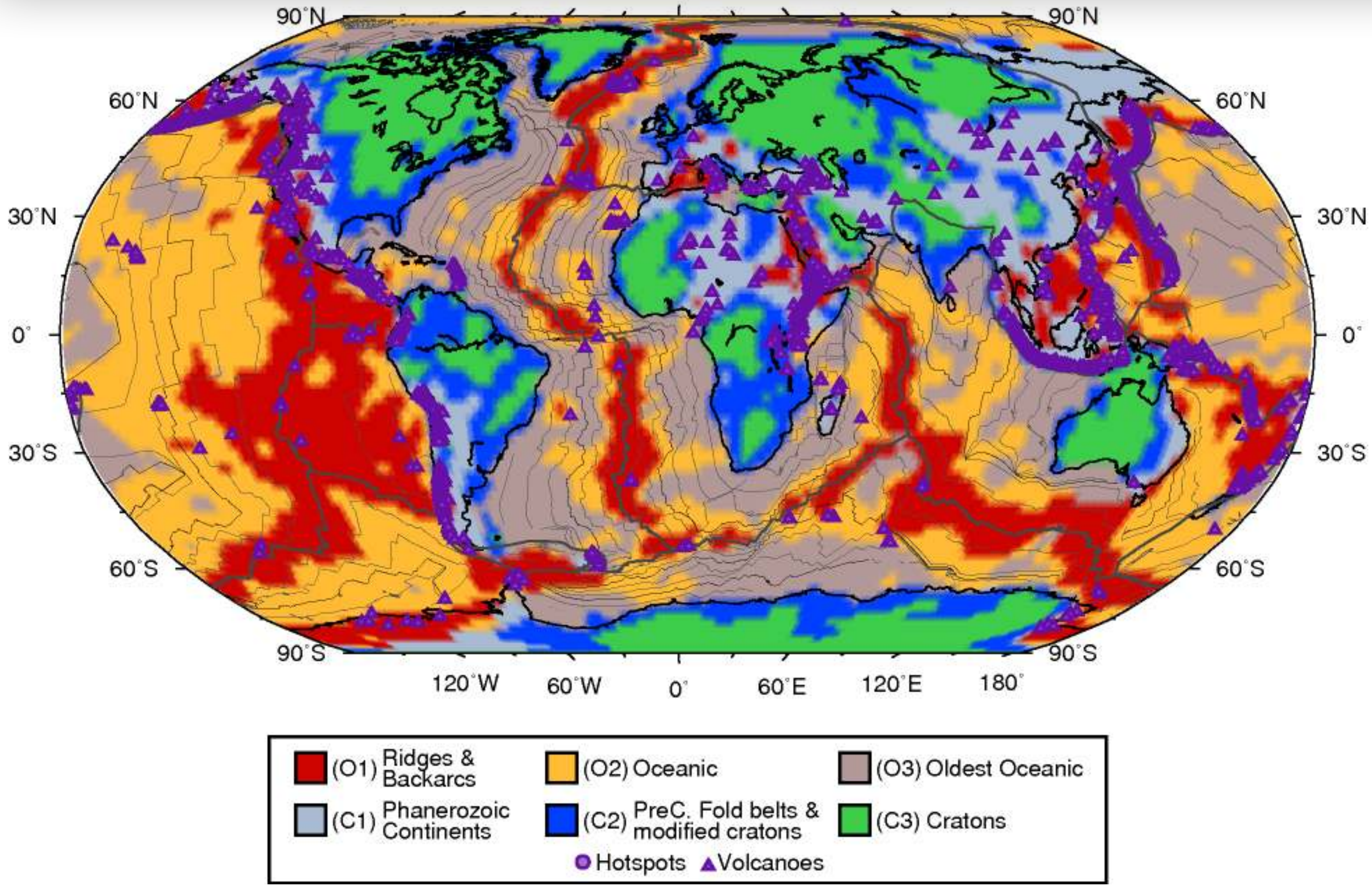

(Schaeffer and Lebedev, 2015)

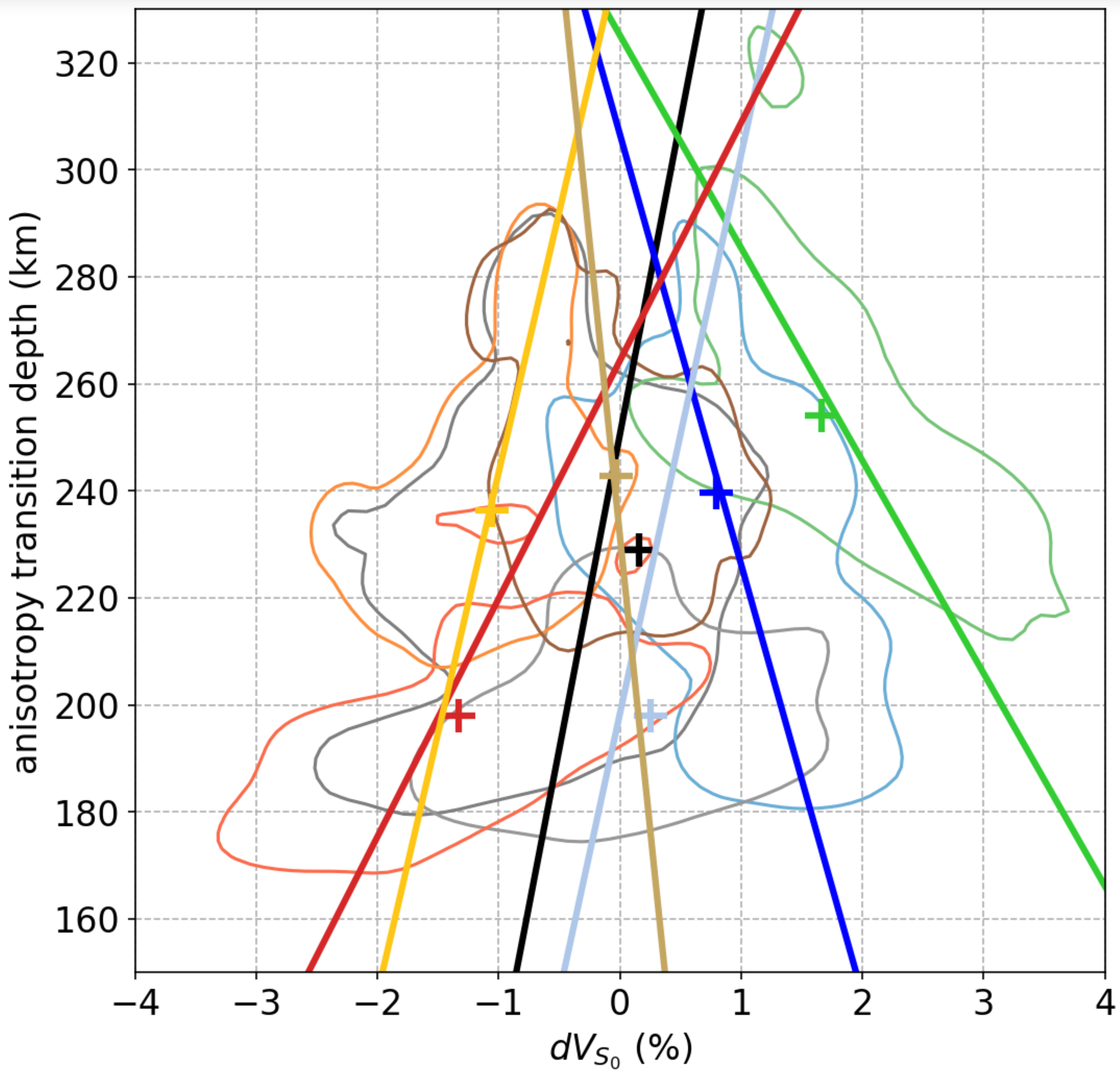

Can we characterize this anisotropy transition? (depth, temperature, Clapeyron slopes?)

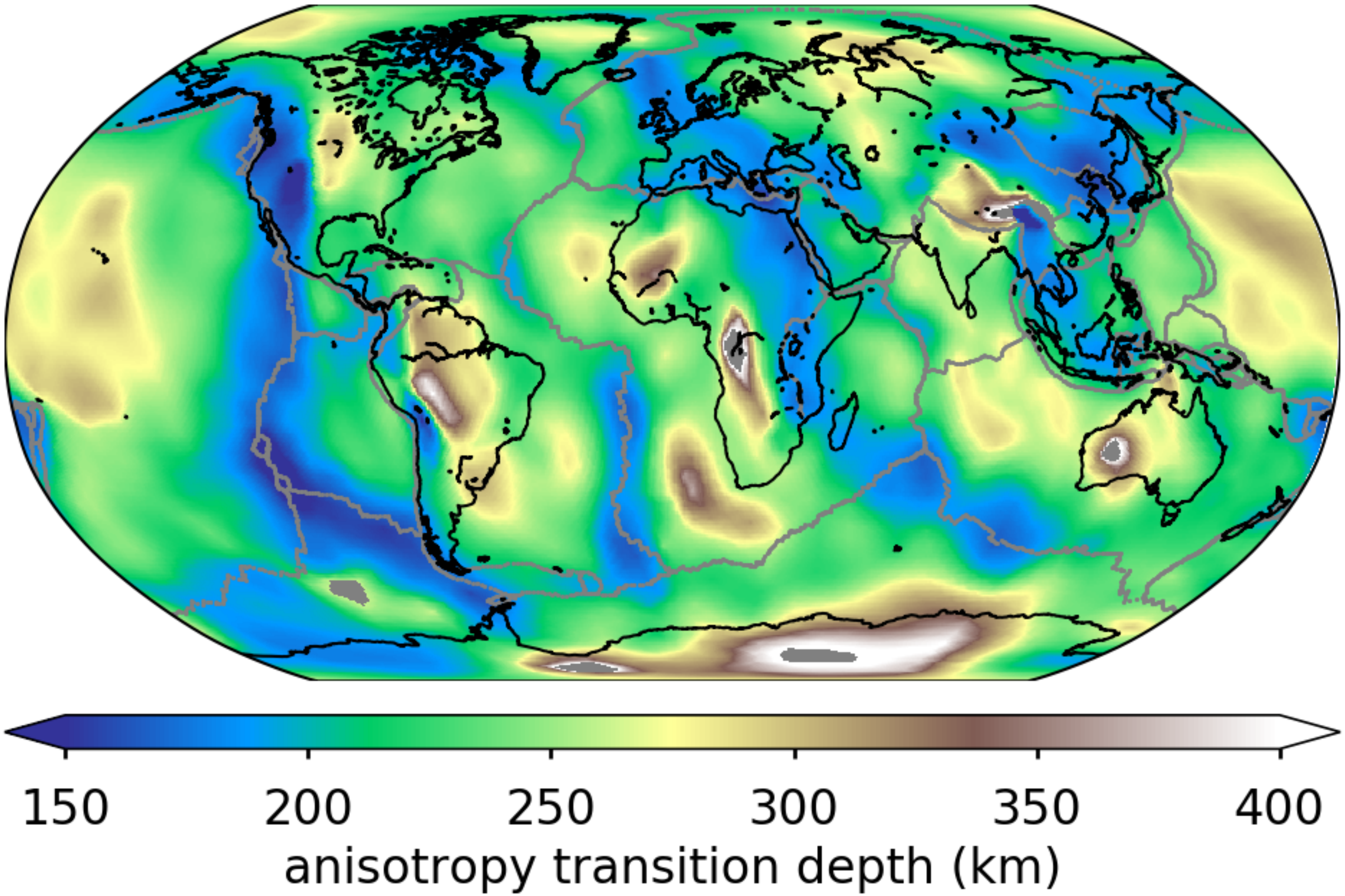

Conclusions

Our models show ***significant anisotropy below 220 km depth*** (unlike PREM and previous studies suggesting diffusion creep below this depth, *e.g. Karato, 1992*) with ***a transition from positive to negative anisotropy between 200 and 300 km*** depth.

This transition has a ***clear tectonic dependence***: shallower under young continents and oceans, deeper under cratons and old oceans, very similar to the one observed for P-wave anisotropy (*Beghein and Trampert, 2003*).

This transition can be interpreted in two ways:

1. Transition from dominantly ***horizontal*** to dominantly ***vertical flow*** in the mantle *(but everywhere?)*.
2. Transition in olivine slip mechanism which would cause a ***horizontal flow*** to induce a ***negative anisotropy*** below a certain depth *(e.g. Mainprice et al., 2005; Mainprice, 2007)*.

These two possibilities are not mutually exclusive, and they do not rule out other mechanisms (e.g. the influence of water, *Jung and Karato, 2001*; *Chang and Ferreira, 2019*).

Thank you!

Questions?

Please feel free to contact us: lavouef@cp.dias.ie

This presentation has emanated from research supported in part by a research grant from Science Foundation Ireland (SFI) under Grant Number 13/RC/2092 and is co-funded under the European Regional Development Fund.

Institiúid Ard-Léinn Bhaile Átha Cliath | Dublin Institute for Advanced Studies

IRISH CENTRE FOR RESEARCH IN APPLIED GEOSCIENCES

TRINITY COLLEGE DUBLIN

Ireland's European Structural and Investment Funds Programmes 2014-2020

Co-funded by the Irish Government and the European Union

European Union
European Regional Development Fund

Science Foundation Ireland For what's next

References

- Auer, L., Boschi, L., Becker, T. W., Nissen-Meyer, T., and Giardini, D. (2014). Savani: A variable resolution whole-mantle model of anisotropic shear velocity variations based on multiple data sets. Journal of Geophysical Research, 119:3006–3034.
- Burgos, G., Montagner, J.-P., Beucler, E., Capdeville, Y., Mocquet, A. and Drilleau, M. (2014). Oceanic lithosphere-asthenosphere boundary from surface wave dispersion data. Journal of Geophysical Research, 119:1079-1093.
- Chang, S.-J., Ferreira, A. M. G., Ritsema, J., Heijst, H. J., and Woodhouse, J. H. (2015). Joint inversion for global isotropic and radially anisotropic mantle structure including crustal thickness perturbations. Journal of Geophysical Research, 120(6):4278-4300.
- Chang, S.-J. and Ferreira, A. M. G. Inference on water content in the mantle tran- sition zone near subducted slabs from anisotropy tomography. Geochemistry, Geophysics, Geosystems.
- French, S. W. and Romanowicz, B. A. (2014). Whole-mantle radially anisotropic shear velocity structure from spectral-element waveform tomography. Geophysical Journal International, 199(3):1303-1327.
- Jung, H. and Karato, S.-i. (2001). Water-induced fabric transitions in olivine. Science, 293(5534):1460–1463.Kennett, B. L. N., Engdahl, E. R., and Buland, R. (1995). Constraints on seismic velocities in the Earth from traveltimes. Geophysical Journal International, 122(1):108–124
- Karato, S.-i. (1992). On the Lehmann discontinuity. Geophysical Research Letters, 19(22):2255-2258, doi:10.1029/92GL02603.
- Karato, S.-i., Jung, H., Katayama, I., and Skemer, P. (2008). Geodynamic Significance of Seismic Anisotropy of the Upper Mantle: New Insights from Laboratory Studies. Annual Review of Earth and Planetary Sciences, 36(1):59-95, doi:10.1146/annurev.earth.36.031207.124120.
- Lebedev, S., Nolet, G., Meier, T., and van der Hilst, R. D. (2005). Automated multimode inversion of surface and S waveforms. Geophysical Journal International, 162:951–964.
- Mainprice, D., Tommasi, A., Couvy, H., Cordier, P., and Frost, D. J. (2005). Pressure sensitivity of olivine slip systems and seismic anisotropy of Earth’s upper mantle. Nature, 433:731–733.
- Mainprice, D. (2007). Seismic anisotropy of the deep earth from a mineral and rock physics perspective. In Treatise on Geophysics, vol. 2, pages 437–491. Elsevier.
- Moulik, P., and Ekström, G. (2014). An anisotropic shear velocity model of the Earth's mantle using normal modes, body waves, surface waves and long-period waveforms. Geophysical Journal International, 199(3):1713-1738.
- Nolet, G. (1990). Partitioned waveform inversion and two-dimensional structure under the network of autonomously recording seismographs. Journal of Geophysical Research, 95(B6):8499–8512.
- Visser, K., Trampert, J., Lebedev, S., and Kennett, B. L. N. (2008). Probability of radial anisotropy in the deep mantle. Earth and Planetary Science Letters, 270:241–250.